Winter 2018

Molecular candidates for Blocking the Transmission of Vector-Borne diseases

Ashish Naresh Vora
Old Dominion University, avora001@odu.edu

MOLECULAR CANDIDATES FOR BLOCKING THE TRANSMISSION OF VECTOR-BORNE DISEASES

by

Ashish Naresh Vora
B.Sc. (Hons.) August 2008, University of Central Lancashire, United Kingdom
M.Sc. January 2009, University of Leicester, United Kingdom

A Dissertation Submitted to the Faculty of
Old Dominion University in Partial Fulfillment of the
Requirements for the Degree of

DOCTOR OF PHILOSOPHY

BIOMEDICAL SCIENCES

OLD DOMINION UNIVERSITY
December 2018

Approved by:

Hameeda Sultana (Director)

Girish Neelakanta (Member)

Emilia Oleszak (Member)

Stephen Beebe (Member)

ABSTRACT

MOLECULAR CANDIDATES FOR BLOCKING THE TRANSMISSION OF VECTOR-BORNE DISEASES

Ashish Naresh Vora
Old Dominion University, 2018
Director: Dr. Hameeda Sultana

Vector-borne diseases (VBDs) require urgent attention as they have a high mortality rate, with 700,000 people dying in a year as of 2017. So far, extremely few reliable vaccination strategies and solutions have emerged. Transmission blocking vaccines are one among many solutions available to manage the control of VBDs. These require identification of both vector and pathogen molecules that play important roles in the transmission, dissemination and establishment of VBDs. Our strategy is to characterize these candidates that play important roles in vector-host-pathogen interactions. This manuscript presents two such studies identifying the participation of two arthropod molecules in vector-host-pathogen interactions. The first study uses quantitative and standard PCR to detect dengue serotypes DENV2/3 RNA and immunoblotting to detect viral proteins within mosquito extracellular vesicles (EVs). The EVs carry infectious viral RNA and are able to establish infection in naïve, recipient cells of various lineages. Mosquito EVs mediate DENV2 transmission through a newly identified mosquito exosome marker, designated as Tsp29Fb, an orthologue of human CD63. Silencing Tsp29Fb reduced DENV2 load, it's interaction with DENV2 E-protein and transmission of DENV2 through EVs.

Our second study identifies another arthropod molecule in ticks. The tick HSP70-like molecule is involved in disrupting the host coagulation pathway through the

induction of fibrinogenolysis. Immunoblotting analysis revealed reduced D-Dimer, a fibrin degradation product, in ticks fed on immunocompromised hosts. In addition, ticks fed on immunocompromised hosts exhibit a lower expression of the arthropod HSP70-like molecule that correlated with higher engorgement weights. This differential activity is linked to the immune states and/or background of the vertebrate host, in this case mice. Inhibition of the tick HSP70-like molecule in the salivary gland lysates of fed ticks abrogates its fibrinogenolytic activity. These studies together identify two strong candidates playing different roles for blocking the transmission of VBDs from two different arthropods.

This manuscript is dedicated to my family. To my parents Nita and Naresh Vora, who due to difficult circumstances could not finish their education but invested heavily in the completion of mine. My sister Sheetal Vora Parikh, without whom I would not be able to live away from home. My wife, who encourages me and teaches me to be the best version of myself as a person and as an academic. To the new generation as well, my nephews and niece Ayaan, Aadiv and Ahana, whose pictures kept me going while I lived away from home.

ACKNOWLEDGMENTS

First and foremost I would like to acknowledge my PhD advisor Dr. Hameeda Sultana for working very closely with me on both these projects. Her guidance has turned me into a professional from a science enthusiast. Dr. Girish Neelakanta, my co-advisor who has contributed significantly to my growth. Drs. Sultana and Neelakanta taught me to never give up, value my work and aim high. I would also like to thank Dr. Emilia Oleszak for being a part of my dissertation committee and for teaching me advanced virology. Thank you to Dr. Stephen Beebe as well, who believed in me and gave me extremely valuable input on this academic work. I would like to acknowledge my colleague Mr. Wenshuo Zhou (shared graduate student with Drs. Sultana and Neelakanta) for generating the DENV2 RNA genome data and for characterizing the role of HSP70 in extracellular vesicles. I sincerely acknowledge the cry electron microscopy facility at UTMB and collaborators Drs. Michael Sherman and Michael Woodson for generating the extracellular vesicle images included in this manuscript and our published work. My sincere thanks also goes to Drs. Tonya Colpitts and Berlin Londono-Renteria for providing the mosquito RNA samples and to Mr. Wenshuo Zhou for performing the QPCR analysis on the same. In addition, I would like to acknowledge the contribution of Mr. Vikas Taank (graduate student with Dr. Neelakanta) for generating the QPCR data for tick HSP70 expression. I acknowledge Dr. Sucharita Dutta for performing the MS/MS analysis and Dr. John Catravas for providing the tick HSP70 inhibitor. I would finally like to thank all the members of Sultana and Neelakanta laboratories, especially Vikas Taank, Wenshuo Zhou, Shovan Dutta and Supreet

Khanal. Their constant support and encouragement helped me in navigating through my degree at ODU. A lot of love and gratitude to my parents and sister for their unconditional love and support. I would finally like to thank my wife Sharmista, who stands by me through thick and thin.

TABLE OF CONTENTS

Page

LIST OF TABLES

LIST OF FIGURES

OVERVIEW

Vector-borne diseases (VBDs) caused over 1.1 million deaths in 2002 and 700,000 deaths in 2017 that comprise of 17% of all infectious diseases (WHO 2004, 2017). Out of the 700,000 deaths in 2017, 400,000 were due to malaria, which remains the leading VBD today (WHO 2017). Other major VBDs include Leishmaniasis, Trypanosomiasis, Yellow fever, Dengue, Chagas disease and Japanese encephalitis fever, in descending order of their mortality rates (WHO 2004, 2017.) There are over 19 million species of arthropods, some of which carry or are known to carry and transmit deadly diseases to humans (Ødegaard, 2000). The leading arthropod vectors of disease are mosquitoes and ticks (Conway et al., 2014; Neelakanta and Sultana, 2015) and can be used as models for studying VBDs.

So far, the VBD management strategies have involved direct treatment of disease, blocking acquisition and transmission of pathogens and finally vector population control (Conway et al., 2014). Out of these the most successful strategy we have today is vector control which involves the use of physical barriers, pesticides, repellents, and attractants (Conway et al., 2014; Foster and Hancock, 1994; Kato et al., 2008). There is also a sterile insect technique involving the release of transgenic insects with dominant lethality to reduce vector population (Harris et al., 2012). Direct treatment of viral infections has not been very successful due to a lack of available antiviral treatment options and the therapy involves just palliative care (Katzelnick et al., 2017a, 2017b; Whitehorn and Simmons, 2011). Blocking acquisition involves either the identification of arthropod molecules important for viral pathogenesis or use of biological

This dissertation is formatted according to the Cell press journal model.

agents like *Wolbachia* that play a role in suppressing viral replication (Cheng et al., 2010; Glaser and Meola, 2010; Mousson et al., 2012; Perera-Lecoin et al., 2013). However, a major problem with these strategies is that it cannot prevent a primary infection from the pathogen.

This leaves transmission blocking strategies as the new promising avenue for investigation. The blocking of transmission would also require the identification of molecular players that facilitate the transmission of pathogen or those that suppress the host's immune system (Conway et al., 2014; Neelakanta and Sultana, 2015; Zhou et al., 2018). The candidates considered as targets for blocking transmission have to match certain criteria to be of high quality. These criteria outline that the target should be indispensable for vector-pathogen interaction and silencing of the target should lead to a direct reduction in pathogen load, dissemination and pathogenesis. The primary amino acid sequence of the candidate should be highly conserved among the population of the vector species. It should be able to generate a high antibody titer and be compatible with multiple adjuvants. Finally, the target molecule should not generate an exaggerated immune response leading to immunological disorders in the host (Neelakanta and Sultana, 2015).

The best place to look for these molecular players lies at the host-vector-pathogen interface i.e. at the bite site of an infected vector. Many studies have been performed to determine the absolute importance of vector-attachment and host-seeking behavior of the vectors in order for them to secure a blood meal (Brossard and Wikel, 2004; Francischetti et al., 2009; Hovius et al., 2008; Ribeiro and Francischetti, 2003; Ribeiro et al., 2007; Wikel, 2013), without which there would not be any physical

channel to transmit the pathogen. Several other studies have been performed to show that vector saliva enhanced the chance of establishing and increased the severity of infection, only some of which are cited here (Ader et al., 2004; Jones et al., 1989; Kročová et al., 2003; Labuda et al., 1993; Le Coupanec et al., 2013; Schneider et al., 2004; Styer et al., 2011; Surasombatpattana et al., 2014). These molecules are of myriad classes and have multiple functions which include behaviors like anti-hemostasis, anti-inflammation, immunosuppression, anti-coagulation, vasodilation etc. (Calvo et al., 2010; Neelakanta and Sultana, 2015; Ribeiro et al., 2007). Hence, this vector-pathogen-host interface provides an ideal area for the search of molecular candidates for blocking transmission of VBDs.

With this in mind, this manuscript highlights two studies that show evidence fulfilling the first requirement of a molecular candidate to block transmission of VBDs. The first study published in 2018, focuses on how a newly identified tetraspanin domain containing glycoprotein mediates the transmission of dengue virus through mosquito extracellular vesicles. The second study published in 2017 focuses on the role of a tick HSP70 and the differential feeding response elicited by ticks upon feeding on hosts with different immune backgrounds.

MOSQUITO EXTRACELLULAR VESICLES MEDIATE DENGUE VIRUS TRANSMISSION THROUGH INTERACTION WITH A TETRASPANIN GLYCOPROTEIN TSP29FB

INTRODUCTION

Dengue is a major VBD, which according to the 2017 WHO report puts 3.9 billion people at risk of infection (Brady et al., 2012). There are 96 million reported cases of dengue with observable symptoms worldwide every year with actual number of infections estimated to be over 300 million (Bhatt et al., 2013). A subset of these infections, around 500,000 are severe infections with symptoms of hemorrhage and multiple organ failure leading to 19,000 deaths every year (Yacoub et al., 2013). Attempts at developing and distributing vaccines for dengue has been challenging, compounded by four serotypes (DENV1-4) and the antibody dependent enhancement of the disease (Halstead and O'Rourke, 1977; Katzelnick et al., 2017a). The only approved vaccine, Dengvaxia for dengue is not broadly protective and has been pulled off the market (Hadinegoro et al., 2015). So far there are no drugs available for treatment and management of the disease is limited to vector control and supportive care (Conway et al., 2014).

The life cycle of dengue virus is like most other flaviviruses. Figure 1 shows the standard model for dengue virus entry into the cells (Cruz-Oliviera et al., 2015). There is a direct interaction of mature viruses with host cell receptors which then leads to receptor mediated endocytosis (Cruz-Oliveira et al., 2015; Perera-Lecoin et al., 2013;

Vega-Almeida et al., 2013). During the late endosomal stage, the low-pH triggers a conformational change in the viral envelope (E)-protein, which fuses with the endosomal membrane. Thus, releasing the genomic content of the virus directly into the cytosol (Cruz-Oliveira et al., 2015; Rodenhuis-Zybert et al., 2010). Once inside, the positive sense RNA genome gets translated to produce the RNA-dependent RNA polymerase encoded by the viral RNA. This polymerase is then further able to replicate the viral genome leading to translation of more viral proteins. Eventually the viral proteins are assembled and the immature virus is passed through the trans-Golgi network (Cruz-Oliveira et al., 2015; Rodenhuis-Zybert et al., 2010). At this stage there is cleavage of furin on the virus that leads to its maturation and subsequent release through budding off from the membrane (Cruz-Oliveira et al., 2015; Rodenhuis-Zybert et al., 2010). The dengue genome is ~11kb long and consists of three structural proteins (M, C and E) and seven non-structural (NS) proteins (NS1, NS2A, NS2B, NS3, NS4A, NS4B, NS5). Out of these, multiple studies have reported the involvement of the dengue NS1 protein in the contribution to viral toxicosis through suppression of the interferon response and increasing viral toxicity (Guzman et al., 2010; Halstead, 2015).

Exosomes or small extracellular vesicles (EVs) have been shown to carry a range of molecules including protein, RNA and even DNA (Colombo et al., 2014; Gonzales et al., 2009; Théry et al., 2002; Villarroya-Beltri et al., 2014). Figure 2 shows multi-vesicular endosomes (MVEs) containing intra-luminal vesicles that are released in the extra cellular space when the endosomes fuse with the plasma membrane

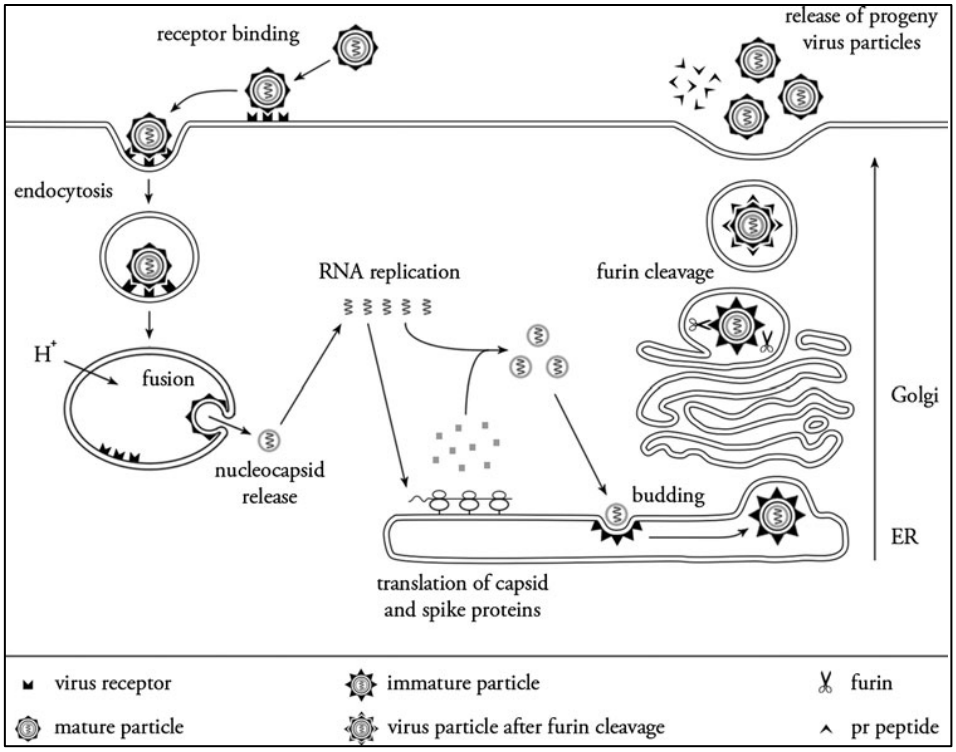

Figure 1. Life Cycle of Dengue Virus. Beginning on the top-left the image shows the receptor mediated endocytosis of a mature dengue virus. The virus once taken inside the cell is present in the endosome which when progresses to the late endosomal stage becomes acidic in pH. The acidic pH triggers the fusion of the viral envelop with the endosomal membrane making the virus release its contents into the cytoplasm. The RNA genetic material of dengue virus begins replicating and simultaneously gets translated to produce the viral proteins. The viral RNA and proteins pass through the trans-Golgi network to produce a mature dengue virus particle which is released into the extra-cellular space through exocytosis**.** This image is reproduced from a paper on the dengue virus life cycle (Rodenhuis-Zybert et al., 2010).

(Colombo et al., 2014; Théry et al., 2002). The small 30-150 nm sized EVs are known as exosomes. Bigger sized EVs with sizes ranging from 150-1000 nm diameters are known to directly bud off from the plasma membrane and are classified as microvesicles (Colombo et al., 2014; Théry et al., 2002). Some studies have shown the presence of virus components in mammalian exosomes (Arakelyan et al., 2017;

Ramakrishnaiah et al., 2013). Previously published work from Dr. Sultana laboratory was the first to characterize the role of arthropod EVs in pathogen transmission (Zhou et al., 2018). This formed the basis of our hypothesis that dengue, which is a positive single-stranded RNA virus could also be transmitted through EVs.

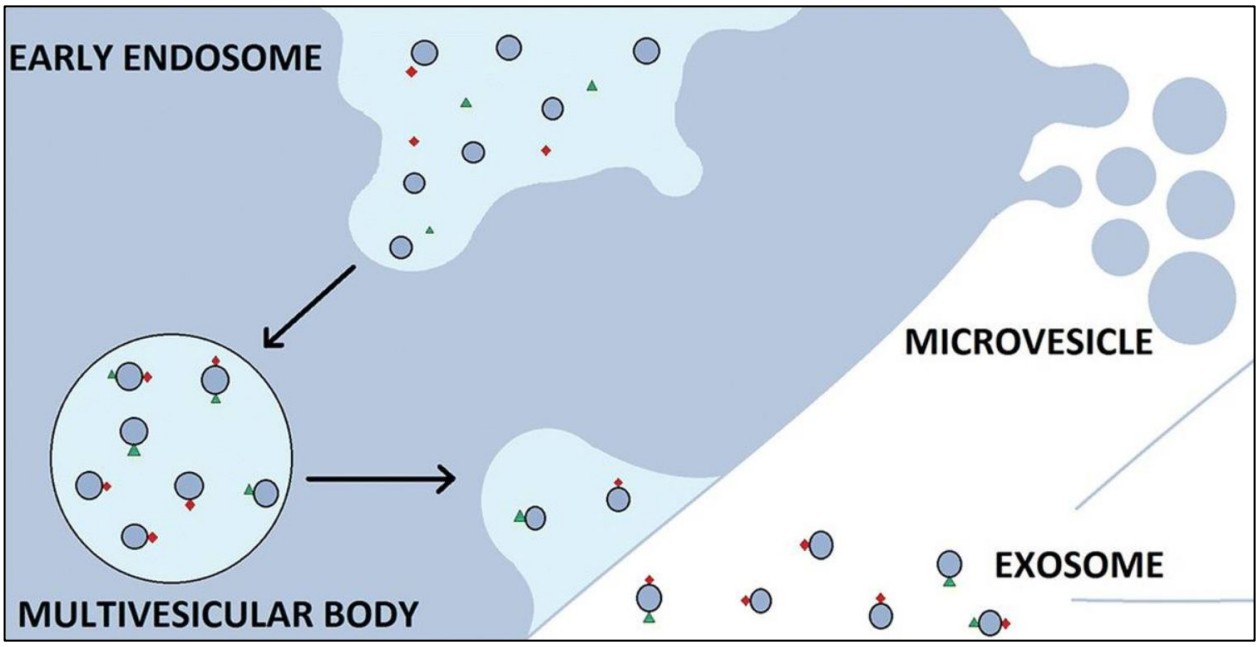

Figure 2. Biogenesis of Extracellular Vesicles. Exosomes (30-150 nm) are formed through invaginations in the early endosome, giving rise to small vesicles called intraluminal vesicles. As these endosome progress to the late endosomal stage known as multivesicular bodies, they contain intraluminal vesicles loaded with various molecules. The multivesicular body through exocytotic mechanisms fuses with the plasma membrane to release these vesicles in the extracellular space which are then known as exosomes. Larger EVs (> 150 nm) can pinch of directly from the plasma membrane and are classified as microvesicles. This image is adapted from a paper published on the recent advancements on the use of exosomes as drug delivery vehicles (Bunggulawa et al., 2018).

This study shows for the first time, the presence of the full-length DENV2 RNA genome and viral proteins in mosquito cell derived EVs and that these EVs are able to establish an infection in naïve recipient cells from different lineages. These findings

provide important data for the current and future avenues in understanding biology of arthropod EVs in pathogen transmission which is a rapidly expanding field (Alenquer and Amorim, 2015; Barile and Vassalli, 2017; Hackenberg and Kotsyfakis, 2018; Madison and Okeoma, 2015; Schorey et al., 2015). To determine whether there are any molecules that can be used to block transmission of disease through EVs, this study investigated two molecules that are enriched in EVs, HSP70 and the mosquito orthologue of human CD63 (LAMP3), Tsp29Fb. The results of which indicate that Tsp29Fb plays an important role in transmission of DENV2 though EVs. The human CD63 has also been implicated in the entry and exit of the human immunodeficiency virus (HIV) (Li et al., 2014). Collectively, this study is not only critical in understanding the molecular basis of the modes of flaviviral transmission from the arthropod vector, but may also potentially lead to the development of better strategies to interfere with the life cycle of this and perhaps other medically important vectors.

RESULTS

Mosquito Cell-Derived EVs Contain DENV2 RNA and Proteins

Figure 3 shows increasing dengue load with time in *Aedes albopictus* mosquito cell line (C6/36). Figure 3A shows a significant increase in the dengue burden in C6/36 cells, Figure 3B in C6/36 EVs and Figure 3C in *Aedes aegypti* mosquitoes (*in vivo*). Since the viral load (both in cell line and *in vivo*) was high at 72 hpi (hours post-infection), we selected this time point for the isolation of EVs from mosquito cells. Figure 4A and 4B show the two different ultracentrifugation techniques used for the isolation of EVs from *in vitro* cultures. Cryo-electron microscopy (cryo- EM) data generated in collaboration with colleagues Drs. Woodsone and Sherman at UTMB were performed on C6/36 EVs showed the presence of 30– 250 nm diameter EVs (Figure 5A), which bear resemblance to EVs isolated from mammalian cells as described in literature (Tauro et al., 2012; Théry et al., 2002). Figure 5B shows the detection of *A. albopictus* HSP70 in each of the infected or uninfected EV fractions 2-6, with the highest level in fraction 4 (Figure 5B). HSP70 was not detected in fraction 1 from EVs isolated from uninfected or DENV2-infected groups (Figure 5B) indicating the absence of EVs (since HSP70 is an EV marker). Figure 5B also shows increased presence of HSP70 in infected EVs in comparison to uninfected fractions. DENV2 E-protein was higher in infected EV fraction 5 in comparison to the other fractions (Figure 5B). Immunoblotting also revealed both DENV2- glycosylated (Figure 5B, upper band) and endogenous (lower band) E-protein in fraction 5 and 6. E-protein was not detected in uninfected controls. The Ponceau S-stained images showed total protein profile in each fraction.

Further quantitative real-time PCR (qRT-PCR) showed DENV2 total capsid transcripts in EVs derived from infected C6/36 cells (Figure 5C). The same result was derived for DENV3 capsid RNA in EVs derived from DENV3 infected *A. albopictus* cells. This suggests that EVs may act as mediators of all serotypes of DENVs (Figure 5D). DENV2 E and nonstructural 1 (NS1) proteins were also detected in C6/36 cell lysates and EVs (Figure 5E). E-protein level was higher in EVs in comparison with cell lysates at 72 hpi, whereas no difference was observed with NS1 protein levels in either EVs or total cell lysates (Figure 5E). Similar pattern of E-protein levels are seen in DENV3-infected C6/36 cell-derived EVs and total cell lysates (Figure 5F). Coomassie-stained gel images show the total protein profiles in both DENV2 and DENV3 groups (Figure 5E and 5F). Quantification of *A. albopictus* EVs showed the highest prevalence of EV sizes were between 50 and 100 nm in both uninfected and DENV2-infected groups (Figure 6A and 6B). Figure 6A and 6B also show that DENV2-infected cell-derived EVs had a higher percentage of EVs in the size range 0-50 nm and fewer 100–150 nm sized EVs in comparison to the uninfected EVs. This suggests that DENV2 may stimulate production of smaller EVs. Figure 6C shows the counts of total number of EVs from uninfected or DENV2-infected *A. albopictus* cells obtained from cryo-EM images collected from at least three independent isolations. The counts did have a significant difference. For biochemical quantification of EVs, we determined their total protein amounts using the Bradford protein assay (BCA). Extracellular vesicles isolated from various number of cells show a linear increase for EV proteins (Figure 6D and 6E). There was a negligible difference in the EV protein amounts from infected or uninfected samples. These data correlate with data in Figure 6A, 6B and 6C. DG-EV isolation performed determined

whether EVs contain viral particles and the size of EVs that contain the viral particles. An independent DG-EV isolation by filtering the culture supernatants with 0.22-μM filters that yielded 12 fractions showed similar results (Figure 6F). To determine if *A. albopictus* cell-derived EVs contain the full-length DENV2 genome, Mr. Wenshuo Zhou (graduate student with Dr. Neelakanta) with support from Dr. Neelakanta performed a PCR analysis (with oligonucleotides producing overlapping amplicons covering entire DENV2 sequence) was performed (Figure 7A). The result shows the presence of the full-length DENV2 genome in C6/36 cell-derived EVs. Fragments 1–10 amplified products of 1,102 bp, 1,110 bp, 1,124 bp, 1,114 bp, 1,118 bp, 1,141 bp, 1,104 bp, 1,135 bp, 1,110 bp, and 1,048 bp. Fragment 11 (3′ end of the genome) amplified multiple products, including the expected size of 717 bp. This may be due to the looped nature of the 3′ end of the genome.

DENV2 RNA and Proteins are Securely Contained Inside the EVs

To eliminate the possibility of DENV2 viruses being present outside of the EVs, we performed cryo-EM analysis on 6 C6/36 cell-derived DG-EV fractions (Figure 7B). The infected EV fractions did not show any virions either inside or outside of these EVs. These data suggest that viral RNA and proteins are perhaps sufficient for the infection of naïve recipient cells. To determine if the viral RNA is bound to the EV exterior and are thus delivered to the recipient cells, we treated our infected cell derived EVs and viral stocks with RNase A (Figure 8A, 8B). DENV2 loads were determined from cells exposed to RNase treated and untreated EVs. We obtained similar results with no difference in the viral load in the C6/36 cells upon incubation with EVs or laboratory viral

stocks prepared from DENV2-infected RNaseA-treated or untreated groups. To confirm that the viral proteins too are contained inside the mosquito cell-derived EVs, and are not on the exterior as contaminants, we designed and performed an E-protein 4G2-antibody bead binding assay. There were no differences in viral loads between infected EV fractions treated with either 4G2 antibody (that binds to viral E-protein) or with the isotype control or the untreated controls (Figure 8C). We also tested the DENV2 laboratory stock as a control that showed reduced DENV2 loads in the recipient C6/36 cells in comparison with the isotype antibody-treated or untreated controls (Figure 8D). In addition, we performed native-PAGE followed by immunoblotting with 4G2 antibody on infected *A. albopictus* EVs treated with 0.1% Triton X-100 for 30 min at room temperature, or treated with multiple freeze-thaw cycles or untreated samples. A higher level of E-protein (in native state at ~200–250 kDa) was detected in Triton X-100–treated EV fractions in comparison with the levels in untreated or freeze-thawed fraction. Ponceau S-stained images showed the total protein profile and served as control. Immunofluorescence analysis with 4G2 antibody showed that EVs treated/lysed with 0.1% of Triton X-100 had a higher fluorescent signal for DENV2 E-protein in comparison with untreated EV fractions (Figure 8F). Enzyme linked immunosorbent assay (ELISA) with 4G2 (an anti-E-protein antibody) further supported the native- PAGE and immunofluorescence analyses, where higher loads of DENV2 E-protein were detected when EVs were permeabilized with 0.1% of Triton X-100 in comparison with untreated controls (Figure 8G). Taken together all of these data suggest that DENV2 RNA and proteins contained inside the *A. albopictus* EVs are not present as contaminants on the outside.

DENV2 Infectious RNA and Proteins are Transmitted to Mosquito, Murine, and Human Cells through *A. albopictus* EVs

To determine if DENV2 RNA and proteins contained in *A. albopictus* cell-derived EVs are viable and infectious to arthropod/ vertebrate host cells, we used EVs and EV-depleted supernatants (EDS; generated during EV pelleting and before PBS wash) (Figure 4B). Immunofluorescence assays performed on naïve C6/36 cells treated with infectious EVs showed a greater fluorescent signal for E-protein in comparison to EDS-treated cells (Figure 9A). Higher concentrations of EVs showed similar results (Figure 9A). Infectious *A. albopictus* EVs and EDS were also tested in plaque assays (Figure 9B). *A. albopictus* cell-derived infectious EV pellet fractions yielded plaques at dilutions of 1:10 that were too numerous to count, and around 25–30 plaques at a dilution of 1:100, and fewer than 5 plaques in dilutions of 1:1000. EDS treatment of *A. albopictus* cells yielded no plaques. Further, we analyzed whether EVs derived from infected *A. albopictus* are capable of transmitting DENV2 to other cell types. The result in Figure 9C shows a successful transmission and reinfection ability of *A. albopictus* EVs to naïve mosquito C6/36 cells, mouse Mo-DCs, HaCaT cells, and HUVEC cells. No viral loads were detected in any tested cell lines incubated with EDS (Figure 9C). The infection of DENV2 in several other cell lines was assessed using dengue stock, which showed detectable a load at 72 hpi (Figure 10B–10E). Infected *A. albopictus* cell derived EVs were introduced to naïve cells used in Figure 10C-10E. Overall, these results suggest that DENV2 viral RNA and proteins exit mosquito cells via EVs, and that these infectious EVs mediate transmission of DENVs to human cells.

Role of *A. albopictus* HSP70 in EV-mediated DENV2 Transmission

The qRT-PCR data in this section was contributed by Mr. Wenshuo Zhou, for the published manuscript (Vora et al., 2018). Figure 5 and 6 demonstrate that the *A. albopictus* HSP70 is present in EVs derived from mosquito cells. To determine if the *A. albopictus* HSP70 plays a role in the EVs mediate transmission dengue, we investigated the role of two isoforms of *hsp70* (GenBank accession nos. JN132154 and XM_019672019). Quantitative RT-PCR revealed that both *hsp70* isoforms were upregulated in C6/36 cells upon infection at 48 h and 72 hpi in comparison with 24 hpi and uninfected controls (Figure 11A, 11B). The *hsp70* transcript (GenBank accession no. JN132154) was undetectable in EVs. The presence of *hsp70* transcript GenBank accession no. XM_019672019 was evident in EVs, without a significant change in expression between uninfected and infected EVs (Figure 11C). Immunoblotting showed an increased expression of HSP70 in EVs isolated from infected cells at 24 hpi in comparison to 48 and 72 hpi and uninfected samples (Figure 11D). No change in expression of HSP70 was observed between uninfected or infected C6/36 cell lysates (Figure 11D). Coomassie-stained gel images show the total protein profiles in EVs and total cell lysates. In addition, we tested the effect of inhibiting HSP70 on DENV2 transmission through EVs. QRT-PCR showed that C6/36 cells treated with VER-155008 (HSP70 inhibitor), followed by infection with DENV2 had significantly reduced expression of *hsp70* (XM_019672019, in comparison to the mock- (DMSO) treated group (Figure 11E). No change was observed in XM_019672019 transcript expression in EVs derived from these inhibitor-treated and DENV2-infected C6/36 cells (Figure 11E). Treatment with VER-155008 inhibitor did not decrease DENV2 load in either total

cell or EV lysates (Figure 11F). The effects of VER-155008 inhibitor-treated infectious EVs and EDS from the same batch were tested on naïve C6/36 cells. No difference was observed in DENV2 loads in the inhibitor-treated group compared to the mock (Figure 11G). Similar results were obtained for EDS treated cells. As expected, DENV2 loads in EV fractions showed significant differences compared with the EDS fractions. All these data indicate that the up-regulation of *A. albopictus* HSP70 as an arthropod stress response during DENV2 infection, but inhibition of this critical chaperone does not lead to the reduction in viral burden or transmission.

Identification of a Mosquito EV Marker Tsp29Fb, a Tetraspanin Domain-containing Glycoprotein

The human CD63 or LAMP-3 proteins are well-established markers for EVs/ exosomes (Colombo et al., 2014; Gonzales et al., 2009; Théry et al., 2002; Villarroya-Beltri et al., 2014). Hence, we decided to investigate the mosquito ortholog of human CD63 as a marker of and mediator for the transmission of DENV2 through EVs. Using a human CD63 primary amino acid sequence, (GenBank accession no. AHI151903) as a query in the VectorBase, we identified tetraspanin domain-containing mosquito orthologs in both *A. aegypti* (AAEL012532-RA) and *A. albopictus* (AALF020630- RA) and designated these orthologs as Tsp29Fb. ClustalW alignment of an *A. aegypti* Tsp29Fb amino acid sequence (Figure 12A) revealed 89% identity with *A. albopictus* Tsp29Fb and 51% identity with *Drosophila melanogaster* tetraspanin 29Fb protein (GenBank accession no. AAF90138). *Aedes aegypti* Tsp29Fb showed 28% and 27% identity with human and mouse CD63 (GenBank accession no. CAJ18387),

respectively. A phylogenetic analysis revealed that *A. aegypti* Tsp29Fb lies within the same clade as *A. albopictus* Tsp29Fb and *D. melanogaster* tetraspanin 29Fb. The human and mouse CD63s form a different clade (Figure 12B). Domain analysis of the *A. aegypti* Tsp29Fb sequence revealed the presence of the tetraspanin domain (amino acids 15–238), four transmembrane regions (amino acids 19–41, 56–78, 90–112, 211–233), four myristoylation sites (amino acids 37–47, 76–82, 92–98, 228–234), and two glycosylation sites (amino acids 125–129, 168–172) (Figure 12C). The identification of an ortholog of the EV/ exosome marker CD63 named Tsp29Fb in the mosquito genome suggests the presence of a putative EV marker in mosquitoes.

DENV2 Infection Up-regulates Tsp29Fb Expression in Mosquito EVs and Cells

To explore the function of Tsp29Fb in EV mediated transmission of DENV2 in mosquitoes, we analyzed its expression in DENV2- infected *A. aegypti* mosquitoes (*in vivo*) (Figure 13A). The results show very significant up regulation of *tsp29Fb* (accession no. AAEL012532-RA) at 24, 48, and 72 hpi, in comparison to uninfected mosquitoes. Similar expression patterns were observed in Aag-2 cells, derived from *A. aegypti* mosquitoes. Quantitative RT-PCR analysis showed that in both Aag-2 EVs and in cells, *tsp29Fb* was up-regulated upon infection at 48 and 72 hpi compared to uninfected samples (Figure 13B, 13C). Quantitative RT-PCR also revealed significantly higher transcripts of tsp29Fb (accession no. AALF020630-RA) at 24 and 48 hpi in C6/36 cell-derived EVs (Figure 12D), and at 48 and 72 hpi in whole-cell lysates (Figure 12E). Time and MOI dependent expression of Tsp29Fb was also analyzed using immunoblotting (Figure 13F and 13B). The results determined that for C6/36 cell-

derived EV fractions and whole-cell lysates at different time points of 24, 48, and 72 hpi, had higher Tsp29Fb protein expression in infected lysates in comparison to uninfected samples (Figure 11F). This correlated with the qPCR data in Figure 13D and 13E. Tsp29Fb expression is also upregulated with increasing infectious dose of DENV2 (Figure 13G). Total protein profiles in all four panels served as loading controls (Figure 13F and 13G). These data show that Tsp29Fb is upregulated both *in vivo* and *in vitro* upon DENV2 infection.

Tsp29Fb Directly Interacts with DENV2 Envelope Protein

For further characterization of Tsp29Fb's function in facilitating DENV2 infection and transmission, we tested if it directly interacts with DENV2 E-protein. Immunoprecipitations (IPs) performed with a human CD63 antibody and DENV2-infected EVs and whole-cell lysates (suspended in modified RIPA protein lysis buffer; 150 µg as input in each group) showed the presence of DENV2 E-protein by immunoblotting with 4G2, an anti- E-protein antibody (Figure 13H). The direct interaction of Tsp29Fb to DENV2 E-protein was increased in cell lysates in comparison to EV lysates. This could be due to a higher total amount of Tsp29Fb protein in cell lysates than in EVs. An E-protein signal was not detected in uninfected controls. Figure 13I shows an IP of Tsp29Fb using PBS suspended intact arthropod EVs (freshly isolated) using human CD63 antibody followed by immunoblotting with 4G2 antibody. This too detected the precipitation of DENV2 E-protein in both mosquito cell-derived EV fractions and whole cell lysates (we used 500 µg as input in each group for IP with PBS suspended EV fractions). Coomassie blue-stained gel images showing total protein

profile of input lysates used for IP served as controls. We also show that Tsp29Fb neither interacts nor co-precipitates with actin in either EVs or total cell lysates (Figure 14B). These data served as a negative control for the direct interaction of Tsp29Fb with DENV2 E-protein (Figure 13H and 13I). Actin protein immunoblots from both cells and EVs lysates (resuspended in RIPA buffer) that were used as input for the IP assay serve as a control (Figure 14C). These data suggest the presence of actin in input lysates that neither interact nor co-precipitate with Tsp29Fb. Immunofluorescence performed on *A. albopictus* cells showed co-localization of Tsp29Fb (Figure 14A) with DENV2 E-protein in infected cells. Uninfected C6/36 cells and nuclei-stained (DAPI) images served as controls. Altogether, these data indicate a role for mosquito EV marker Tsp29Fb in facilitating infection and transmission of dengue virus through direct interaction with the viral E-protein.

Inhibition of Tsp29Fb Reduces DENV2 Infection

We investigated the effect of inhibiting Tsp29Fb function to study its effect on dengue replication and transmission through EVs. We generated the dsRNA against the *tsp29fb* gene and sequenced it (Figure 15A and 15B) Transfection with *tsp29fb* dsRNA resulted in lower *tsp29Fb* transcripts (Figure 16A) in Aag-2 cells and EVs. DENV2 load in the same samples was significantly reduced (Figure 16B). Immunoblotting showed the same result, with reduced E-protein and Tsp29Fb protein expression in both EVs and total cell lysates compared to mock (Figure 16C). Total protein profiles shown by Coomassie-stained gel served as loading controls. Blocking Tsp29Fb using the human CD63 antibody in mosquito cells resulted in a reduced dengue load in EVs, cells at the

transcriptional and translational level (Figure 16D-16F). Total protein profiles shown by Coomassie-stained gels served as controls (Figure 16F). Significant differences with CD63 antibody treatments and silencing suggest that inhibition of Tsp29Fb reduces DENV2 load in cells that ultimately inhibits transmission of viral RNA and proteins via EVs.

GW4869 Inhibitor Reduces DENV2 load, Transmission and Tsp29Fb Interaction with DENV2 E-protein

Treatment of C6/36 cells with GW4869 an EV/ exosome release inhibitor followed by DENV2 infection showed reduction in the DENV2 capsid transcript in EVs, compared with the DMSO control (Figure 16G). Similar results were obtained with immunoblotting analysis with anti- E-protein antibody at 18 and 24 hpi, in both infected C6/36 cell-derived EVs and cell lysates in comparison with the DMSO controls (Figure 16H). Longer incubation duration with the inhibitor resulted in further reduction of E-protein expression at 24 hpi in comparison to 18 hpi. Total protein profiles shown by Coomassie-stained gels served as control. Infection of naïve C6/36 cells with EVs derived from GW4869 inhibitor treated, infected mosquito cells showed reduced DENV2 viral RNA in the recipient cells in comparison with the DMSO control (Figure 16I). A transwell assay was performed with C6/36 cells on top and HUVEC cells at the bottom. The C6/36 cells were infected with DENV2 stock, EVs or EVs in addition to GW4869 (Figure 16J). The dengue load was determined in the HUVEC cells 48 hpi and shown to be reduced in the inhibitor treated samples. The exosome inhibitor was also shown to reduce the direct interaction of Tsp29Fb with the dengue E-protein through an IP

performed with CD63 antibody and lysates from infected C6/36 cells. DMSO treated samples were used as control (Figure 16K). These data indicate that the reduction in EV release reduces dengue load and that the direct interaction of Tsp29Fb with E-protein is not only required for DENV2 infection and pathogenesis in the arthropod host, but also is essential for transmission of infectious EVs to the human host.

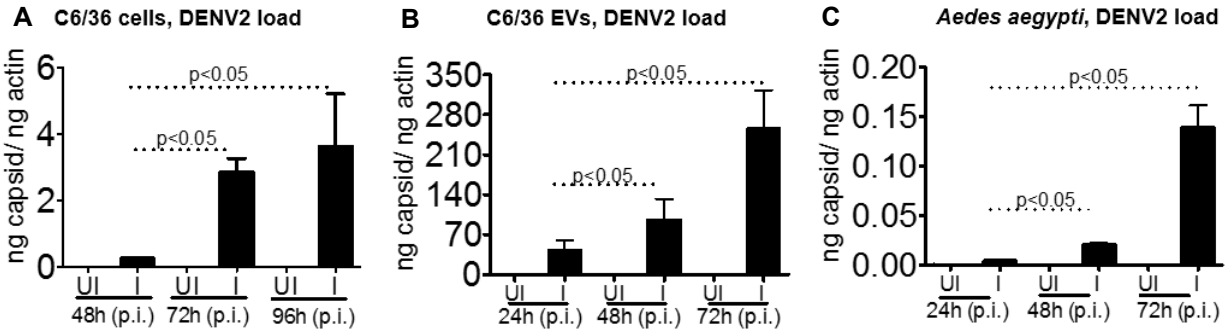

Figure 3. DENV2 Infection Kinetics in C6/36 Cells, EVs and Mosquitoes.

(A and B) QRT-PCR analysis showing viral loads in DENV2-infected (5 MOI) C6/36 cells (n = 4) or in EVs (n = 6) derived from DENV2-infected C6/36 cells Uninfected C6/36 cells or cell-derived EVs were used as controls.

(C) QRT-PCR analysis showing DENV2 load in *A. aegypti* mosquitoes (n = 4). (Note: The data in panel C was contributed by Mr. Wenshuo Zhou towards the publication of this data in Vora et al., 2018) DENV2 capsid mRNA levels were normalized to mosquito *actin* level. The value of p determined by Student's two-tailed *t* test is shown.

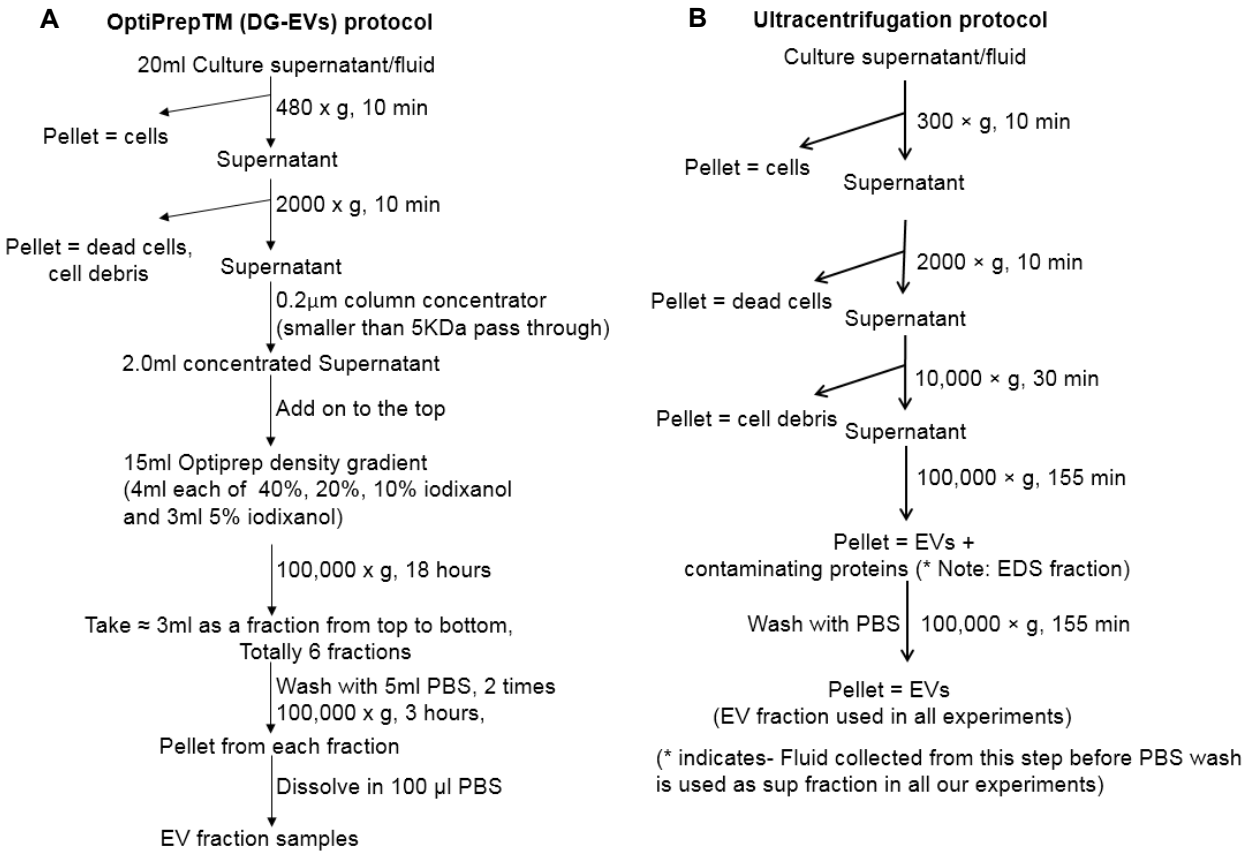

Figure 4. Schematic Representation of the Methods Used for EV Isolation from Mosquito Cells.

(A) Schematic representation of OptiPrep TM (DG-EVs-iso) using density gradients of iodixanol.

(B) A regular ultracentrifugation technique used for EV isolation.

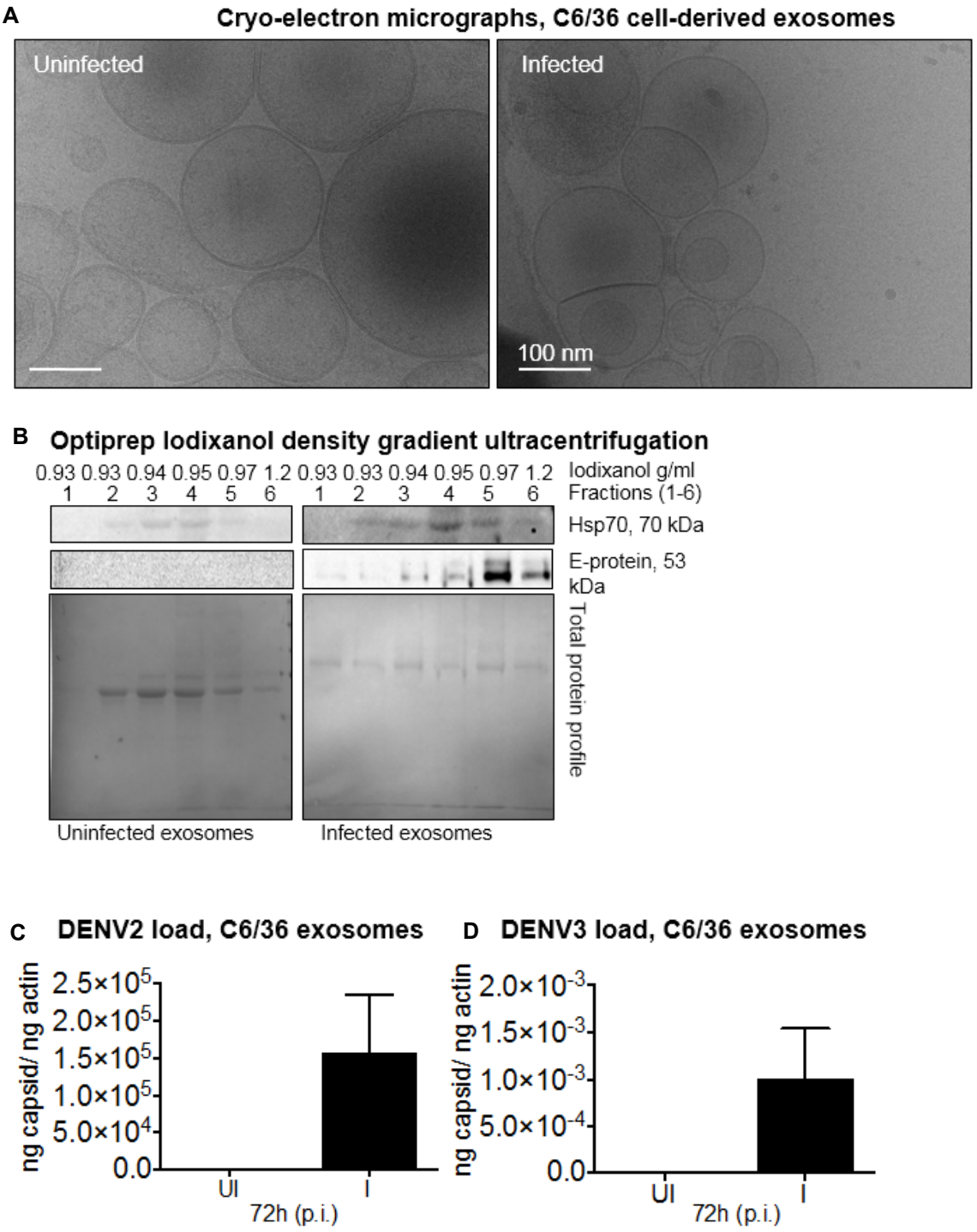

Figure 5. EVs Derived from Mosquito Cells Contain DENV2/DENV3 RNA and Proteins.

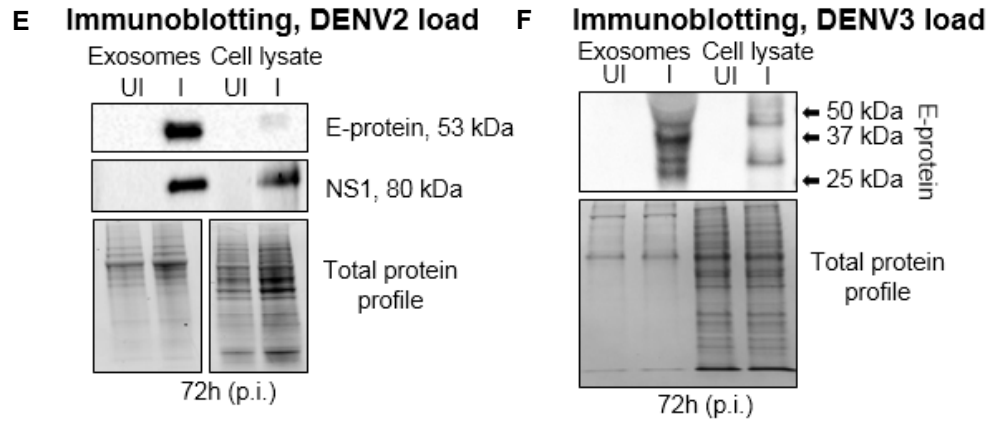

Figure 5. Continued.

(A) Cryo-EM images showing EVs isolated from uninfected or DENV2-infected (MOI 5, 72 hpi) C6/36 cells. Scale bar, 100 nm. (Note: The cryo-EM images were contributed by Drs. Woodson and Sherman at UTMB).

(B) Immunoblotting from DG-EV-iso preparation showing enhanced DENV2 E-protein level and HSP70 in fractions 4–6. EVs derived from uninfected cells serve as control. Total protein profiles from both groups shown for comparison. Fraction number and calculated iodixanol density (g/mL) shown for reference.

(C and D) QRT-PCR analysis showing DENV2 or DENV3 load in EVs isolated from C6/36 cells at 72 hpi (n = 5). DENV2/ DENV3 capsid mRNA levels were normalized to mosquito *actin* levels. The p value determined by Student's two-tail *t* test shown.

(E) Immunoblotting showing detection of DENV2 E-protein and NS1 in EVs and total lysates from whole cells prepared from uninfected (UI) or infected (I) C6/36 cells at 72 hpi (MOI 5).

(F) DENV3-specific E-protein in EVs and total cell lysates from uninfected (UI) or infected (I) C6/36 cells at 72 hpi (MOI 5) is shown. Protein sizes are indicated as kilo Daltons. Images showing total protein profiles serve as loading controls in both (E) and (F).

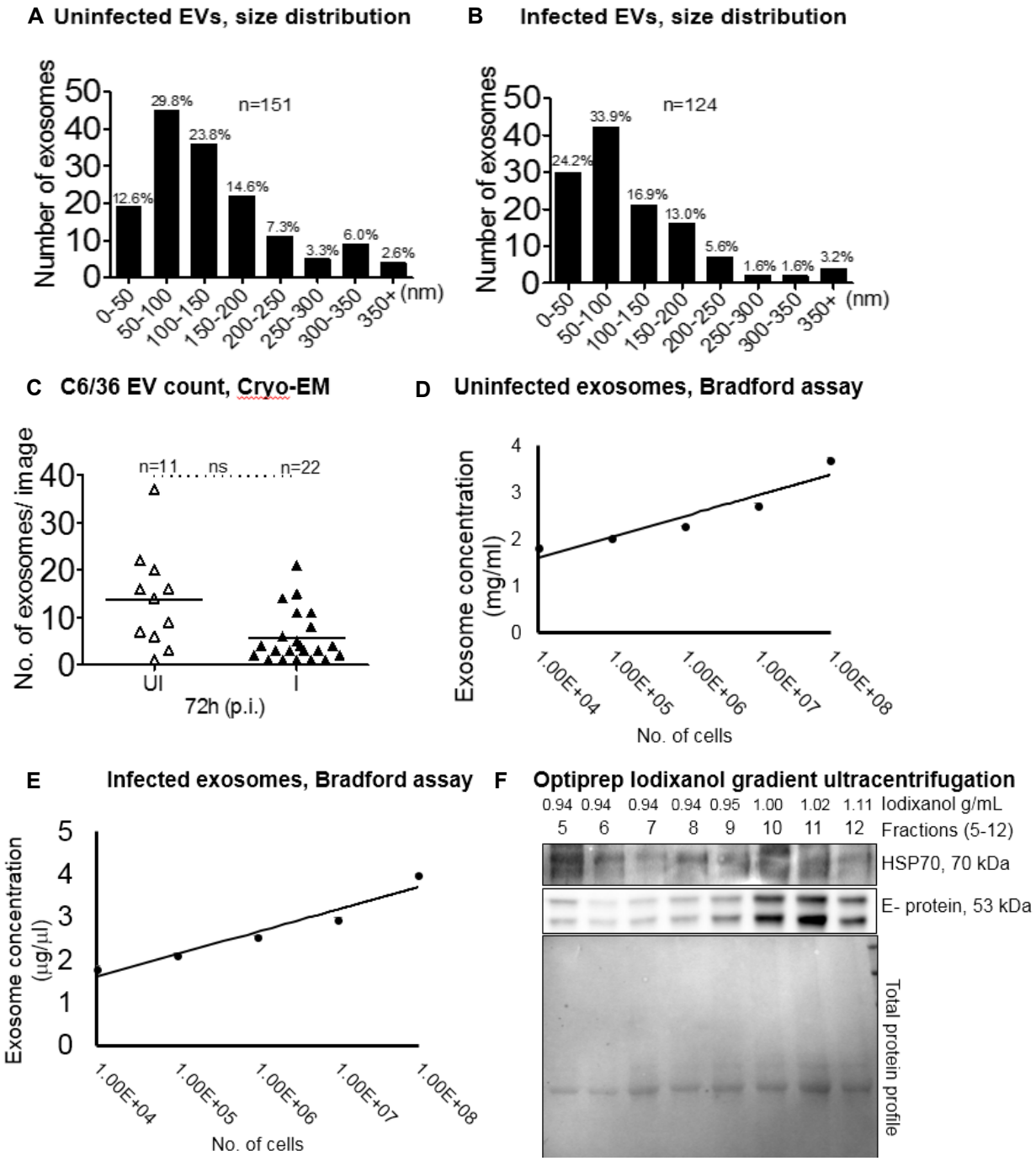

Figure 6. Estimation and Quantification of C6/36 EVs upon DENV2 Infection.

(A and B) Heterogeneous size distribution of EVs isolated from uninfected or DENV2-infected C6/36 cells is shown. Y-axis represent number and X-axis indicate size range (e.g. 0-50 nm, in diameter) of EVs in each group. The total number of EVs considered from different cryo-EM images is indicated as 'n'. Percentages were calculated based on the total number of EVs in each size range.

(C) EVs numbers were counted from uninfected and DENV2-infected (MOI 5, 72 hpi) groups. The Y-axis represents EVs number. ‘n’ indicates total number of images used in this quantification. Data shown in (A-C) was generated by Mr. Wenshuo Zhou.

(D) and E) Quantification of arthropod EVs by measurement of total protein amounts (BCA method) from uninfected or DENV2-infected (MOI 5, 72 hpi) EVs isolated from increasing density of 10^4, 10^5,10^6, 10^7 and 10^8 cells is shown from respective groups. Total EV protein concentration (measured as µg/µl) is plotted against increasing cell number/density.

(F) Detection of DENV2 E-protein and EVs marker HSP70 in EVs derived as twelve fractions during independent DG-EV isolation. Immunoblotting analysis from iodixanol density gradient EVs preparations filtered through 0.22 µm showing enhanced DENV2 E-protein levels in fractions 9-12 from infected (MOI 5; 72 hpi) C6/36 cells. HSP70 was detected in all fractions and serve as EV marker. Total protein profile from each fraction is shown for comparison. Fraction number and calculated iodixanol density (g/mL) is shown on top for reference.

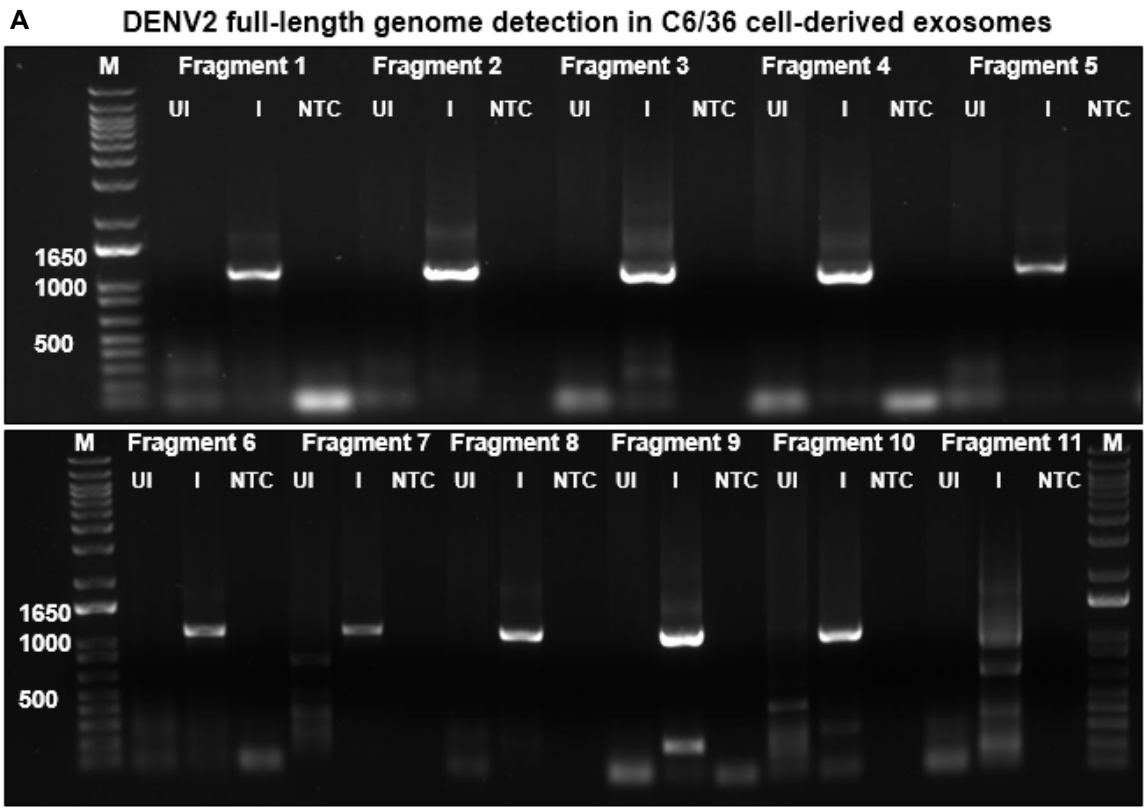

Figure 7. EVs Derived from C6/36 Cells Contained DENV2 Full Length Genome and No Viral Particles.

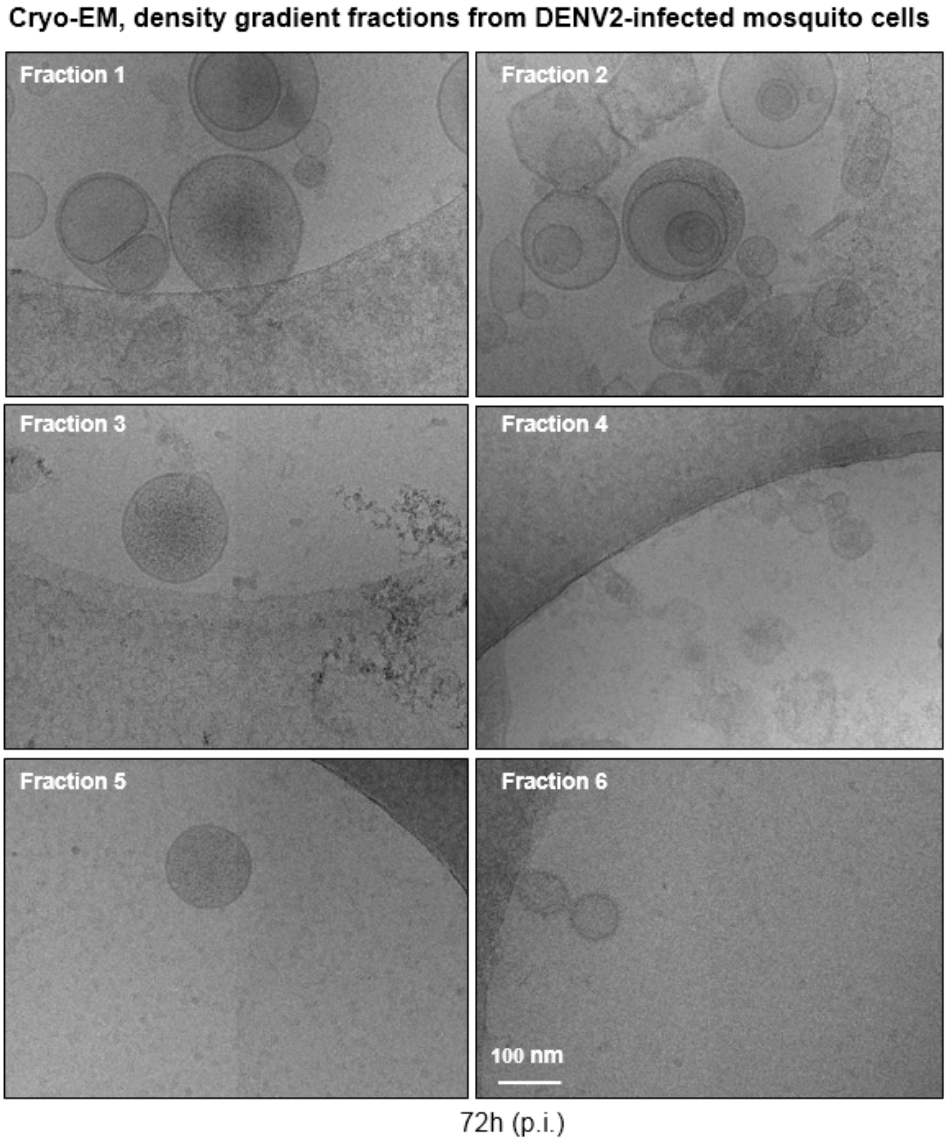

Figure 7. Continued.

(A) Agarose gel images showing amplification of overlapping fragments from full-length genome in arthropod EVs derived from DENV2-infected (5 MOI, 48 hpi) C6/36 cells. The cDNA derived from total RNA was used as template. PCR generated 11 fragments (fragment sizes are shown in methods) show the full-length DENV2 genome amplification. UI and I indicate uninfected and infected groups respectively. NTC indicates no template control. M indicates DNA marker.

(B) Cryo-EM images showing EVs isolated from DENV2-infected (MOI 5; 72 hpi) C6/36 cells. EVs isolated by density gradient (DG-EVs-iso) fractions are shown. Fractions are labeled from 1-6. Scale bar indicates 100 nm in all six fractions. Panel (A) PCR was performed by Mr. Wenshuo Zhou and Panel B images generated by Drs. Woodson and Sherman.

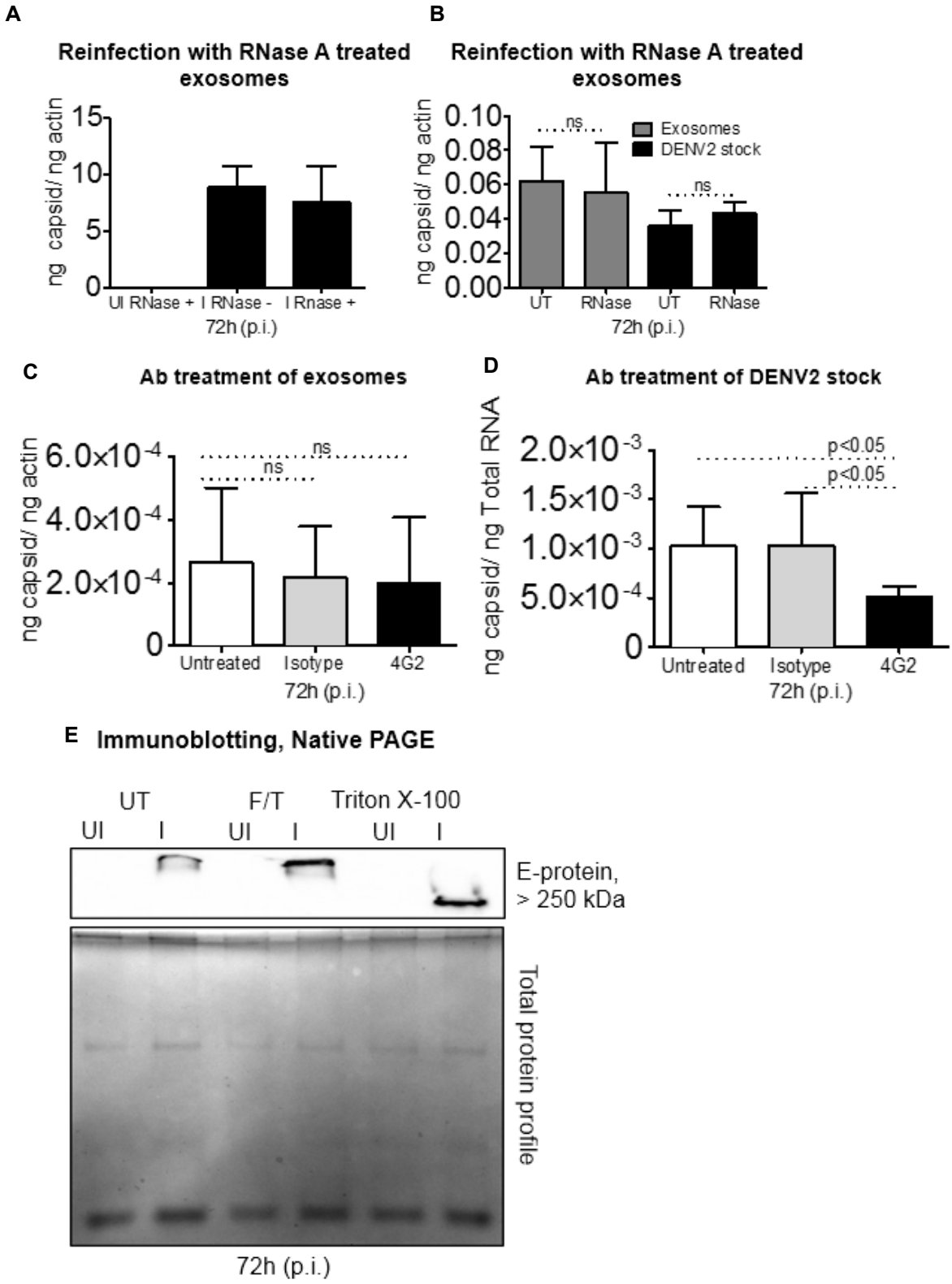

Figure 8. DENV2 RNA and Proteins Are Securely Contained Inside EVs.

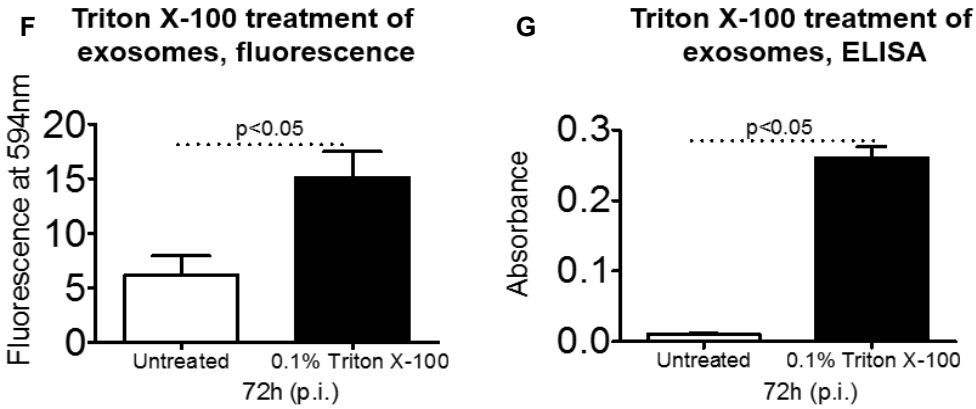

Figure 8. Continued.

(A) QRT-PCR analysis showing DENV2 loads in naïve C6/36 cells (incubated with EVs derived from independent batch of DENV2 infected (MOI 5; 72 hpi) C6/36 cells treated with RNase A). Uninfected treated samples serve as control (n = 4).

(B) QRT-PCR analysis showing DENV2 loads in naïve C6/36 cells infected via either infectious EVs derived from DENV2-infected (MOI 5, 72 hpi) C6/36 cells from an independent batch or DENV2 laboratory viral stocks with known virus titer (MOI 5) and treated with RNase A. The untreated samples serve as control (n = 6).

(C) QRT-PCR analysis showing viral load in EVs samples isolated from C6/36 DENV2-infected cells (MOI 5; 72 hpi) that were treated with 4G2 or isotype matched control antibodies. Untreated EVs samples served as control (n = 6). 'ns' indicates not significant in (B) and (C). DENV2 capsid mRNA levels were normalized to mosquito *actin* levels in (A, B and C).

(D) QRT-PCR analysis showing viral loads in DENV2 laboratory viral stocks (MOI 5) that were treated with 4G2 or isotype matched control antibodies. Untreated group was used as control (n = 6). DENV2 levels were normalized to total RNA in (D) as *actin* is not detectable.

(E) Native-PAGE followed by immunoblotting analysis showing presence of E-protein from DENV2-infected (MOI 5; 72 hpi) C6/36 cell-derived EVs (I) treated with Triton-X-100 (0.1%), or freeze-thaw cycles or untreated samples held on ice. Ponceau S stained blot image showing total protein profiles serve as loading control. EVs isolated from uninfected cells (UI) were used as controls.

(F) Relative fluorescence measurements from EVs (derived from DENV2-infected C6/36 cells at 72 hpi) treated with 0.1% Triton X-100 is shown. Untreated group was used as control (n = 6).

(G) ELISA showing increased detection of E-protein from EVs isolated from C6/36 DENV2-infected cells (MOI 5; 72 hpi) upon treatment with 0.1% Triton X-100 in comparison to untreated control (n = 4). The p value was determined by Student's two-tail *t* test is shown.

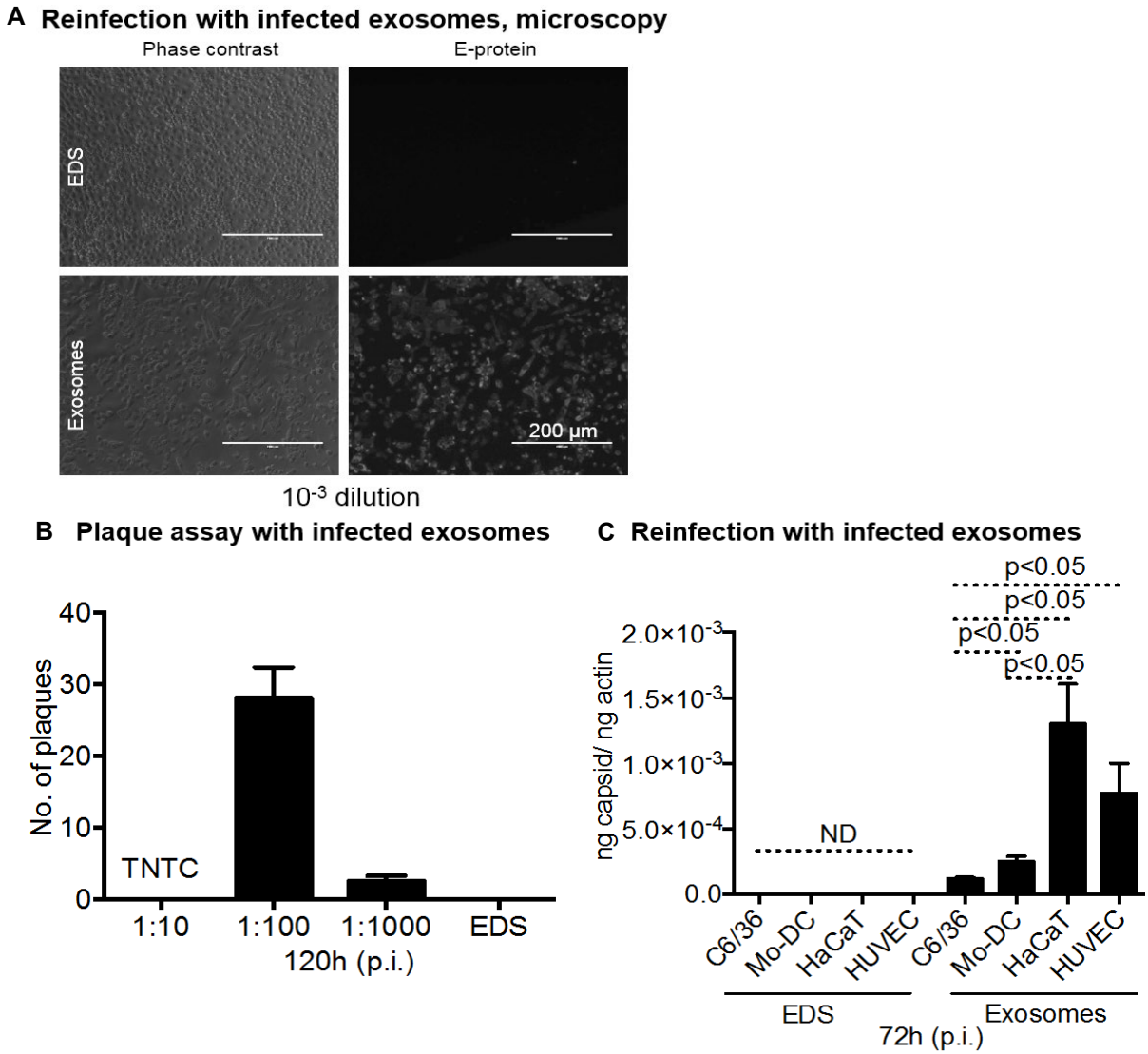

Figure 9. EVs Derived from Mosquito Cells Are Infectious and Transmit DENV2 to Both Arthropod and Mammalian Cells.

(A) Fluorescent microscopic images showing detection of E-protein in C6/36 cells infected via EVs derived from independent batch of DENV2-infected (MOI 5; 72 hpi) C6/36 cells. EDS-treated cells serve as control (n = 5) (Scale bar, 200 µm.).

(B) Quantitative assessment of number of plaques on Vero cells treated with EVs (in different dilutions) or EDS fractions (as similar dilution) derived from DENV2-infected (MOI 5, 72 hpi) C6/36 cells are shown. TNTC indicates “too numerous to count” (n = 2).

(C) QRT-PCR analysis showing viral loads at 72 hpi in naïve C6/36 or mouse dendritic or human HaCaT or HUVEC cells treated with EVs or EDS fractions derived from DENV2- infected (MOI 5, 72 hpi) C6/36 cells are shown (n = 3 for each cell line). ND indicates not detectable. Depending on the cells that were used, DENV2 capsid mRNA levels were normalized to mosquito, mouse, or human *actin* levels.

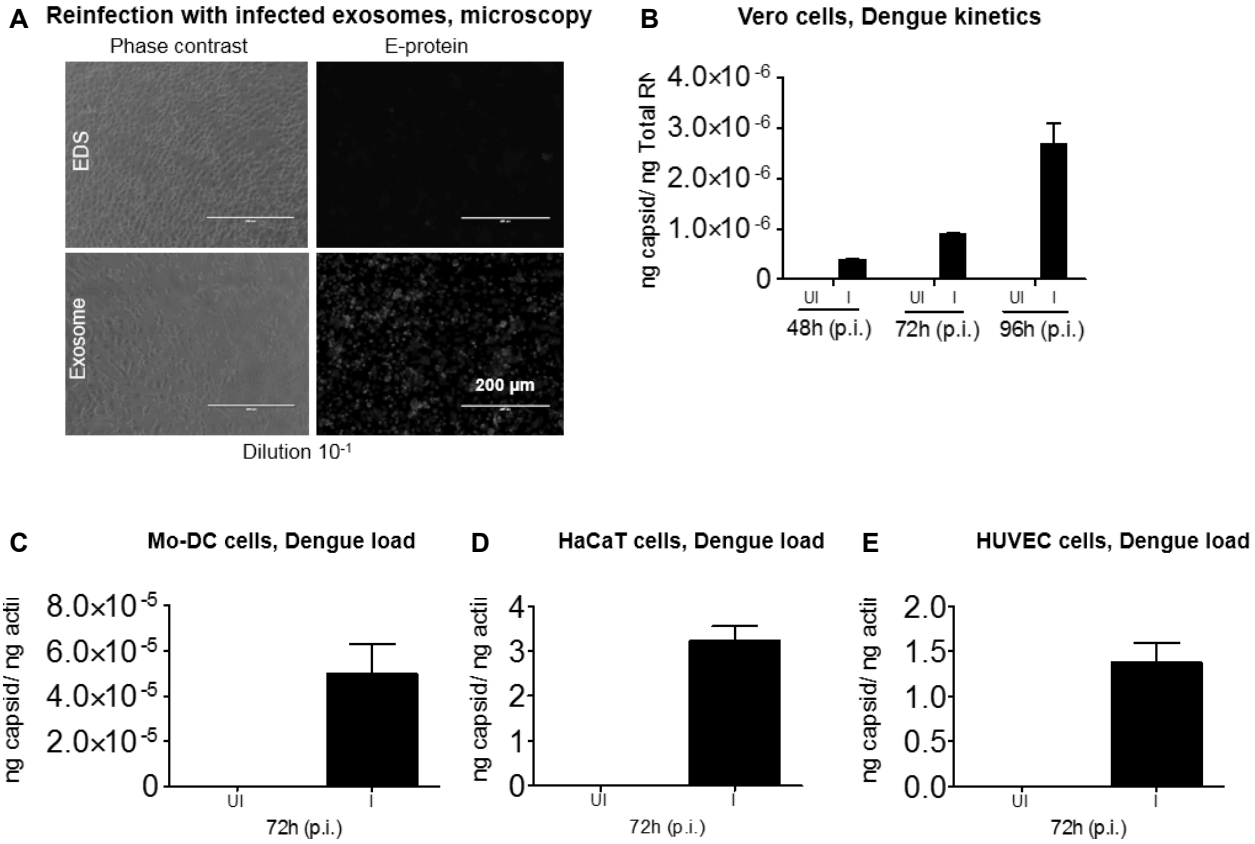

Figure 10. Re-Infection of Mosquito Cells via Infectious EVs and Infection Kinetics of DENV2 in Various Mammalian Cell Lines.

(A) Fluorescent microscopic images showing detection of E-protein in C6/36 cells infected with EVs diluted 10-fold that corresponds to 12.6 µg of total EVs protein as estimated by the BCA, derived from independent batch of DENV2-infected (MOI 5; 72 hpi) C6/36 cells. The C6/36 cells treated with EVs-depleted supernatant (EDS) fractions serve as control (n = 5). Scale bar indicates 200 µm in each image.

(B, C, D and E) QRT-PCR analysis showing viral loads in DENV2-infected Vero cells at indicated time

points (of 48, 72 and 96 hpi), mouse-derived dendritic cells at 72 hpi, human HaCaT cells at 72 hpi, and human HUVEC cells at 72 hpi. Cells were infected with laboratory virus stocks (MOI 5). Uninfected cells were used as controls (n = 3). DENV2 capsid mRNA levels were normalized to mouse or human *actin* levels, respectively. Human *actin* primers were used to determine the *actin* levels in Vero cells.

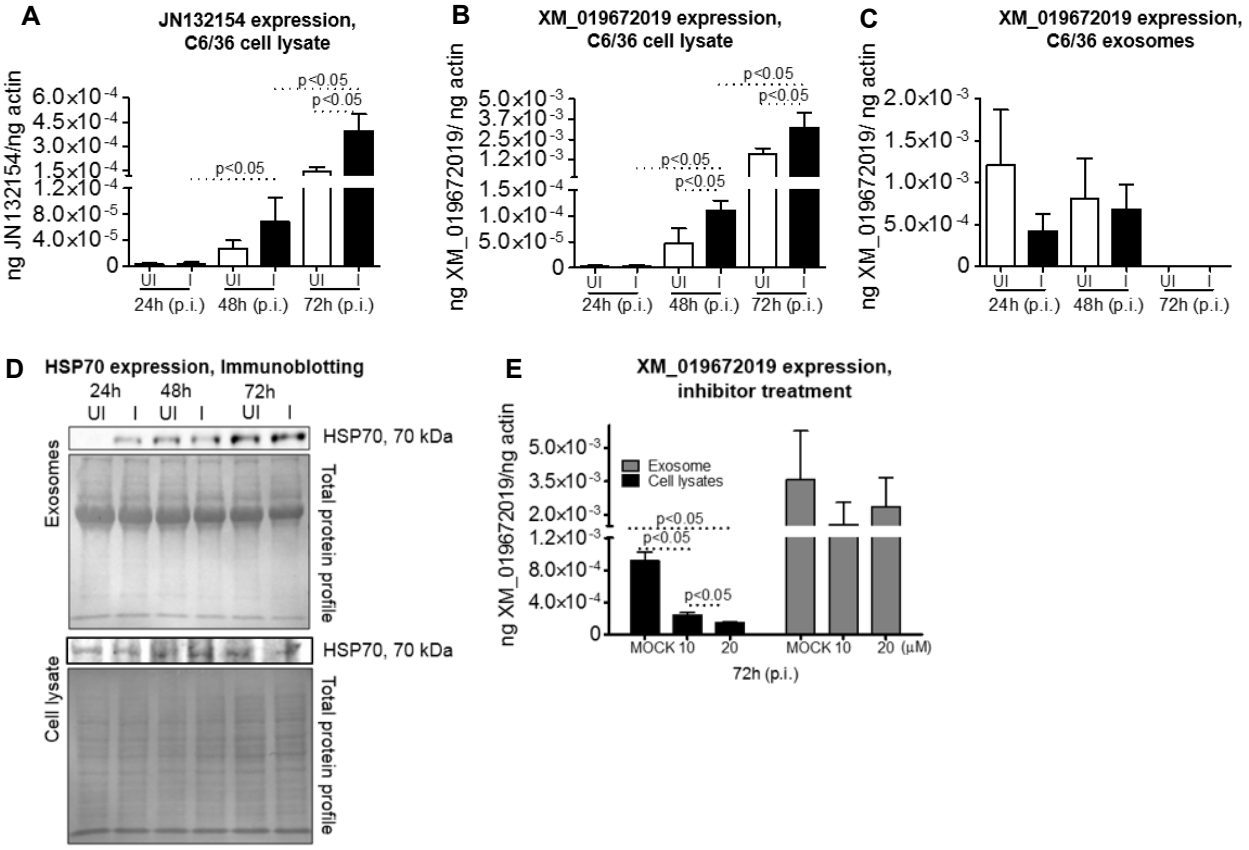

Figure 11. Role of HSP70 in *A. albopictus* EV-Mediated DENV2 Transmission.

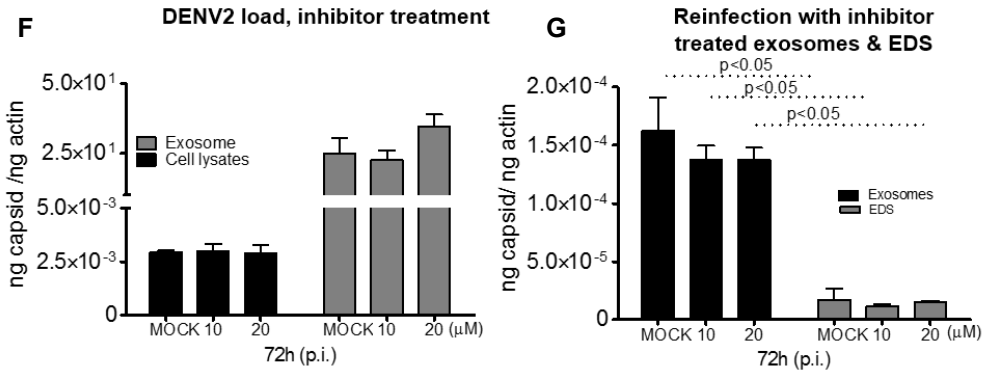

Figure 11. Continued.

(A and B) QRT-PCR analysis showing expression of *A. albopictus*- HSP70 isoform-1 (Accession number JN132154) (n = 6) or expression of HSP70 isoform-2 (Accession number XM_019672019) (n = 6) in C6/36 cell lysates collected from uninfected (UI) or DENV2-infected (I) (MOI 5; 72 hpi) groups. Samples analyzed from 24, 48, and 72 hpi are shown for both isoforms.

(C) XM_019672019 levels in EVs derived from DENV2-infected (MOI 5) C6/36 cells at 24, 48 and 72 hpi is shown. Uninfected C6/36 cell-derived EVs collected at similar time points serve as control (n = 6).

(D) Immunoblots showing expression levels of HSP70 in EVs derived from uninfected or DENV2- infected (MOI 5) samples and total cell lysates is shown from different time points (24, 48 and 72 hpi) of infection. Total protein profiles from Coomassie stained gel images serve as controls for both cell and EVs lysates. HSP70 molecular mass is indicated as 70 kDa.

(E) QRT-PCR analysis showing expression of HSP70 isoform-2 in C6/36 cells treated with VER-155008 inhibitor for 4 h followed by DENV2 (MOI 5, 72 hpi) infection is shown. Also, EVs lysates collected from these C6/36 cells treated and infected (as shown above) is shown for comparison (n = 4).

(F) DENV2 load in C6/36 cells or EVs is shown. C6/36 cells were treated with VER-155008 inhibitor at indicated doses followed by DENV2 infection (MOI 5, 72 hpi) and EVs were derived from the same cells (n = 4).

(G) Reinfection of naïve C6/36 cells with EVs derived from VER-155008 inhibitor treated and DENV2-infected (MOI 5, 72 hpi) or EDS is shown. C6/36 cells were treated with mock (DMSO) serve as controls in (E, F and G) (n = 4). HSP70 or DENV2 capsid mRNA levels were normalized to mosquito *actin* levels. The p value determined by Student's two-tail *t* test is shown. The qPCR analysis for this figure was performed by Mr. Wenshuo Zhou.

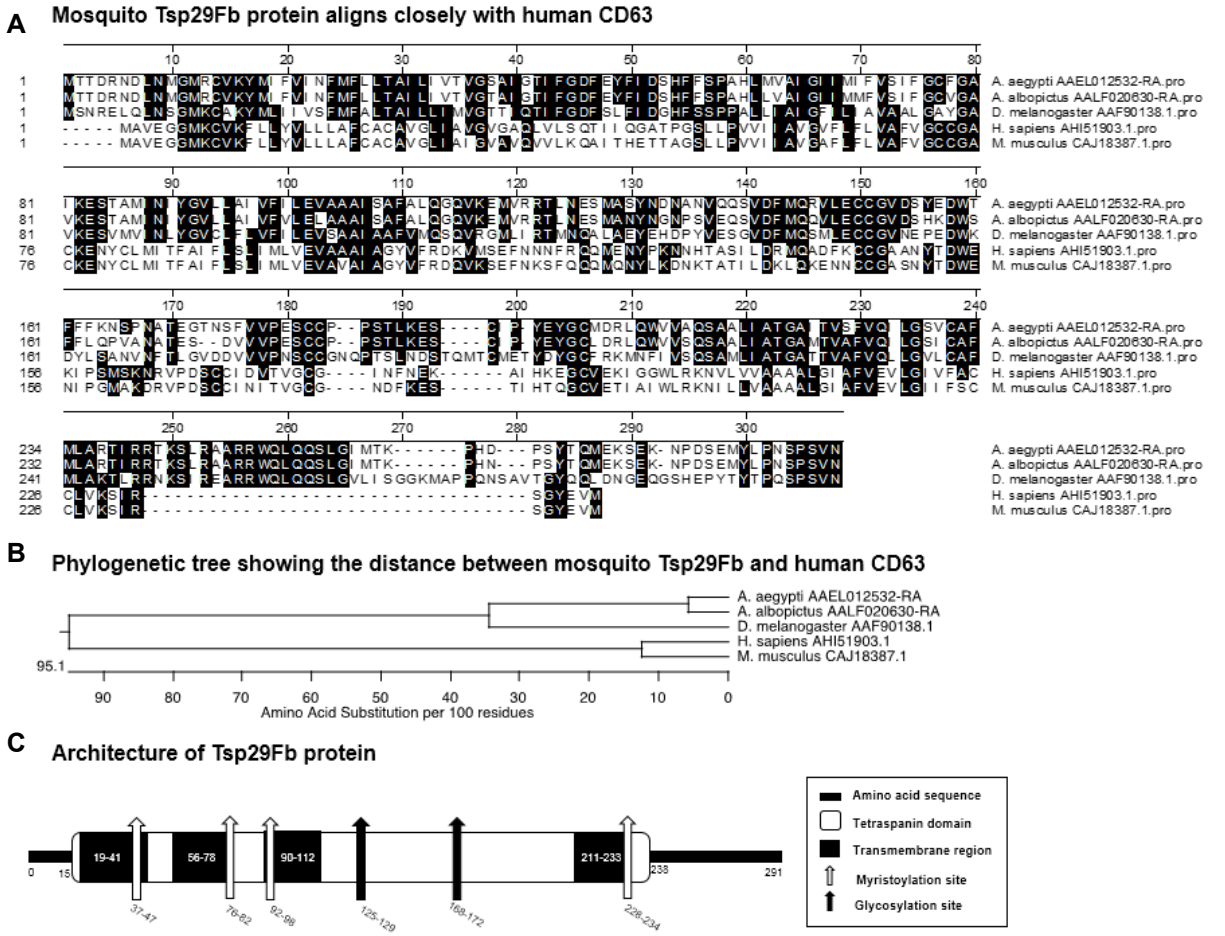

Figure 12. Alignment and Phylogenetic Analysis of *A. aegypti* Tsp29Fb.

(A) The deduced *A. aegypti* Tsp29Fb amino acid sequence alignment (with other orthologs) using ClustalW program in DNASTAR Lasergene is shown. Residues that match are shaded in black color. GenBank accession numbers for *D. melanogaster* tetraspanin 29Fb, *M. musculus* and *H. sapiens* CD63 sequences are shown. VectorBase accession numbers for *A. aegypti* and *A. albopictus* Tsp29Fb are provided. Ruler on the top of alignment indicates number of amino acids. Total length of the amino acid sequence is provided at one end of each sequence.

(B) Phylogenetic analysis was performed in DNASTAR by ClustalW slow/ accurate alignment method. Scale at the bottom denotes amino acid substitutions per 100 amino acid residues.

(C) Domain analysis of *A. aegypti* Tsp29Fb primary amino acid sequence at PROSITE (ExPASy) is shown. *A. aegypti* Tsp29Fb contain one highly conserved tetraspanin domain, 4 transmembrane regions, 4 myristoylation sites and 2 glycosylation sites.

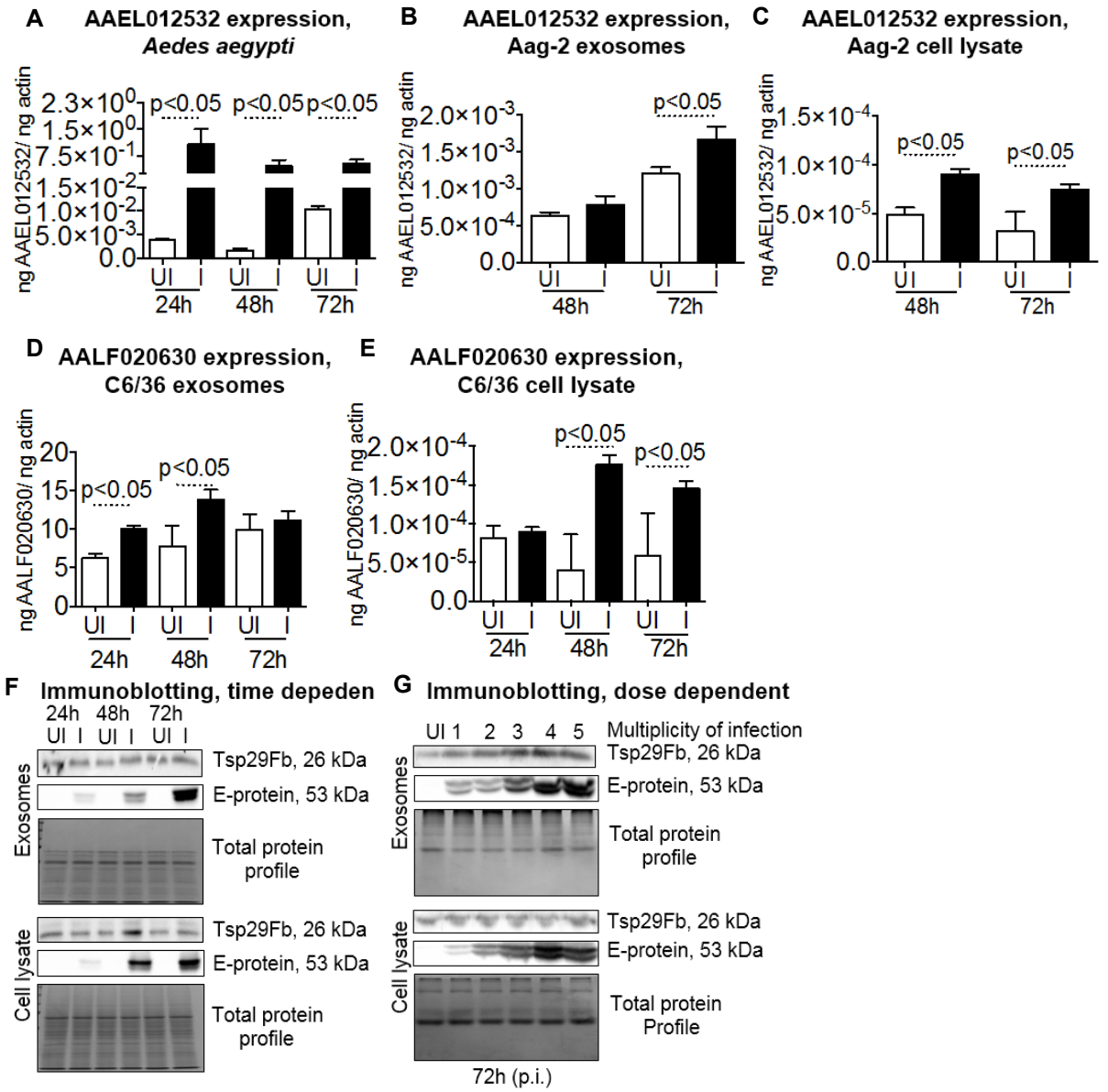

Figure 13. DENV2 Induces the Expression of Tsp29Fb, a Putative EV-Enriched Marker in Mosquito Cells.

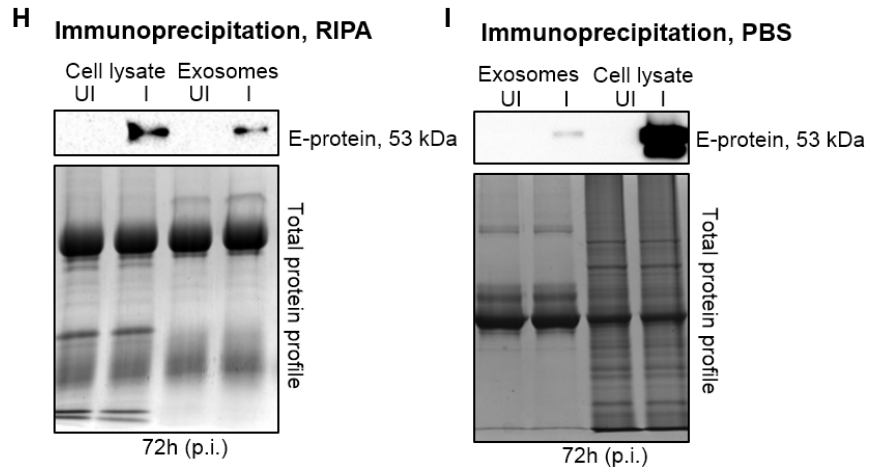

Figure 13. Continued.

(A, B and QRT-PCR analysis showing expression of *A. aegypti tsp29fb* in uninfected (UI) or DENV2-infected (I) whole mosquitoes at 24, 48, and 72 hpi (n = 4), or in EVs isolated from an uninfected or infected (MOI 5) *in vitro* cell line or in Aag-2 whole-cell lysates at (n = 4).

(D and E) QRT-PCR analysis showing expression of *A. albopictus tsp29fb* in EVs isolated from uninfected or infected (MOI 5) C6/36 cells or in whole-cell lysates at 24, 48, and 72 hpi (n = 8). DENV2 capsid mRNA or *tsp29fb* levels were normalized to mosquito *actin* levels. The p value determined by Student's two-tail *t* test is shown.

(F) Immunoblotting analysis showing levels of Tsp29Fb and viral E-protein in EV derived from uninfected or DENV2-infected (MOI 5) C6/36 cells or in whole-cell lysates at 24, 48, and 72 hpi.

(G) Immunoblotting analysis showing presence of Tsp29Fb and viral E-protein in EVs derived from uninfected or DENV2-infected (MOI 5, 72 hpi) C6/36 cells or in whole-cell lysates upon infection with different viral doses (MOI 1–5) is shown.

(H and I) Immunoblotting analysis of Tsp29Fb IP proteins in RIPA or in 1 x PBS buffer with 4G2 antibody showing detection of viral E-protein in EVs or whole-cells lysates derived from DENV2-infected (MOI 5, 72 hpi) C6/36 cells. Uninfected cells were used as controls in all assays. Gel images showing total protein

profiles in (F–I) serve as loading control for respective immunoblots. Tsp29Fb and DENV2 E-protein molecular mass is indicated as kilo Daltons.

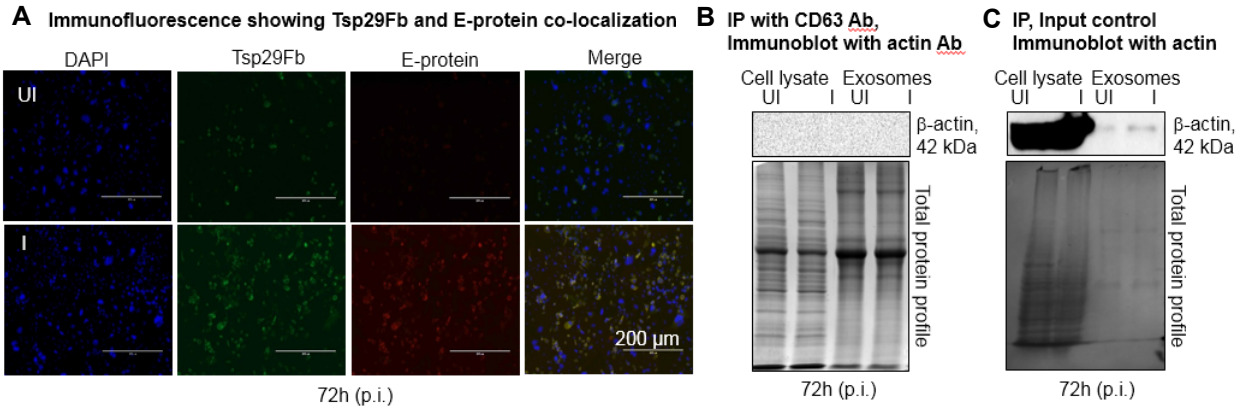

Figure 14. Tsp29Fb Co-Localizes with DENV2 E-protein and Does Not Precipitate with Actin.

(A) Fluorescent microscopic images of uninfected (UI) or DENV2-infected (I) (MOI 5) C6/36 cells at 72 hpi, probed with DAPI (blue), Tsp29Fb (green) and E-protein (red) is shown. Merged images show co-localization of E-protein with Tsp29Fb (yellow) (n = 5) and counter staining with DAPI. Scale bar indicates 200 µm.

(B) Immunoblotting analysis of Tsp29Fb immunoprecipitated proteins in RIPA buffer with actin monoclonal antibody revealed no co-precipitation in either EVs or whole cells lysates derived from DENV2-infected (MOI 5; 72 hpi) C6/36 cells. Uninfected cells were used as controls.

(C) Immunoblotting analysis of input lysates from DENV2-infected (MOI 5, 72 hpi) and uninfected C6/36 cells showing level of actin being present in the same lysates used for immunoprecipitation assay. Total protein profile images showing Coomassie stained proteins serve as control. Expected actin molecular mass is indicated as kDa.

Figure 15. PCR Amplification of *A. aegypti* Tsp29Fb DNA Fragment

(A) Agarose gel image showing amplification of *A. aegypti tsp29fb* DNA fragment used for synthesis of dsRNA. Oligonucleotides were designed based on AAEL012532 sequence.

(B) Nucleotide sequence of *A. aegypti tsp29fb* dsRNA clone is shown.

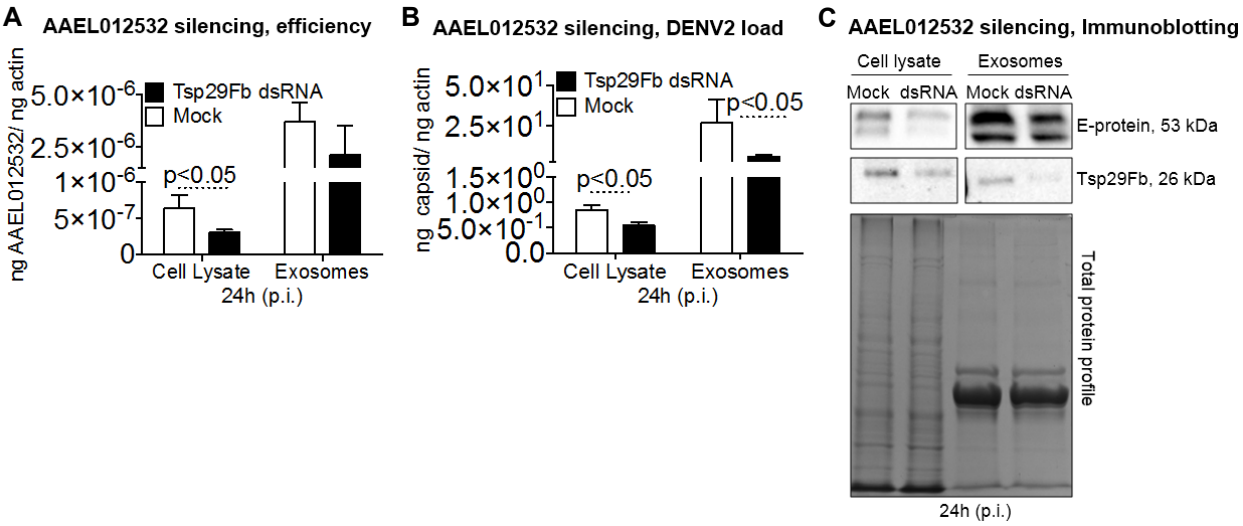

Figure 16. RNAi-Mediated Silencing or Antibody Blocking of Tsp29Fb or Treatment with GW4869 Inhibitor Affects DENV2 Burden in Mosquito Cells and EVs.

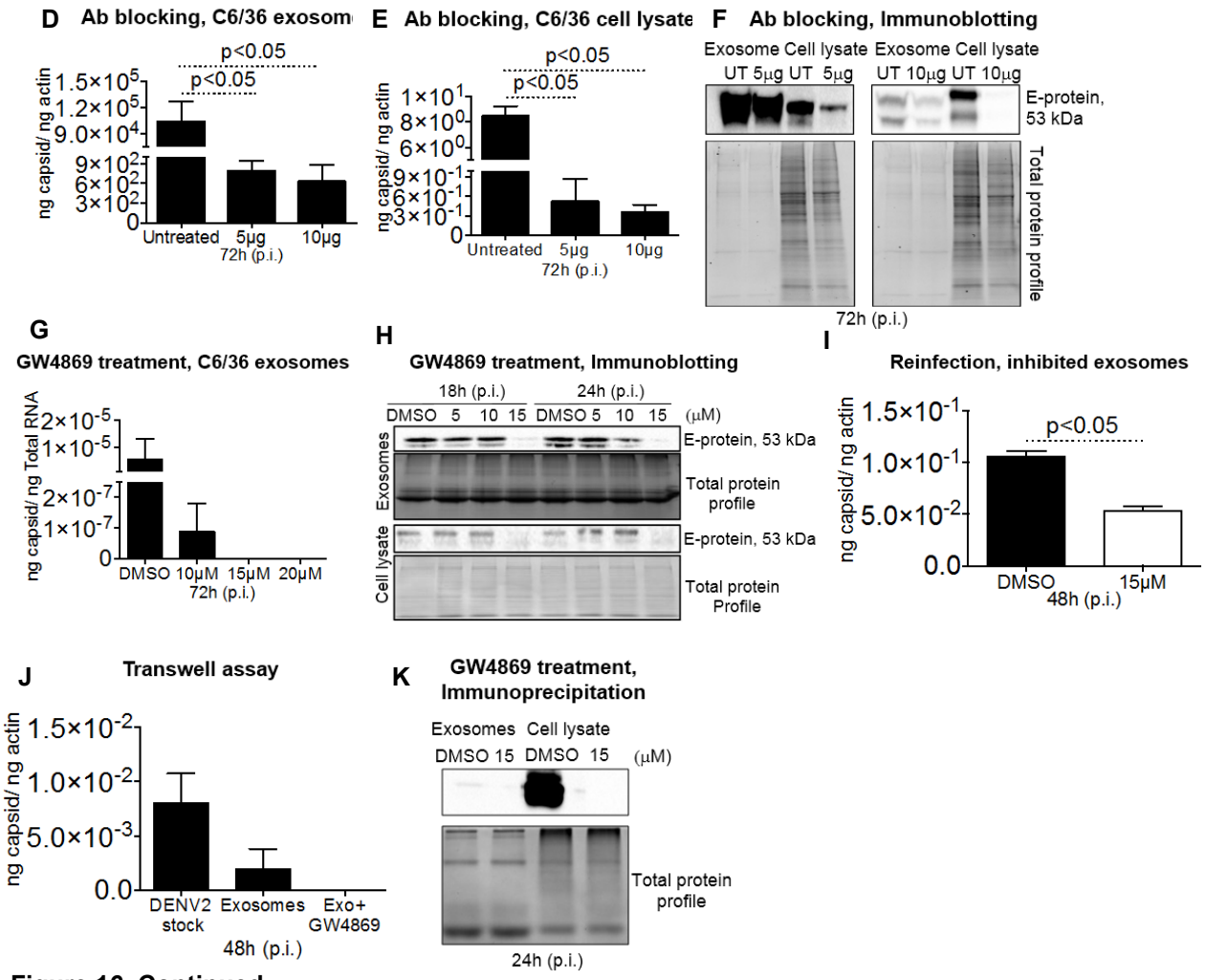

Figure 16. Continued.

(A) QRT-PCR analysis showing expression of *A. aegypti tsp29fb* to reveal silencing efficiency or,

(B) viral burden in whole-cell lysates or EVs derived from DENV2- infected (MOI 2, 24 hpi) Aag-2 cells treated with mock or Tsp29Fb dsRNA (n = 6).

(C) Immunoblotting analysis showing levels of *A. aegypti* Tsp29Fb or viral E-protein in whole-cell lysates or EVs derived from DENV2-infected (MOI 2, 24 hpi) Aag-2 cells treated with mock or *tsp29fb* dsRNA.

(D and E) QRT-PCR (n = 3) or,

(F) immunoblotting analysis showing viral burden in EVs or whole-cell lysates derived from DENV2-infected (MOI 5, 72 hpi) C6/36 cells treated with Tsp29Fb antibody at different doses (of 5 and 10µg). Untreated, infected (MOI 2, 72 hpi) C6/36 cells were used as controls in (D–F).

(G) QRT-PCR (n = 4) or,

(H) immunoblotting analysis showing viral burden in EVs or whole-cell lysates derived from DENV2-infected (MOI 2) C6/36 cells at 72 hpi or at 18 or 24 hpi. Samples in (H) were treated with GW4869 inhibitor at different doses (of 5–20 μM).

(I) QRT-PCR analysis showing viral burden in naïve C6/36 cells at 48 hpi, (reinfection) upon treatment with EVs derived from DMSO- or GW4869-treated DENV2-infected (MOI 2, 72 hpi) C6/36 cells (n = 4).

(J) QRT-PCR analysis showing viral load at 48 hpi in HUVEC cells in a transwell assay performed with C6/36 cells (in upper chamber) and naïve HUVEC cells (in lower chamber) treated with EVs derived from DENV2-infected (MOI 2, 72 hpi) C6/36 cells (25 μL, in upper chamber) in the presence or absence of GW4869. C6/36 cells infected with DENV2 laboratory stocks were used as control (n = 4). The p value determined by Student's two-tailed *t* test is shown.

(K) Immunoblotting analysis of Tsp29Fb IP proteins with 4G2 antibody and EVs or whole-cell lysates derived from DMSO- or GW4869-treated infected (MOI 2, 24 hpi) C6/36 cells. Tsp29Fb and DENV2 E-protein molecular mass is indicated in kilo Daltons. Coomassie-stained gel images showing total protein profiles in (C, F, H, and K) serve as a loading control for the respective immunoblots.

Table 1. Oligonucleotides Used for DENV, *tsp29fb, hsp70* and *actin*

Primers (5'-3')	**Purpose**
AATATGCTGAAACGCGAGAGAAACCGCG	Dengue 2, QPCR
CTCTTCAGTATCCCTGCTGTTGG	Dengue 2, QPCR
AATATGCTGAAACGCGTGAGAAACCGTG	Dengue 3, QPCR
CTAGCCAAGACTCCTGCTGTTGG	Dengue 3, QPCR
CCATGTACGTCGCCATCCA	Mosquito *actin*
GCGGTGGCCATTTCCTG	Mosquito *actin*
AGTTGTTAGTCTACGTGGACCGACA	Dengue 2, fragment 1 amplification
GAGTGGCAGGTTGTTTGGCT	Dengue 2, fragment 1 amplification
CAGGAGGAAGCTGGGTTGACA	Dengue 2, fragment 2 amplification
GTCCCGGCTCTACTCCTATGATGA	Dengue 2, fragment 2 amplification
GTCAACCCAATCGTAACAGAAAAAGA	Dengue 2, fragment 3 amplification
CTCCAGAGGGTGTGTGACTTTG	Dengue 2, fragment 3 amplification
CGATATGGGTTATTGGATAGAAAGTG	Dengue 2, fragment 4 amplification
GTTGGTTCTTGAAAGGGTTGTTAGA	Dengue 2, fragment 4 amplification
CCTCACAGCAGAAAGCGGA	Dengue 2, fragment 5 amplification
GACTATGGCCGGAAGGTATCTCT	Dengue 2, fragment 5 amplification
CAATCCAGAGATCGAAGATGACA	Dengue 2, fragment 6 amplification
GCCTTCAGCTGCCACTCTGT	Dengue 2, fragment 6 amplification
CAGAGCGTGAAAAGGTGGATG	Dengue 2, fragment 7 amplification
GAGCTGCTGTGAGAGTTATGGGGT	Dengue 2, fragment 7 amplification
GTTAATGGGTCTTGGGAAAGGA	Dengue 2, fragment 8 amplification
GGCTCCTCCATATTTCCTTTGTAGT	Dengue 2, fragment 8 amplification
CCCAATTTTGCATAAAGGTTCTCA	Dengue 2, fragment 9 amplification
CTTCTAGTGTGATTCTTGTGTCCCA	Dengue 2, fragment 9 amplification
CTTGAGTGGAGTGGAAGGAGAAG	Dengue 2, fragment 10 amplification
CCCAATCAATGAGCCGCA	Dengue 2, fragment 10 amplification
GGAACAGGGTGTGGATTCAAGA	Dengue 2, fragment 11 amplification
AGAACCTGTTGATTCAACAGCACCA	Dengue 2, fragment 11 amplification
GGACGAGAAGGACGGTGAGA	JN132154, *A. albopictus hsp70*, QPCR
GCACAGCGCGGTTGTCCT	JN132154, *A. albopictus hsp70*, QPCR
GACGGCGGCATTGGCA	XM_019672019, *A. albopictus hsp70*-like, QPCR
CCGCTCGGCATTGGTGA	XM_019672019, *A. albopictus hsp70*-like, QPCR
CGCCGGCCCACCTGAT	AAEL012532 QPCR and RNAi analysis
GAGTTCGGCGAACCATCTCCT	AAEL012532 QPCR and RNAi analysis
CGCCGGCCCACCTGCT	AALF02630 QPCR
GATATTAATCATAGCGGTGCTCTCCT	AALF02630 QPCR
CCAGATCTGACCGGAACGACCTCAACA	AAEL012532 dsRNA fragment cloning
CGGGTACCCATGGCGGTGCTTTCCTTGA	AAEL012532 dsRNA fragment cloning

DISCUSSION

This study has established that dengue virus is able to use extracellular vesicles as vehicles for transmitting itself from infected mosquito cells to various naïve recipient cells. Viruses other than DENV that are implicated in the use of EVs for transmission include the human immunodeficiency virus, hepatitis C virus and Langat virus (Ramakrishnaiah et al., 2013; Wiley and Gummuluru, 2006; Zhou et al., 2018). These evidences supported our hypothesis that dengue virus, which is a flavivirus with a positive-sense single stranded RNA genome might also be transmitted through similar mechanisms. The multiple pieces of evidence generated in this work are shown starting with Figure 3 & 5 that show *A. albopictus* cells (C6/36) can be infected with DENV2 & 3 and that EVs isolated using techniques described in Figure 4, also carry the viral RNA and protein at different time points post infection. Figure 7 further provides evidence that the entire DENV2 genome is present in the EVs derived from infected C6/36 cells. The genomic RNA of flaviviruses is single-stranded, ~11 kb in length and is infectious with positive polarity, encoding the viral proteins required for RNA replication (Apte-Sengupta et al., 2014; Gritsun et al., 2014). The abundant amount of E-protein and viral RNA in C6/36 EVs in comparison with the cell lysates suggests package of higher amounts of viral molecules for transmission to human and other vertebrate host cells. The dissemination of infectious EVs within mosquitoes from hemolymph to the salivary glands and subsequently to the mosquito saliva may efficiently facilitate the transmission of the infectious viral RNA and proteins to the vertebrate host through an infected mosquito bite during blood feeding. These data suggest that the full-length

genomes of other serotypes of DENVs and perhaps related flavivirus genomes are contained in arthropod EVs for transmission. In addition, a previous study from the Sultana lab has shown that the tick-borne Langat virus and mosquito-borne West Nile Virus (other members of *Flaviviridae*) RNA and proteins are also contained inside *Ixodes scapularis* tick or mouse neuronal cell derived exosomes and that exosome-mediated Langat virus and West Nile Virus transmission to recipient cells is through receptor-dependent endocytosis (Zhou et al., 2018). We hypothesize that the presence of DENV2/3 RNA and proteins inside EVs could facilitate the viruses to escape the host's antibodies, immune cells and defense response. This could allow enhanced fusion of EVs with naïve recipient cells through clathrin-dependent, receptor-mediated endocytosis for the establishment of infection.

In the multiple cryo-EM analyses (Figures 5 and 7), the presence of intact virions inside or outside the EVs was not detected. One of the reasons for this could be that all our analyses were performed 72 hpi. To make virus preparations, concentrated supernatants from longer times of infection (7–14 dpi) with higher titers (10^9 to 10^{12} PFU/mL) and centrifugal forces of 200,000 × g have been used (Fragnoud et al., 2015) that are not similar to the one used for our EV preparations (Figure 4). To avoid longer incubation days and peak of infection resulting in cell death, we performed all our experiments at 72 hpi. It is possible that longer times of infection (days 7–14 pi) may reveal intact mature viruses in EVs. Mosquito cell-derived EVs were found to have a wide ranging size distribution, varying from diameters of 30–150 nm (exosomes) and sizes of 150–350 nm (microvesicles). The quantification of EVs using the cryo-EM microscopy data suggested a smaller number of microvesicles in the DENV2-infected

group compared with the number of EVs from the uninfected group (Figure 6). In addition, the infected samples had an abundance of smaller EVs or exosomes of 0-100 nm size. The DG-EVs isolation showed the presence of HSP70, an EV-enriched/ marker protein confirming the presence of EVs. Detection of DENV2 E-protein in denser fractions, along with HSP70 shows that the EVs, with size ranges of 50–100 nm carry the highest amount of viral E-protein (Tauro et al., 2012).

Higher expression of HSP70 in infected samples could be due to the fact that EV marker presence has been correlated with a general increase in vesicle secretion, or rather with an increase in biomarker density on the surface of vesicles (Figure 5) (Chia et al., 2017; Rupert et al., 2017). The reference to the total protein concentration (determined by the BCA technique) each time has given us very reliable and consistent results with the routine isolation of EVs (Figure 6). Negligible differences in the viral loads in the 4G2 antibody-bead binding assay (Figure 8) suggests that E-protein is contained exclusively inside the EVs. If E-protein or viral particles were present outside the EVs as contaminants, the 4G2 antibody would bind E-protein, resulting in lower viral loads in comparison with the isotype antibody-treated or untreated controls. Treatment of DENV2 viral stocks with 4G2 antibody showed binding of surface-exposed E-protein, but not in the EV group, as E-protein was contained in the lumen of EVs and hence was unavailable to bind to the 4G2 antibody. RNase A-treatment assays were in agreement with the antibody-bead binding assay that further suggests no viral RNA was bound to the exterior of the EVs or was not present as a contaminant in our EV preps. If viral RNA was present in PBS suspensions containing EVs, we should expect an enhanced viral load in samples not treated with RNase A in comparison with the treated group.

These data are further supported by native-PAGE immunoblotting with 4G2 antibody and ELISAs that showed more intense signal in the Triton X-100 detergent–treated group in comparison with the untreated controls. Native-PAGE analysis indicated detection of either higher complexes of E-protein as dimer or oligomers or perhaps the presence of viral polyprotein (at higher molecular mass) under non-reducing conditions and in the native state. The observation of lower molecular mass of E-protein upon Triton X-100 treatment is possibly due to breakdown of the viral polyprotein.

Figure 9 and 10 firmly establish that EVs derived from infected mosquito cells infectious, confirming the observations in a recent publication from Dr. Sultana's laboratory (Zhou et al., 2018). Naïve recipient cells exposed to EVs in contrast with the EDS showed a much higher load of dengue indicating that the majority of the infectious agents are contained within the EVs at 72 hpi. These data show that mosquito derived infectious EVs are able to establish infection in cells that they would encounter during the early stages during an *in vivo* infection of a vertebrate host i.e. human skin keratinocytes, murine dendritic cells as well as human vascular endothelial cells. Perhaps the viruses quickly insert their genome through EVs in the early stages of the infection and then when it has enough copies, the viremia with detectable mature virions occurs at later stages.

To identify a molecular player facilitating receptor-mediated endocytosis of infectious EVs, we first looked at some EV markers. Starting with HSPs which include both constitutive and stress-inducible members that interact with native and denatured proteins to facilitate the proper folding of native proteins or refolding of the denatured proteins (Lancaster and Febbraio, 2005; Takeuchi et al., 2015). The presence of

mosquito HSP70s have been documented to increase during several environmental stresses, and several *hsp* genes are upregulated following a blood meal in mosquitoes (Benoit et al., 2010; Sanders et al., 2003). Upregulation of HSP70 homologs upon DENV2 infection suggested a protective role of this molecule during DENV2-induced stress. Figure 11 shows the presence of only one isoform (XM_019672019) of HSP70 in EVs suggesting its importance possibly in the chaperone activity inside EVs. The lack of any effect on DENV2 loads in EVs upon treatment with VER-155008 HSP70 inhibitor suggests that HSP70 is perhaps not required for DENV2 replication in cells and release into EVs. In addition, no differences in the DENV2 loads in naïve C6/36 cells upon treatment with infectious EVs derived from HSP70-inhibitor–treated and DENV2-infected C6/36 cells suggests that HSP70 may not be required for EV-mediated transmission of DENV2 RNA and proteins.

We then identified another EV associated protein, the transmembrane/ tetraspanin domain containing glycoprotein Tsp29Fb in *A. aegypti* mosquito cells and EVs derived from both *A. aegypti* (Aag-2) and *A. albopictus* cells (C6/36) (Figure 12). Figure 13 shows the up-regulation of Tsp29Fb upon DENV2 infection at both transcriptional and translational levels, *in vivo*, in cells and EVs confirmed the link between this molecule and DENV2 infection in mosquitoes. Identification and characterization of this arthropod EV-enriched marker provides information on a molecular determinant that facilitates transmission of DENV2 from vector to the vertebrate host. Furthermore, the direct interaction and association of Tsp29Fb with DENV2 E-protein suggests a potential role of this molecule in mediating DENV2 entry, replication and transmission via the mosquito endo-exosome pathway. The enriched

signal for E-protein in both IP assays could be because of the abundance of Tsp29Fb to bind with DENV2 E-protein in cells compared with the EVs.

Silencing of Tsp29Fb in Aag-2 cells showed a significant reduction in DENV2 cellular loads and significantly reduced export of the viral RNA and E-protein in EVs (Figure 16). Functionally blocking of Tsp29Fb clearly showed reduced DENV2 loads in both EVs and C6/36 cells. These data clearly showed the prominence of this arthropod molecule in mediating DENV2 replication, release, and transmission via EVs. The use of exosome release inhibitor GW4869 at lower tested doses of 10–20 μM further confirmed that DENV2 transmission is mediated via EV release. The exosome inhibitor treatment significantly reduced the DENV2 capsid mRNA and E-protein. In addition, blocking of EVs/ exosome release by GW4869 reduced the infectious viral RNA and protein transport, thereby dramatically blocking the transmission to human blood endothelial cells. The direct interaction of the viral E-protein with Tsp29Fb was also affected by treatment with GW4869, suggesting a role for this arthropod marker in the EVs/ exosome release pathway. It would be an interesting future avenue to investigate the mechanism of this viral inhibition through blocking the release of EVs from arthropod saliva. The finding that inhibition of EVs/ exosome release/ exocytosis upon GW4869 treatment in arthropod cells suggests the presence of neutral sphingomyelinase in mosquitoes.

Overall, this study suggests that inhibition of mosquito tetraspanin domain-containing glycoprotein Tsp29Fb or inhibition of EV/ exosome release through the GW4869 inhibitor treatment can both be potential therapeutics to block transmission of DENV2 and perhaps other mosquito-borne flaviviruses.

METHODS AND MATERIALS

Cell Culture and Infection of *In Vitro* Cell Lines

Aedes albopictus (C6/36 cells) and *Aedes aegypti* (Aag-2) cell lines were grown in either MEM medium or in Schneider's insect medium with 10% FBS, respectively. Vero and HaCaT cells were grown in complete DMEM medium containing 10% heat-inactivated FBS. Mouse monocyte-derived dendritic cells isolated from bone marrows of C57BL/6 wild-type mice were plated in RPMI medium containing 10% FBS and 10 ng/mL of GM-CSF (Peprotech). Four days later, cells were re-plated in the same medium for experiments. HUVEC cells were grown in human lung MVEC medium (M199 medium; SIGMA, containing 150 mg ECGF- bovine brain extract and 20% FBS) and as per the instructions from Dr. Catravas laboratory. All culture medium and required supplements were purchased from Invitrogen/ThermoScientific Inc.

To determine infection, 1 x 10^5 of C6/36 or Vero or mouse-DCs or HaCaT/HUVEC cells were seeded in 12-well plates, infected with Multiplicity Of Infection (MOI 5) of DENV2 (TVP2176 provided by Dr John Anderson and New Guinea C strain) or DENV3 (DENV-3/US/BID-V1619/2005). Cells were collected at different time points (24, 48, 72 and 96 hpi) and processed for RNA extraction. Briefly, for re-infection experiments with EV fractions containing infectious DENV2 RNA and proteins, 1 x 10^5 C6/36 cells or HaCaT/HUVEC cells or mouse dendritic cells were co-incubated with 25 µL of mosquito cell-derived EV fractions (that corresponds to 126 µg of total EV protein as estimated by Bradford assay). We used 625 µL (same ratio) of EV depleted supernatant (EDS) fraction from C6/36 cells (collected from the step before PBS

washes during EV isolation, See Figure 4B). For re-infection studies, mosquito or mammalian cells (infected via EVs or EDS fractions collected from 72 hpi. DENV2-infected C6/36 cells) were collected at 72 hpi, and processed for RNA extractions. The IBC number for the all the cell culture performed for this study is 15-014.

Cryo-Electron Microscopy

Purified concentrated suspensions of EVs in PBS were vitrified on carbon holey film grids (R2x2 Quantifoil®; Micro Tools GmbH, Jena, Germany; or C-flat™, Protochips, Raleigh, North Carolina) and as previously described (Sherman et al., 2006, 2009). EVs were applied to the holey films in a volume of ca. 3 µl, blotted with filter paper, and plunged into liquid ethane cooled in a liquid nitrogen bath. We used computerized Vitrobot plunger (FEI, Hillsboro, OR) for freezing. Frozen grids were stored under liquid Nitrogen and transferred to a cryo-specimen holder (70 deg. 626, Gatan, Inc., Pleasanton, CA, or 2550 Cryo-Tomography holder, E.A. Fischione Instruments, Inc., Export, PA) under liquid Nitrogen before loading into a JEOL 2200FS, or a JEOL 2100 electron microscopes (JEOL Ltd., 3-1-2 Musashino, Akishima, Tokyo 196-8558, Japan). JEOL 2200FS was equipped with in-column energy filter (omega type) and a field emission gun (FEG); JEOL 2100 had a LaB_6 filament, both were operating at 200 keV. Grids were maintained at near-liquid Nitrogen temperature (-172 to -180°C) during imaging. Preliminary screening and imaging of EVs was done using a 4k x 4k Gatan US4000 CCD camera (Gatan, Inc., Pleasanton, CA), and final imaging was done at indicated 40,000x magnification with a 5k x 4k Direct Electron Detector Camera (DE-20, Direct Electron, Inc., San Diego, CA) using a low-dose imaging

procedure. An in-column omega electron energy filter was used during imaging with a zero-loss electron energy peak selected with a 20 eV slit. Images were acquired with a ca. 20 electrons/Å^2 dose; the pixel size corresponded to 1.5 Å on the specimen scale. We used a 2.0 – 2.3 µm defocus range for imaging. Individual EV images were acquired from three independent isolated batches. For quantitation of EV size ranges, we manually analyzed the sizes using scale bar from cryo-EM images and counted EVs of different sizes per image in each group. Three independent estimations and counts were performed without any bias. Percentages (for size determination) were calculated based on the total number of EVs in each size range.

OptiPrep^{TM} Density Gradient EV (DG- EVs) Isolation

2 x 10^8 or 1 x 10^9 of C6/36 cells were infected with either 2 or 5 MOI of DENV2, respectively or were maintained as uninfected controls. The detailed protocol is shown in Figure 4A or described in (Zhou et al., 2018). Supernatants (20 mL) from uninfected/infected cells were collected and centrifuged at 4°C (480 x g followed by 2000 x g for 10 min each to remove cell debris and dead cells). Cell culture supernatants were (either filtered through 0.22 µm and then) concentrated to 2 mL using the Corning Spin-X UF concentrators or centrifugal filter device with a 5 k nominal molecular weight limit (NMWL). 15 mL volume of discontinuous gradient of 40% (w/v), 20% (w/v), 10% (w/v) and 5% (w/v) solutions of iodixanol was prepared from the stock solution of OptiPrep^{TM} 60% (w/v) of aqueous iodixanol (Axis-Shield PoC, Norway) with 0.25 M Sucrose/10 mM Tris, pH 7.5. Polycarbonate bottles were loaded with discontinuous gradient of iodixanol (4 mL each of 40% (w/v), 20% (w/v), 10% (w/v) and

3 mL of 5% (w/v) from bottom to top). Concentrated cell culture supernatants (1-2 mL) were overlaid onto the top of the gradient, and centrifuged at 100,000 x g for 18 h at 4°C. Either 6 or 12 (12 in case of 0.22 µm filtered group) individual uninfected or infected fractions of ~2.6 mL or 1.3 mL (filtered) were collected (from top to bottom) manually (with increasing density of iodixanol) and diluted with 5 mL of sterile PBS. Fractions were centrifuged at 100,000 x g for 3 h at 4°C, followed by another PBS wash and spin at similar centrifugal forces. DG-EVs fractions were resuspended in 100 µL of PBS and stored at -80°C until further analysis. For cryo-EM images obtained from different fractions, EVs were isolated from DENV2-infected (MOI 5, 72 hpi) C6/36 cells (2×10^9) and samples were immediately shipped on dry ice to imaging facility. Similar processing methods were used to collect images from each fraction.

Isolation of EVs from Cell Culture Supernatants

EVs were also isolated by differential ultracentrifugation method (Tauro et al., 2012; Théry et al., 2006; Zhou et al., 2018). EVs isolation procedure and modifications are schematically shown in Figure 4B and respective figure legend. Briefly, 2×10^6 C6/36 or 1×10^6 Aag-2 cells were seeded for EVs isolation in respective medium for overnight. Next day, cells were changed to respective medium containing bovine exosome-free FBS (Systems Biosciences Inc; SBI). After 4-5 hour of medium replacement, cells were infected with DENV2 (MOI 5). Cell culture supernatants were spun as shown in Figure 4B. Increased centrifugation times and rotor types are shown to improve EVs yield and purity (Cvjetkovic et al., 2014) and, hence were used for isolation of EVs from mosquito cells. Supernatants were spun at 100,000 x g, for 155

min. Supernatants collected after this spin served as EVs depleted supernatant (EDS) fractions (used as controls in our study and indicated with asterisk in Figure 4B). The pellet containing EVs and any contaminants were washed with ice-cold PBS and spin at 100,000 x g, for another 155 min. Resulting EVs pellet is referred as EVs fraction in this study. Freshly prepared EVs pellets were resuspended in PBS and stored frozen at -80°C for subsequent evaluations and assays or were directly resuspended in RNA lysis buffer (Bio-Rad) or modified RIPA buffer (G-Biosciences, BioExpress) for total RNA or protein extractions, or were immediately used in RNaseA and Triton-X-100 treatment studies, respectively. We also isolated EVs from mosquito cells using the commercial total EVs isolation reagent and extracted total RNA and proteins using total EVs RNA and Protein Isolation kit (Invitrogen/ThermoScientific Inc.) and as per the manufacturer's instructions.

PCR-Amplification of Full Length DENV2 Genome

The cDNA generated from total RNA isolated from C6/36 cell derived EVs was used as template for the amplification of DENV2 genome. The oligonucleotides used for the amplification are shown in Table 1. We amplified fragments 1-10 of variable sizes by regular PCR and fragment 11 (3' end) by touchdown PCR. Regular PCR was performed with the following conditions: Initial denaturation at 95 ºC for 4 min followed by 40 cycles of steps including 95 ºC for 10s, 58ºC for 20s, and 72ºC for 1min. Fragments 1-10, amplified products of following sizes 1102 bp, 1110 bp, 1124 bp, 1114 bp, 1118 bp, 1141 bp, 1104 bp, 1135 bp, 1110 bp and 1048 bp, respectively (Figure 7A). The fragment 11 amplified a product of 717 bp by touchdown PCR, performed with method

as described (Korbie and Mattick, 2008) . The PCR reactions were later run on 1% agarose gels, imaged using the Chemidoc MP imaging system, and processed using Image Lab software obtained from the manufacturer (Bio-Rad).

RNA Extraction, cDNA Synthesis, and qRT-PCR Analysis

RNA from mosquito - C6/36 cells and Aag-2 cells, mouse monocyte-derived dendritic cells, HaCaT cells, Vero and HUVEC cells infected with various MOI of DENV2 or uninfected controls at indicated time-points pi, was extracted using Aurum Total RNA Mini kit (Bio-Rad) and following manufacturer's instructions. RNA was converted to cDNA using the Bio-Rad iScript cDNA synthesis kit. The generated cDNA was used as template for the amplification and determination of the viral burden. For detection of DENV2 RNA, published forward and reverse primers for dengue virus (Serotype 2) were used (Sultana et al., 2009). For DENV3 RNA detection, we used specific primers designed for Serotype 3, shown in Table 1. To normalize the amount of templates, either mosquito or mouse or human *beta actin* amplicon were quantified with published primers (Sultana et al., 2010, 2012). Primers for *beta-actin* were used in parallel for qRT-PCR normalization. Equal amounts of mosquito or mouse or human cDNA samples were used in parallel for beta *actin* and DENV2 capsid gene.

The ratio of DENV2 capsid gene copy/*beta actin* gene copy was used as an index to determine the rate of infection in each analyzed sample. In some experiments, with undetectable amounts of *actin* in EVs samples, we normalized to the total RNA loads. QRT-PCR was performed using iQ-SYBR Green Supermix (Bio-Rad, USA). Standard curves were prepared using 10-fold serial dilutions starting from standard 1 to

6 of known quantities of *actin* or DENV2 capsid gene fragments and qRT-PCR reactions were performed as described (Sultana et al., 2009, 2010, 2012). Primer sequences for all mosquito genes (including both *hsp70* isoforms, *tsp29Fb* and *actin*) used in this study are provided in Table 1. For RNase A treatment, we isolated fresh EVs from either uninfected or DENV2-infected C6/36 cells (2 x 10^6), distributed the infected EVs as treated (5 µg/mL RNase A, 37°C for 15 min) or untreated groups. For laboratory virus stocks (generated by collecting cell culture supernatants from 14 days post infection C6/36 cells and held as frozen stocks), similar treatments with RNase A were performed on DENV2 (5 MOI). Naïve C6/36 cells (2 x 10^5) were infected (72 hpi) and either treated or untreated DENV2-infected EVs samples (25 µL) were processed for RNA extraction and qRT-PCR analysis. Untreated EV samples from uninfected group served as internal controls.

Protein Estimation and Immunoblotting

2 x 10^6 of C6/36 or Aag-2 cells was seeded in six well dishes/plates for overnight. Next day, we changed the media containing bovine EVs free FBS (Systems BioSciences Inc.; SBI). After 4-6 hours of media replacement, cells were infected with DENV2/DENV3 (MOI 5). For EVs quantitation assay, C6/36 cells were plated in six well plates at densities of 10^4, 10^5, 10^6, 10^7, and 10^8 and followed by infection with DENV2 (MOI 5, 72 hpi). Uninfected cells plated with similar densities were used as controls for estimation of total number of EVs. Cell culture supernatants were collected (at 72 hpi) and processed for EV isolation. EV fractions were collected after PBS wash and the adherent cells collected from the same plates (washed twice with 1 x PBS), were all

resuspended in modified RIPA buffer. Total protein amounts were estimated using Bradford assay (BCA kit from Pierce/ThermoScientific Inc.) as three replicates. Total cell and EV lysates (30 µg) were separated on 12% or 4-20% SDS-PAGE gradient stain-free gels (Bio-Rad or NuSep; BioExpress) or processed for Coomassie blue staining. Followed by gel electrophoresis, blots were blocked in either 5% milk buffer or BSA and probed with either highly cross-reactive 4G2 monoclonal antibody (obtained from Dr. Michel Ledizet, L2 Diagnostics or Millipore, Sigma) to detect DENV2 or DENV3 E-protein (obtained from BEI resources) or human CD63 (Santa Cruz Biotechnology, Inc.) or human HSP70 (Cell Signaling Technologies, Inc. or Bio-Rad) or monoclonal anti-DENV2 NS1 (Abcam) antibodies or actin monoclonal antibody (Abcam), followed by mouse or rabbit monoclonal HRP-conjugated secondary antibodies (Santa Cruz Technologies, Inc.), respectively. Total protein profiles were images obtained from either stain free gels, Coomassie stained gels, or Ponceau S stained blots that served as loading controls. Antibody binding was detected with WesternBright ECL kit (Advansta, BioExpress/VWR). Blots were imaged using Chemidoc MP imaging system and processed using Image Lab software obtained from the manufacturer (Bio-Rad).

E-Protein-Antibody-Beads Binding Assays

Freshly isolated EVs from 2 x 10^6 C6/36 cells (infected with MOI 5) were seeded on plates for overnight incubation, changed to exosome-free FBS medium after 4h, followed by infection with DENV2 for 72 hpi. EVs collected were resuspended in PBS and grouped into three categories as; untreated, treated with 4G2 antibody (that recognizes DENV2 E-protein) or relevant isotype control antibody (R & D Systems)

groups. In a similar way, we used DENV2 laboratory virus stocks (with known titers; 5 MOI, suspended in MEM complete growth medium from C6/36 cells), also grouped as three categories (untreated, 4G2 or isotype antibodies treated, respectively). EVs fractions or DENV2 laboratory virus stocks were incubated for 1 h. (RT) with respective antibodies followed by incubation (4°C) with protein A/G agarose beads (Pierce/ ThermoScientific, Inc.) for another 30 min. The antibody-bead complexes were spun (13k rpm) at 4 °C for 30 min and supernatants were collected and lysed in RNA lysis buffer, processed for RNA extractions, followed by cDNA synthesis and qRT-PCR to analyze the DENV2 loads from either EVs samples or DENV2 laboratory viral stocks.

Native-Poly Acrylamide Gel Electrophoresis (PAGE)

For this analysis, we seeded C6/36 cells (2 x 10^6) in complete MEM medium for overnight incubation, then replaced with exosome-free FBS medium followed by infection with DENV2 (MOI 5) for 72 hpi. Cell culture supernatants were processed for isolation of EVs (Figure 4B) and resuspended in PBS. EVs were separated as three groups (from the same preparations); group that was either held as untreated on ice, or group treated with Triton-X-100 (0.1%; 30 min, RT) or group treated with three cycles of freezing at -80°C (for 1 h.) followed by thawing at 4 °C. After treatments, protein lysates were prepared for non-reducing and non-denaturing sample conditions (62.5 mM Tris-HCL, pH 6.8, 25% Glycerol and 1% Bromophenol blue) that maintained the proteins secondary structures and native charge density. Gels were pre-run for 60 min in gel running buffer (25 mM Tris and 192 mM Glycine). Uninfected or DENV2-infected EVs preparations with treatments or untreated samples were separated on 12% Native-

PAGE gel, transferred on to nitrocellulose membrane, probed with 4G2 antibody followed by mouse monoclonal HRP-conjugated secondary antibody. Total protein profiles (Ponceau S stained image) served as loading control. WesternBright ECL kit (Advansta, BioExpress) detected antibody binding and blots were scanned using Chemidoc MP imaging system as described for immunoblotting analysis.

Measurement of Relative Fluorescence

C6/36 cell-derived EVs (derived from 2 x 10^6 cells infected with DENV2 MOI 5; 72 hpi) were resuspended in PBS (250 µL/sample). EVs were plated as five replicates of 50 µL each that corresponds to 254 µg of total EVs protein, as estimated by BCA method. EVs fractions held in PBS were either treated with 0.1% of Triton-X-100 for 30 min or kept untreated. Samples were incubated with 4G2 monoclonal antibody (1:500 dilution) for 1 h, followed by three times washes with PBS and secondary Alexa-Fluor 594 mouse monoclonal secondary (1:2500 dilution) for 1 hour at RT. Relative fluorescence was measured using a Fluorimeter (Tecan, USA) with excitation at 590 nm and emission at 617 nm.

Enzyme Linked Immunosorbent Assay

Freshly isolated mosquito cell-derived EVs (from 2 x 10^6 of DENV2-infected MOI 5; 72 hpi cells) resuspended in PBS (250 µL/sample) were either treated with 0.1% of Triton-X-100 for 30 min or kept untreated. Nunc grade ELISA plates were coated with 50 µL (that corresponds to 254 µg of total EVs protein as estimated by BCA method) of untreated or Triton-X-100 treated- uninfected or infected samples for overnight at 4 °C.

Samples were blocked with BSA and incubated with 4G2 antibody for 1 h, followed by HRP-conjugated mouse monoclonal secondary antibody for another 1 h for detection (Sultana et al., 2009). SureBlue TMB Microwell Peroxidase substrate and Stop solution (KPL) were used following manufacturer's instructions. After stopping the reactions with TMB Stop solution, using a Multimode infinite M200 Pro Microplate reader (Tecan) optical density was measured from triplicate samples in two independent experiments and absorbance at 450 nm was recorded.

Viral Immunofluorescence Assay

Dilution assays were performed as described in (Schoepp and Beaty, 1984). Briefly, C6/36 cells were seeded (at a density of 1 x 10^5 cells/well in 225 µL of MEM complete medium) into 96 well plates. Cells were incubated overnight and treated with either EVs fractions (20 µL; that corresponds to 101 µg of total EVs protein as estimated by the BCA method) or EVs depleted supernatant fractions (EDS; 675 µL) for 24 hours. Each of the group had six different dilutions (1-6) and at least 7-10 independent replicates in addition to the uninfected negative controls. Data is shown from dilution 1 or 10 fold dilution (Figure 9A, 10A) or from dilution 3 or 1000 fold dilution (shown as Figure 9A). Cells were fixed with acetone-PBS mixture (3:1, for 20 min at -20º C) and plates were air dried, washed with 1 x PBS and blocked with 5% FBS-PBS-0.05% Sodium Azide for 15 min at RT. E-protein was detected by incubation with 4G2 antibody (for overnight at 4º C), followed by three washes with PBS. Samples were incubated with Alexa-594 labeled mouse secondary antibody for 1 hour at RT, followed by washes (3X) with PBS. Plates were analyzed using EVOS fluorescence system (Invitrogen or

ThermoScientific, Inc.) and cells were scored for fluorescence or the presence or absence of infection in comparison to the infected positive controls or uninfected negative controls. Representative images from dilutions 10^{-1} and 10^{-3} are shown.

Plaque Formation Assays

Plaque assays were performed as described in (Sultana et al., 2009). EVs and EDS, were tested for infectious dose and capability of DENV2 viral RNA replication and formation of infectious plaques. Briefly, we seeded Vero cells in 6-well plates at densities of 2 x 10^6 cells per well, allowed them to adhere and grow as monolayers reaching 65-85% confluence (for ~24h.). EVs fractions containing unknown PFU (plaque forming units) of DENV2 viral genomes collected from C6/36 cells (5 x 10^6 cells; resuspended in 100 µL of PBS; 30 µL of this suspension) were used for plaque assays. EVs free supernatants (600 µL) corresponding to similar amounts of EVs fractions were used as controls. Serial dilutions (1:10, 1:100 and 1:1000) of the EVs or EDS fractions were prepared in duplicate (from two independent experiments). Medium was removed 4 hpi, and warm 2% Seaplaque agarose (Lonza) overlay with complete MEM media (1:1 ratio) containing antibiotic and anti-mycotic solution (1% each; Sigma) was added. Plates were incubated for 6-7 days, at 37°C, 5% CO_2. Plaques were stained with 0.03% Neutral Red (Sigma) for 4 h, and were counted on the same day or otherwise incubated (inverted and covered in foil) for overnight, and then plaques were counted to determine the viral titers during next day.

Immunoprecipitation Assays

Mosquito whole cell and EVs fractions were collected (either in RIPA modified protein lysis buffer containing protease and phosphatase inhibitors; SIGMA or in cold 1 x PBS) from uninfected and DENV2 infected (MOI 5) cells (2 x 10^8 cells, 72 hpi). Before immunoprecipitation, lysates in RIPA buffer or samples resuspended in PBS were precleared with protein A/G agarose beads (Pierce/ ThermoScientific, Inc.) at a 1:10 volume of 50% bead slurry and centrifuged at 12,000 rpm at 4ºC for 10 min. Supernatants were collected and protein concentrations were determined using the Bradford assay (BCA kit; Pierce/ ThermoScientific, Inc.). Samples were aliquoted as input (20 µg shown in total protein profile as controls) or used for immunoprecipitation (150-500 µg of lysates suspended in RIPA buffer or 500 µg of PBS suspended samples). Lysates/PBS suspended samples were incubated with 5 µg of highly cross-reactive human CD63 antibody (Santa Cruz Biotechnology, Inc.) that recognizes the Tsp29Fb for overnight at 4ºC, followed by incubation with protein A/G agarose beads for 4 h to complex with antibody. Samples were washed thrice with cold 1 x PBS and beads were resuspended in 40 µL of SDS sample Laemmeli buffer, boiled and loaded on 12% SDS-PAGE gels. Immuno-precipitates were further processed for immunoblotting (as described above) using the 4G2 antibody or actin monoclonal antibody (as control) to detect DENV2 E-protein or actin precipitation with Tsp29Fb.

Immunofluorescence and Microscopy

1 x 10^5 C6/36 cells were plated on 18 mm coverslips in complete MEM medium and allowed to adhere for overnight. Cells were infected with DENV2 (MOI 2) for 72 hpi.

Uninfected and infected cells were fixed with 3.7% (wt. /vol.) paraformaldehyde (37ºC for 20 min), permeabilized with 0.2% (vol. / vol.) Triton X-100 (10 min at room temperature), and blocked with 3% bovine serum albumin (30 min at RT) in PBS, respectively. Cells were immuno-stained with antibodies directed against human CD63 (that detect Tsp29Fb), or 4G2 (that detect DENV2 E-protein), and detected by anti-rabbit (human CD63) or mouse (4G2) secondary antibodies conjugated with Alexa Fluor 488 or 594, respectively. Cells were counterstained for nuclei with DAPI and were detected below 300 nm wavelengths. Alexa Fluor conjugates and DAPI (obtained from Invitrogen/ ThermoScientific, Inc.). Images were obtained using the EVOS Fluorescence System (Invitrogen/ ThermoScientific, Inc.). Representative images are shown for co-association between Tsp29Fb and DENV2 E-protein.

RNAi, dsRNA Synthesis and Transfections

A. aegypti Mosquito cDNA was used as template to amplify the DNA encoding a fragment of *Aedes tsp29Fb* (Accession Number AAEL012532). Gene specific primers containing the BglII and KpnI restriction enzyme sites used in the PCRs are shown in Table 1. The amplified *Aedes tsp29Fb* fragment was purified by gel extraction (Using Qiagen kit) and cloned into the BglII and KpnI sites of the L4440 double T7 Script II vector (Sultana et al., 2010). *Escherichia coli* DH5alpha strain was used as a cloning host. Using the MEGAscript RNAi kit (Applied Biosystems/ ThermoScientific) and user manual instructions, we synthesized the dsRNA complementary to the *Aedes tsp29Fb* sequence. For dsRNA transfections and silencing of Tsp29Fb, we plated 1 x 10^6 of Aag-2 cells in complete medium (Schneider medium with 10% FBS and L-glutamine),

allowed to adhere overnight, and used Lipofectamine transfections reagent (Invitrogen/ ThermoScientific). 750 ng of dsRNA mixed with Lipofectamine reagent was added on to cells and 6 hours post addition, 2x complete medium was added and plates were further incubated for additional 16 h. Cells were infected with DENV2 (MOI 2) and collected at 24 hpi for further analysis. Silencing efficiency of *tsp29Fb* was analyzed by qRT-PCR and primers used are shown in Table 1.

Inhibition Studies

For inhibition of HSP70, we used the commercially available inhibitor VER-155008 (obtained from SIGMA-Aldrich), a small molecule ATP-derivative inhibitor of HSP70 (Lancaster and Febbraio, 2005; Takeuchi et al., 2015b). First we examined the cytotoxic effects of the VER-155008 inhibitor and found no changes at the tested doses of 10 and 20 μM, in comparison to the untreated group. C6/36 cells (2×10^6) were plated in 6 well plates and treated with VER-155008 inhibitor for 4 h. (at tested doses of 10 and 20 μM) and followed by DENV2-infection (5 MOI) for 72 hpi. DMSO vehicle was used as mock control as VER-155008 was dissolved in DMSO. Cell supernatants were collected and processed for EVs isolation. Both cells and EVs were processed for RNA extractions followed by qRT-PCR to detect *hsp70* expression or DENV2 loads. For re-infection studies, we used EVs derived from VER-155008 inhibitor treated (for 4 h), followed by DENV2-infected (MOI 5, 72 hpi) C6/36 cells. EDS fractions (used in similar dilution to the use of suspended EVs per reaction) collected during EVs isolation (after pelleting of EVs) served as control. Fresh C6/36 cells were incubated (re-infection) with

either EVs (derived from VER-155008 treated and DENV2 infected C6/36 cells) or EDS fractions as controls.

For EVs inhibition studies, we used either the highly cross-reactive human CD63 antibody or GW4869, a cell permeable and selective commercial inhibitor for Neutral Sphingomyelinase (N-SMase) (Santa Cruz Biotechnologies, Inc.) dissolved in DMSO. For the inhibitor and antibody studies, EVs were isolated using the isolation reagent (Invitrogen/ThermoScientific, Inc.). For antibody functional blocking studies, we treated C6/36 cells (2×10^5) for 2 h with either 5 or 10 µg of CD63 antibody, followed by DENV2 infection (2 MOI) for 72 hpi. The untreated cells were used as controls. Cytotoxicity of the inhibitor was first analyzed and cells did not show any toxicity at tested doses (1-20 µM). For the inhibitor studies, C6/36 cells (2×10^5) were plated in complete MEM medium for overnight, changed to exosome-free FBS medium for 4 h and then treated with the GW4869 inhibitor (with doses of 5, 10 15 or 20 µM) for another 4 h, followed by DENV2 infection (2 MOI) for 72 hpi (in case of qRT-PCR analysis) or for 18 or 24 hpi, for immunoblotting analysis. Cells were treated with similar volume of DMSO as control groups. For infection kinetics using incubations with infectious EVs, HaCaT cells (2×10^5) were treated with DENV2-infected (2 MOI; 72 hpi) and 15 µM of inhibitor treated 2×10^5 of C6/36 cell-derived EVs and respective DMSO vehicle. Viral loads were determined from HaCaT cells at 48 hpi by qRT-PCR analysis. For immunoprecipitation assay, 1×10^7 of C6/36 cells were plated in regular complete MEM medium for overnight, changed with exosome-free FBS medium for 4 h., treated with 15 µM inhibitor or respective volume of DMSO as control, followed by infection with DENV2 (5 MOI) for 24 hpi. Cell culture supernatants were processed for EVs isolation and whole cells and

EVs lysates (500 µg) were processed for immunoprecipitation with human CD63 antibody, followed by immunoblotting with 4G2 antibody to detect viral E-protein.

Transwell Assays

Transwell assays were performed to analyze the migration of infectious EVs released from infected C6/36 cells (seeded in inserts; upper chamber) to uninfected/ naïve HUVEC cells seeded in 12-well plates (lower chamber). Sterile, polycarbonate tissue culture-treated transwell inserts (12 mm insert size) with 0.4 µm microporous membrane pore size were used in our assays (Corning/VWR). We plated, 2 x 10^5 C6/36 cells in inserts (upper chamber) and 2 x 10^5 HUVEC cells in 12-well plates (lower chamber). Inserts with C6/36 cells were first kept in a separate 12-well plate containing 0.5 mL (in order to keep microporous membranes moist/wet) of MEM medium. Inhibitor-treated group in transwell assays was treated with 20 µM of GW4869 inhibitor, and at 24 h post treatment, C6/36 cells were either infected with EVs containing DENV2 (25 µL of the EVs fraction, that corresponds to 126 µg of total EVs protein as estimated by BCA method, collected from independent batch of DENV2 (MOI 5; 72 hpi) infected C6/36 cells) or with DENV2 from laboratory viral stocks (MOI 5) prepared from infected C6/36 cell (14 days pi) culture supernatants. The laboratory viral stocks with known titers were included as internal controls. Twenty-four hours post-infection, inserts with C6/36 cells (with change of new media) were moved to 12-well plates containing uninfected or naïve HUVEC cells. EVs containing viral RNA and proteins produced from C6/36 cells were allowed to transmigrate and infect HUVEC cells (that were kept uninfected/naïve). After, 48 h post-incubation (with infected C6/36 cells released EVs from inserts/upper

chambers) HUVEC cells from lower chamber were washed twice with ice-cold PBS and collected for RNA extractions, cDNA synthesis, and qRT-PCR to determine viral loads from HUVEC cells.

Statistics

Statistical significance of difference observed in data sets was analyzed using GraphPad Prism6 software and Microsoft Excel. The non-paired, two-tailed Student *t* test was performed (for data to compare two means) for the entire analysis. Error bars represent mean (+SD) values, p values of < 0.05 were considered significant in all analysis. Statistical test and p values are indicated for significance.

IXODES SCAPULARIS HSP70 IS RESPONSIBLE FOR VARIABLE FIBRINOGENOLYSIS IN RESPONSE TO FEEDING ON HOSTS WITH DIFFERENT IMMUNE STATUS

INTRODUCTION

Ixodes scapularis ticks are hard-bodied, obligate hematophagous arthropods. These ectoparasites during the process of taking a blood meal can transmit many pathogens to the host (Anderson and Magnarelli, 2008). Understanding molecular interactions at the tick-host interface involve knowledge of the participation of host defense mechanisms against tick infestations and counter measures employed by ticks (Wikel, 2013). Tick feeding, egg production and viability affecting vector competence can be influenced and modulated by the acquired resistance by the host through both humoral and cellular immuno-regulatory pathways (Brossard and Wikel, 2004). Ticks have many strategies for successfully avoiding the host response too. It involves the suppression of the host's antibody production, complement activation and cytokine production from both antigen-presenting cells and T cells (Brossard and Wikel, 2004; Francischetti et al., 2009; Hovius et al., 2008). *Ixodes scapularis* ticks have been known to transmit pathogens like *Borrelia burgdorferi*, *Anaplasma phagocytophilum*, *Babesia microti*, *Ehrlichia muris*-like agent, Powassan virus and *B. miyamotoi*. The cause Lyme disease, human anaplasmosis, babesiosis, human ehrlichiosis, encephalitis and relapsing fever respectively (Anderson and Armstrong, 2012; Anderson and Magnarelli, 2008; Krause et al., 2014; Pritt et al., 2011).

To establish a successful feeding niche, commence blood feeding and engorgement to repletion, *I. scapularis* ticks secrete a range of molecules through their

saliva responsible for anti-hemostatic, anti-inflammatory, immunosuppressive and immune-modulators against the host's immunity pathways (Brossard and Wikel, 2004; Hovius et al., 2008; Ribeiro and Francischetti, 2003; Wikel, 2013). Tick-borne pathogens exploit these molecules present in tick saliva to enhance their ability to transmit themselves and infect vertebrate hosts (Jones et al., 1989; Kročová et al., 2003; Labuda et al., 1993). Many studies have explored the role of pathogens in the modulation of tick gene expression (Neelakanta et al., 2010; Pal et al., 2004; Sultana et al., 2010). However, the influence of different genetic or immune backgrounds of the vertebrate hosts on tick biology and behavior during acquisition of a blood meal has not yet been fully evaluated. Previous studies have reported significant variations in many basic hematological and coagulation factors among many mouse strain backgrounds (Emeis et al., 2007; Peters et al., 2002). It also been recently shown that T-cells participate in coupling coagulation with inflammation implicating a direct role of host immune status with coagulation (Green et al., 2015). These studies provide a strong rationale to test whether different genetic or immune status of hosts influence feeding and gene expression in *Ixodes scapularis* ticks. The results presented in this study report that the host's genetic background and/ or immune status does influence specific tick gene expression that subsequently impact variable fibrinogenolysis during feeding though the involvement of a tick HSP70-like molecule.

RESULTS

Engorgement Weights Are Greater in Ticks Fed on Immunodeficient vs Immunocompetent Mice

The first analysis was to determine if the immune status of hosts influence tick engorgement weights. Two sets of age and background matched immunocompetent (C57BL/6J and BALB/c) or immunodeficient ($RAG^{-/-}$ and SCID) mice with independent housing conditions were ordered from two different vendors. These mice were infested with uninfected *I. scapularis* larvae. After repletion, the engorgement weights of individual larvae were measured using an analytical balance. The post-feeding weight of larvae that fed on immunodeficient mice (0.499 ± 0.06 mg for $RAG^{-/-}$; 0.517 ± 0.05 mg for SCID) was significantly ($P < 0.05$) higher in comparison to the larvae that fed on immunocompetent (0.479 ± 0.06 mg for C57BL/6J; 0.467 ± 0.06 mg for BALB/c) mice (Figure 17A & B).

Presence of a Host Fibrin Degradation Product- D-Dimer Was Reduced in Ticks Fed on Immunodeficient Mice

During feeding, ticks may acquire host proteins like fibrinogen and its degradation products along with the vertebrate blood (Villar et al., 2016). Hence, we decided to check for the presence of D-dimer, which is a degradation product of fibrin (Cesarman-Maus and Hajjar, 2005), in the lysates of whole ticks fed on immunodeficient vs. immunocompetent animals. The total protein profile of ticks that were fed on either group of mice did not show any significant difference (Figure 18A & B). Immunoblotting

showed negligible presence of D-dimer in the whole tick lysates obtained from ticks fed on immunodeficient mice in comparison to the respective control groups of ticks fed on immunocompetent animals (Figure 18C & D, respectively). Densitometry of the same immunoblots show that the difference in D-dimer presence is statistically significant ($P < 0.05$) (Figure 18E & F). An independent experiment shown in Figure 19A-19C corroborated this data. Immunoblotting assays performed with purified D-dimer protein along with total lysates from ticks fed on immunocompetent mice validated that the observed band at size ~ 200 kDa in these samples is D-dimer which was found to be negligible in total lysates prepared from ticks fed on immunodeficient animals (Figure 18G & H, and Figure 20A & B). Densitometry was performed as a graphical representation of the immunoblot analysis (Figure 18C and 19C). Taken together, these results show that there is a significant decrease in fibrinogen degradation at the bite site when ticks feed on immunodeficient animals.

Salivary Gland Lysates Prepared from Ticks Fed on Immunodeficient Animals Show Reduced Fibrinogenolytic Activity *In Vitro*

Next we tested whether salivary gland lysates prepared from nymphal ticks fed on immunodeficient animals show a decrease in fibrinogenolytic activity *in vitro* in comparison to salivary gland lysates prepared from nymphs that fed on immunocompetent animals. Immunocompetent and immunodeficient mice were infested with nymphs. The nymphs were collected upon repletion and were processed for salivary gland isolation. Purified fibrinogen was incubated with the salivary gland lysates over time. The sample when subjected to PAGE showed a reduction in the degradation

of Aα chain of fibrinogen in the presence of $CaCl_2$ at 2 and 4 hours post-incubation vs. the salivary gland lysates prepared from nymphs fed on immunocompetent animals (Figure 21A & B). Densitometry was performed to graphically represent this observation (Figure 21C & D). The salivary gland lysates prepared from nymphs fed on immunocompetent mice showed increased degradation of Aα chain of fibrinogen in the presence of $CaCl_2$ even at shorter incubation times of 15 and 30 min in vs. salivary gland lysates from nymphs fed on immunodeficient mice as shown in Figure 22. The degradation of fibrinogen Aα chain (in all cases) was abrogated in the presence of EDTA. Increased fibrinogenolytic activity was observed with the salivary gland lysates prepared from ticks fed on BALB/c mice even upon exposure to EDTA (Figure 21F & H). $CaCl_2$ or EDTA did not result in any degradation of fibrinogen as seen in Figure 23. The salivary gland lysates used in the fibrinogenolysis assay by themselves did not show any prominent bands that coincided with the size of the fibrinogen (Figure 21).

The Expression of the Tested Metalloprotease Genes Did Not Show Any Alteration in Ticks That Fed on Immunocompetent Mice vs Immunodeficient Mice

A tick metalloprotease belonging to reprolysin family containing pre- and pro-enzyme domains, zinc-binding motif and cysteine-rich region from salivary glands of *I. scapularis* has been suggested to participate in fibrinogenolytic activities (Francischetti et al., 2003). Therefore, we analyzed expression of four tick metalloproteases (GenBank acc. nos. XM_002416249, XM_002416250 and XM_002412196) along with the salivary gland metalloprotease (GenBank acc. no. AY264367) that was previously suggested to participate in fibrinogenolysis (Francischetti et al., 2003). QRT-PCR analysis revealed

that the expression of the tested metalloproteases did not show significant ($p > 0.05$) difference in expression between ticks that were fed on immunocompetent or immunodeficient animals (Figure 24A-D).

LC-MS/MS Based Identification of Proteins Showing Differential Expression in the Salivary Glands of Ticks Fed on Immunocompetent vs Immunodeficient Mice

A 1-D PAGE with the salivary gland lysates prepared from ticks fed on immunocompetent or immunodeficient animals was performed (Figure 25A). A band showing increased intensity at ~ 100 kDa in the salivary glands of ticks fed on C57BL/6J mice was chosen for further analysis (Figure 25A and Figure 26A & B). Similar results were obtained for the ~ 100 kDa band in the salivary gland lysates prepared from ticks fed on BALB/c mice in comparison to salivary gland lysates prepared from ticks fed on SCID mice (Figure 26C and D). Since the ~ 100 kDa band was upregulated in both sets of immunocompetent mice, this band was excised from the C57BL/6J fed tick samples and subjected to LC-MS/MS analysis. The result revealed higher peptide matches for tick HSP70-like proteins (Table 2, Figure 27A & B). The LC-MS/MS experimental procedures were performed by our collaborator Dr. Sucharita Dutta.

One Isoform of the Tick HSP70-Like Molecules is Upregulated in Nymphs Fed on Immunocompetent Animals vs Immunodeficient Animals

QRT-PCR analysis was performed with the samples generated from whole larvae fed on C57BL/6J or $RAG^{-/-}$ mice for all six tick HSP70-like isoforms that were identified in LC-MS/ MS analysis (Table 2). The mRNA levels for five of the HSP70-like

genes (GenBank Acc. Nos. XM_002433611, XM_002407088, XM_002406516, XM_002415881, and XM_002402518) were found to be unchanged in larvae fed on either group of mice (Figure 25B-F). However, one of the HSP70-like molecules (GenBank Acc. No. XM_002412155) was found to be significantly ($P < 0.05$) upregulated in ticks fed on immunocompetent mice in comparison to ticks fed on immunodeficient mice (Figure 25G). Alignment of the amino acid sequences of all HSP70-like molecules analyzed in this study using ClustalW program revealed a high degree of conservation across the entire sequence (Figure 28). The tick HSP70-like molecule (XM_002412200) corresponding to the nucleotide sequence (GenBank acc. no. XM_002412155) shares approximately 82, 47, 72, 81, 59% identity respectively with other tick HSP70-like molecules (GenBank acc. nos. XP-002406560, XP_002402562, XP_002407132, XP_002415926, XP_002433656) analyzed in this study (Figure 28). Mr. Vikas Taank (graduate student with Dr. Neelakanta) performed the qRT-PCR analysis for the HSP70- like tick genes, published in Vora et al., 2017. Taken together, the results from LC-MS/MS and qRT-PCR analysis provide important insights on the novel role for the participation of specific tick HSP70-like molecule in fibrinogenolysis during blood feeding.

Treatment of Salivary Gland Lysates with VER-155008 (HSP70 inhibitor) or with Anti-HSP70 Antibody Resulted in Reduced Fibrinogenolytic Activity

To validate whether HSP70-like molecules in ticks participate in fibrinogenolysis, salivary gland lysates prepared from ticks fed on C57BL/6J were incubated with VER-155008 or with mock (DMSO). Salivary gland lysates treated with HSP70 inhibitor

showed reduced Aα chain degradation in comparison to the mock-treated lysates (Figure 29A & B). Similar assays were performed with salivary gland lysates prepared from ticks fed on C57BL/6J in the presence of anti-HSP70 antibody vs. isotype-matched antibody (Figure 29C). Salivary gland lysates treated with anti-HSP70 antibody showed reduced Aα chain degradation in comparison to the isotype-treated controls at 15 and 30 min incubations (Figure 29C & D). Collectively, these results support a novel role for the participation of tick HSP70-like molecule in variable fibrinogenolysis during blood feeding on hosts with different immune backgrounds.

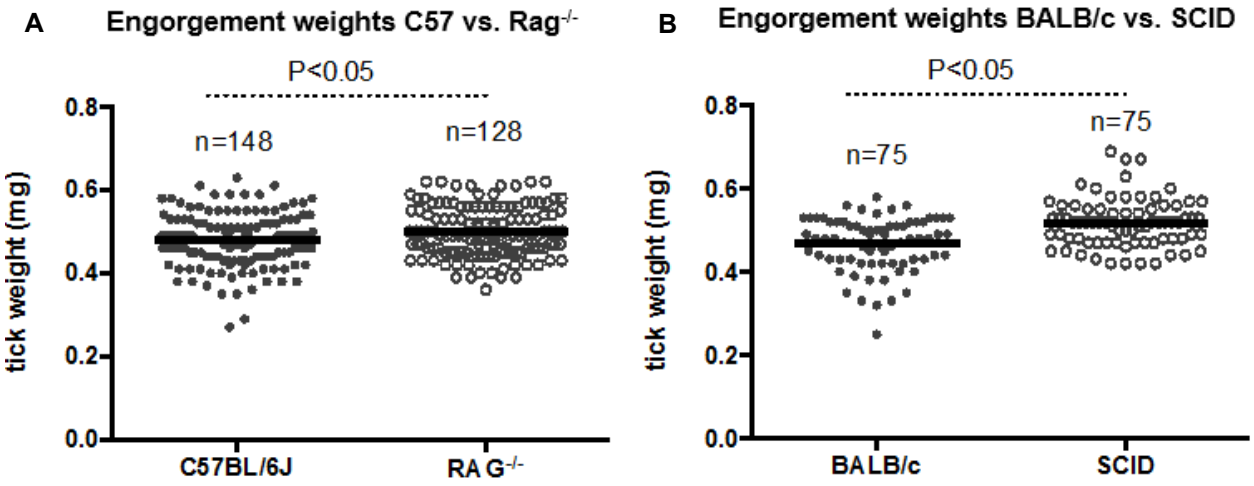

Figure 17. Engorgement Weights of Ticks Increase upon Feeding on Immunodeficient Animals

(A and B) Uninfected, unfed larvae were fed on gender and age matched immunocompetent mice (C57BL/6J, BALB/c) or immunodeficient (RAG$^{-/-}$, SCID) mice. Data from C57BL/6J and RAG$^{-/-}$ and

BALB/c and SCID NCr mice is shown. In both sets, the weights are greater in ticks fed on immunodeficient mice vs. immunocompetent. Each circle represents one individual tick.

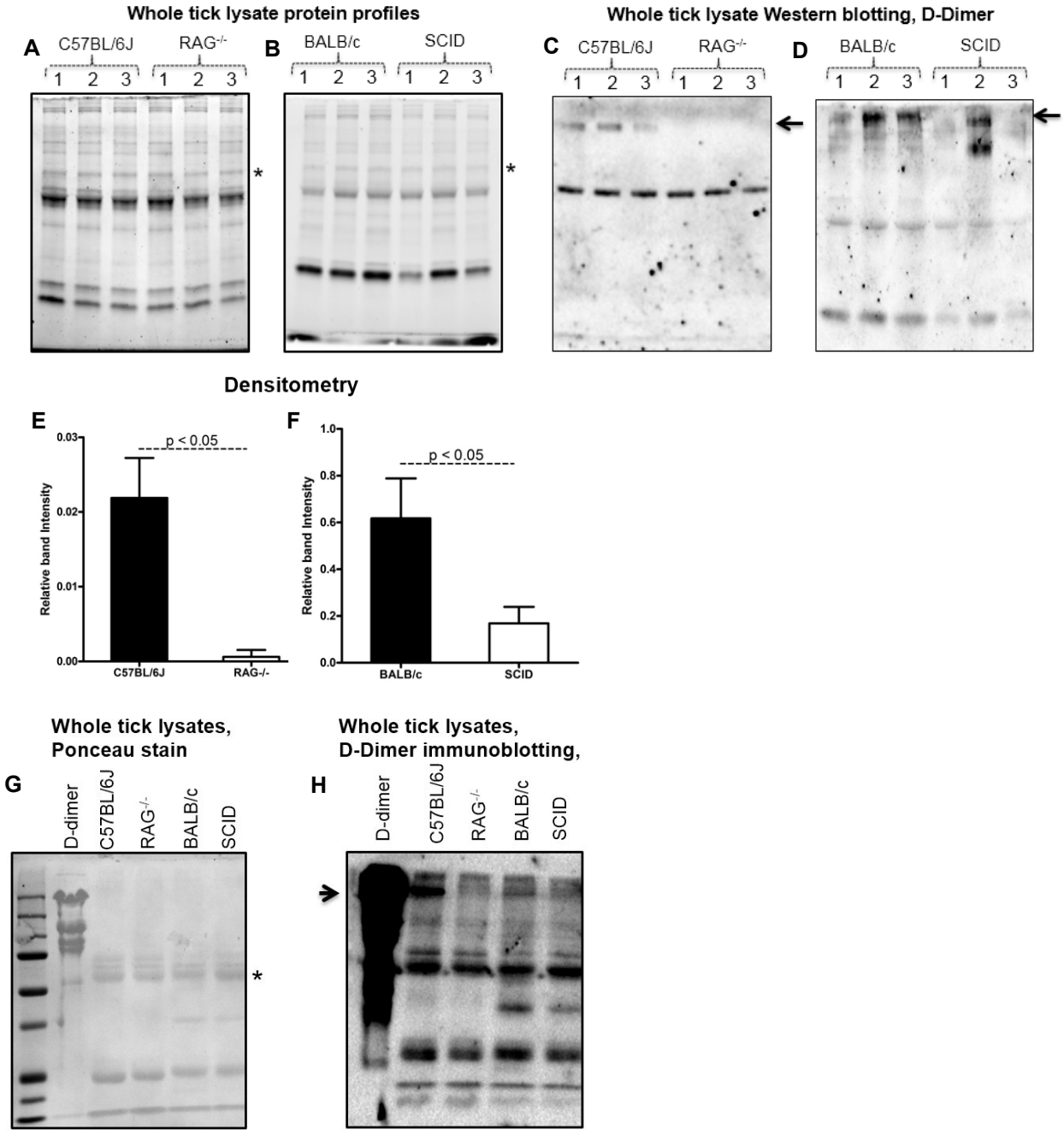

Figure 18. Fibrin Degradation Product (D-dimer) Was Reduced in Ticks Fed on Immunodeficient Animals

(A and B)The total protein profile from ticks fed on individual mice (3 mice/group) is shown.

(C and D) Immunoblotting performed with larval total lysates and anti-D-dimer antibody showed negligible or reduced D-dimer in ticks fed on immunodeficient animals vs. immunocompetent groups.

(E and F) Densitometry analysis showing presence of D-dimer in C57BL/6J, RAG$^{-/-}$ samples and BALB/c, SCID samples relative to the respective bands seen in (A) and (B) (marked with asterisk).

(G) Ponceau S stained membrane image showing D-dimer along with tick total lysates.

(H) Immunoblotting assays with anti-D-dimer antibody show the presence of D-dimer in lysates prepared from ticks fed on immunocompetent animals at the same position (~ 200 kDa) as native D-dimer protein. Arrow next to the immunoblots (C, D & H) indicates position of D-dimer.

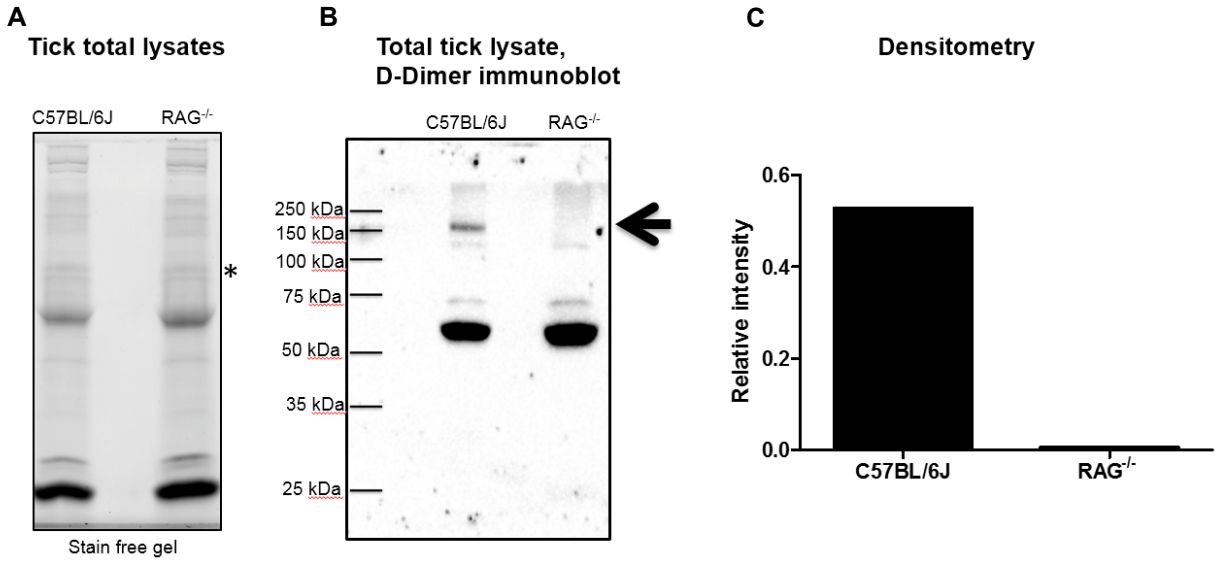

Figure 19. Independent Experiment Showing Presence of D-Dimer in Ticks Fed on Immunocompetent Animals

(A) 3-5 larvae fed on C57BL/6J or RAG$^{-/-}$ were pooled and total lysates were prepared. Total protein profile of the two samples are shown.

(B) Immunoblotting performed with tick total lysates and anti-D-dimer antibody showed significantly reduced level of D-dimer in ticks fed on immunodeficient animals in comparison to ticks fed on immunocompetent animals.

(C) Densitometry for the immunoblot shown in (B). D-dimer presence was calculated relative to the respective bands seen in (A) marked with asterisk.

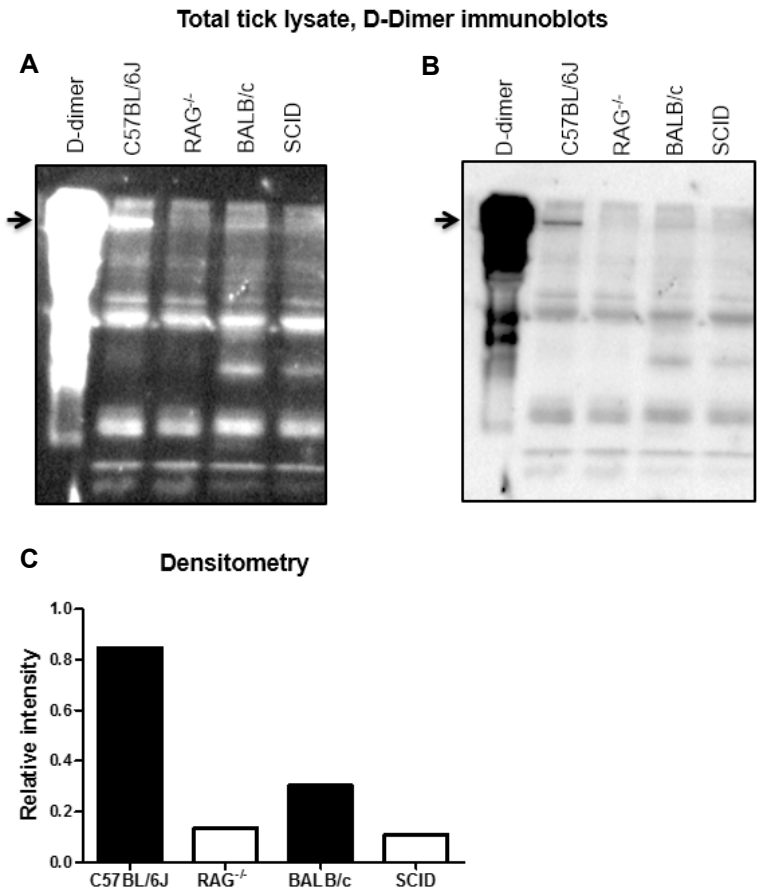

Figure 20. The Amount of D-Dimer is Reduced in Ticks Fed on Immunodeficient Animals

(A) Inverted image or,

(B) low intensity image for data in Figure 18H is shown. Immunoblotting with anti-D-dimer antibody showed presence of D-dimer in lysates prepared from ticks fed on immunocompetent animals (C57BL/6J, BALB/c) at the same position (~ 200 kDa) as native D-dimer protein. The arrow indicates position of D-dimer.

(C) Densitometry analysis for the immunoblot in B showing the level of D-dimer in ticks fed on immunocompetent or immunodeficient mice. The level of D-dimer for each sample was measured relative to the control band indicated with an asterisk in Figure 18G.

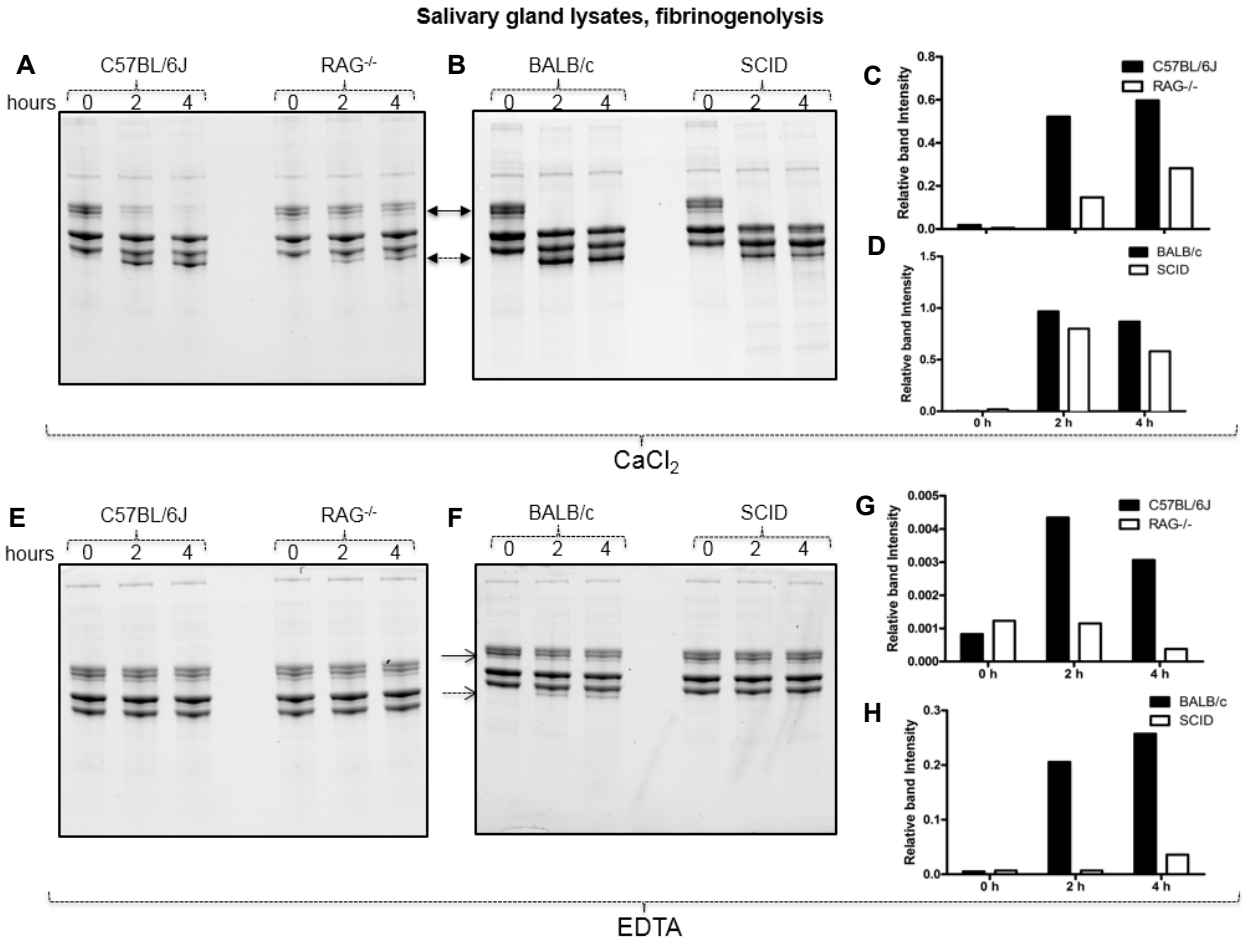

Figure 21. Salivary Gland Lysates Prepared from Ticks Fed on Immunodeficient Animals Show Reduced *In Vitro* Fibrinogenolytic Activity

(A and B) Purified fibrinogen was incubated with the salivary gland lysates for the indicated times (in hours) in the presence of 1 mM $CaCl_2$ where there is increased fibrinogenolysis with time in immunocompetent samples vs. immunodeficient. Solid arrow indicates Aα chain of fibrinogen and dotted line indicates degradation product.

(C and D) show densitometry of bands observed in (A and B).

(E and F) Reactions incubated with 1 mM EDTA do not show any fibrinogenolysis or show abrogated fibrinogenolysis.

(G and H) show densitometry of bands observed in (E and F).

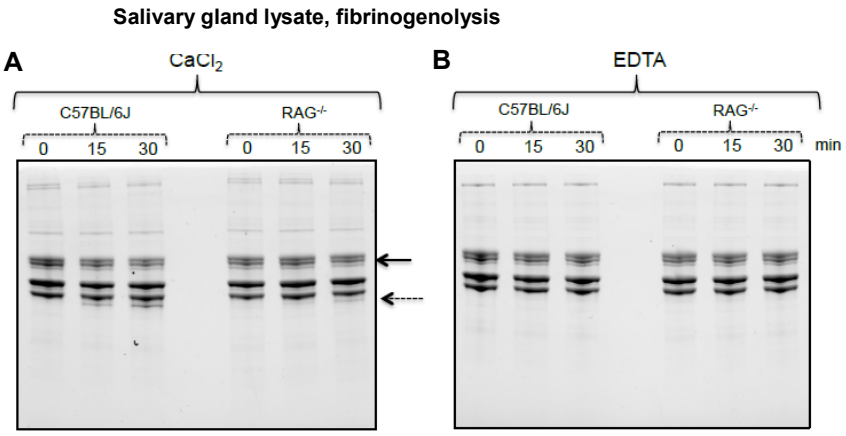

Figure 22. Salivary Gland Lysates Prepared From Ticks Fed on Immunocompetent Animals Show Increased Fibrinogenolytic Activity Even at Early Time Points

(A) Purified fibrinogen was incubated with tick salivary gland lysates for the indicated times (in minutes) in the presence of 1 mM $CaCl_2$ or,

(B) 1 mM EDTA showing similar results as Figure 21.

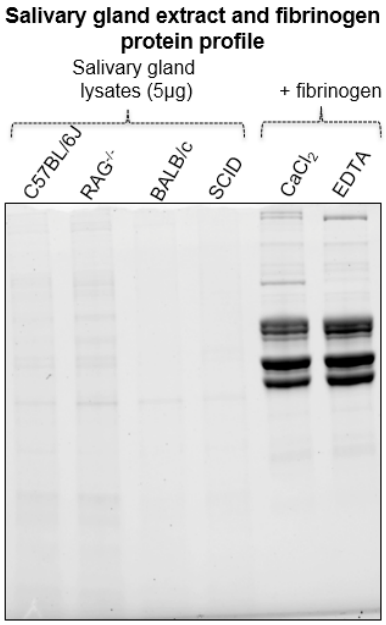

Figure 23. Treatment of $CaCl_2$ or EDTA Alone Had No effect on Fibrinogen Degradation

SDS-PAGE analysis of salivary gland lysates prepared from ticks fed on immunocompetent or immunodeficient mice showed no prominent fibrinogen degradation products. Incubation of fibrinogen with $CaCl_2$ or EDTA alone had no effect on fibrinogen degradation.

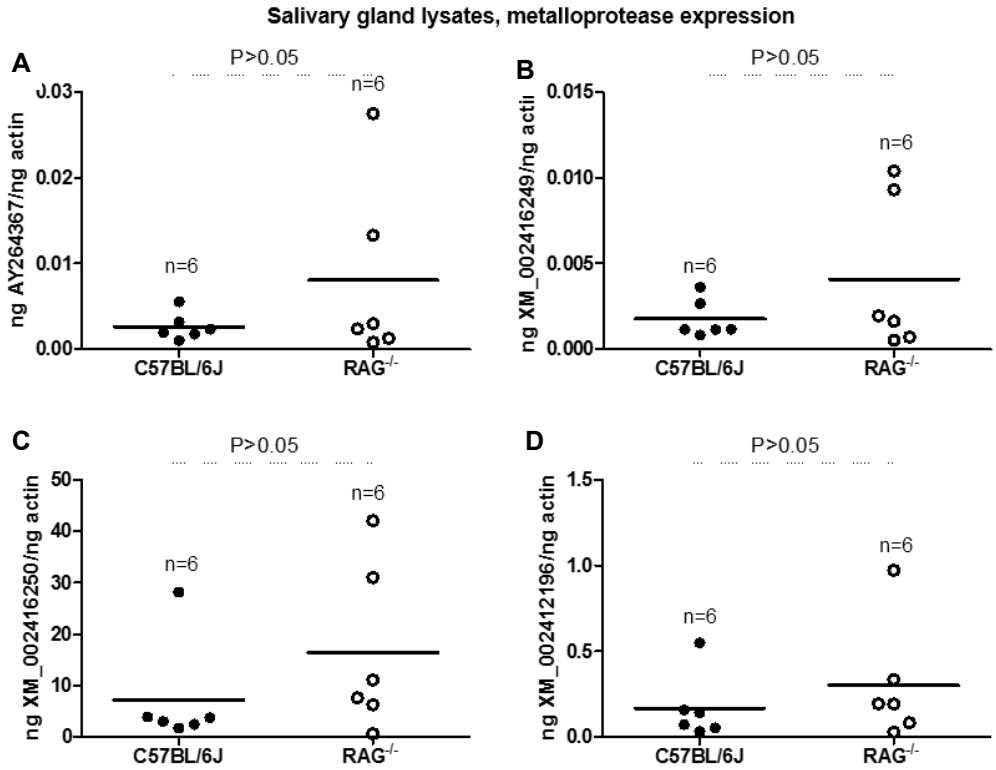

Figure 24. Expression of Metalloproteases is Unaltered in Ticks upon Feeding on Immunocompetent or Immunodeficient Animals

(A, B, C and D) QRT-PCR results showing levels of four arthropod metalloproteases, GenBank acc. nos. AY264367 (A), XM_002416249 (B), XM-002416250 (C) and XM_002412196 (D), transcripts in ticks fed on immunocompetent (C57BL/6J) or immunodeficient ($RAG^{-/-}$) animals. The mRNA levels for metalloproteases are normalized to tick *beta-actin*. Each circle represents one tick.

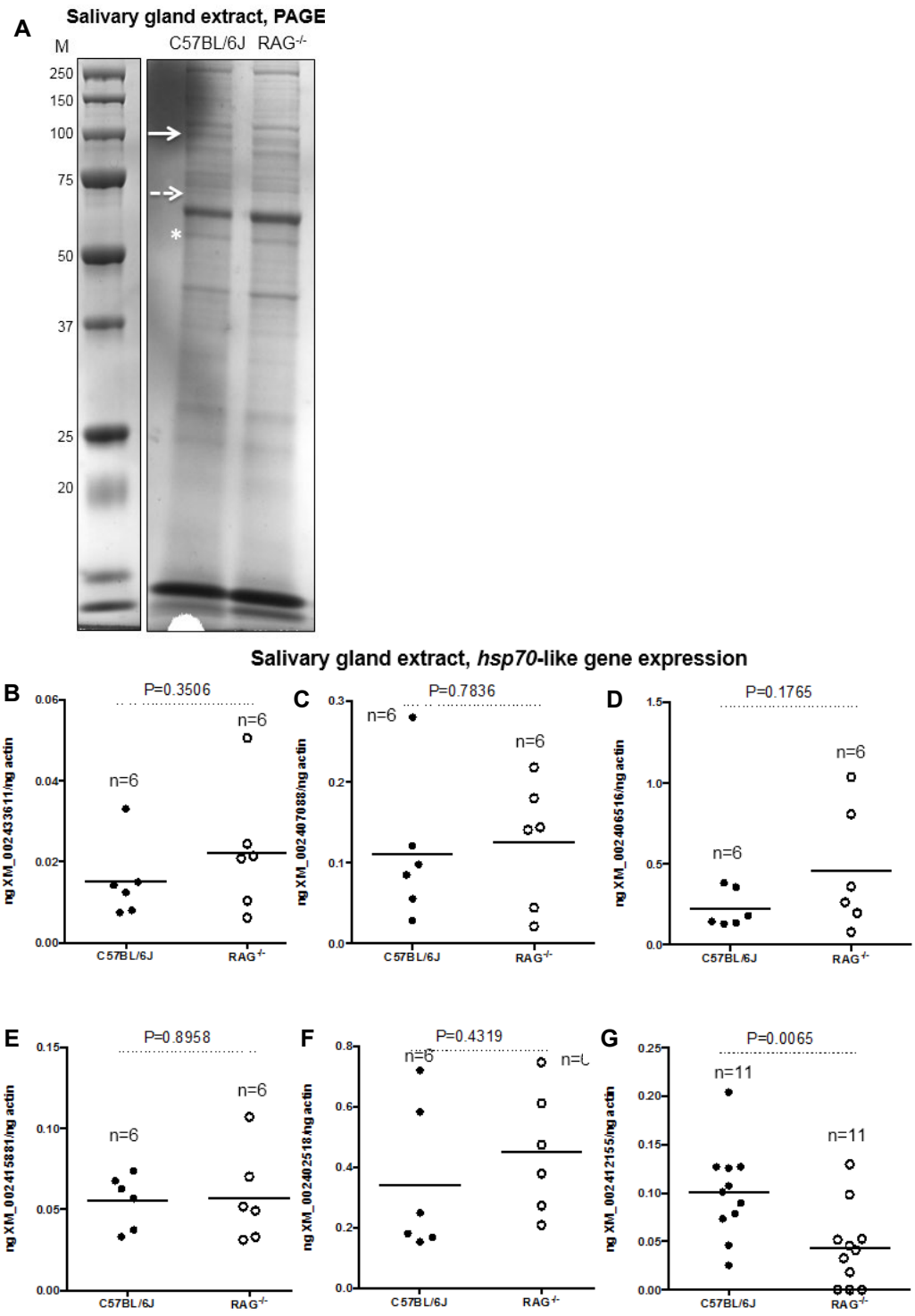

Figure 25. Transcripts of Arthropod HSP70-Like Proteins are Downregulated in Immunodeficient Animals

(A) 1-D SDS-PAGE profile in salivary glands of ticks fed on C57BL/6 J or RAG$^{-/-}$ mice is shown. Solid arrow indicates around 100 kDa band (that was excised and processed by LC-MS/MS analysis) and

dotted arrow indicates another band around 73 kDa that were found to be upregulated in salivary gland lysates prepared from ticks fed on immunocompetent mice.

(B, C, D, E, F and G) QRT-PCR results showing levels of XM_002433611 (B), XM_002407088 (C), XM_002406516 (D), XM_002415881 (E), XM_002402518 (F) and XM_002412155 (G) transcripts in ticks fed on immunocompetent or immunodeficient mice.

(G) Transcript XM_00241255 was undetectable or had very low threshold levels in some of the ticks that were fed on immunodeficient animals.

Each circle represents one tick. Student's *t* test p values are shown. Mr. Vikas Taank performed the qRT-PCR analysis for this figure.

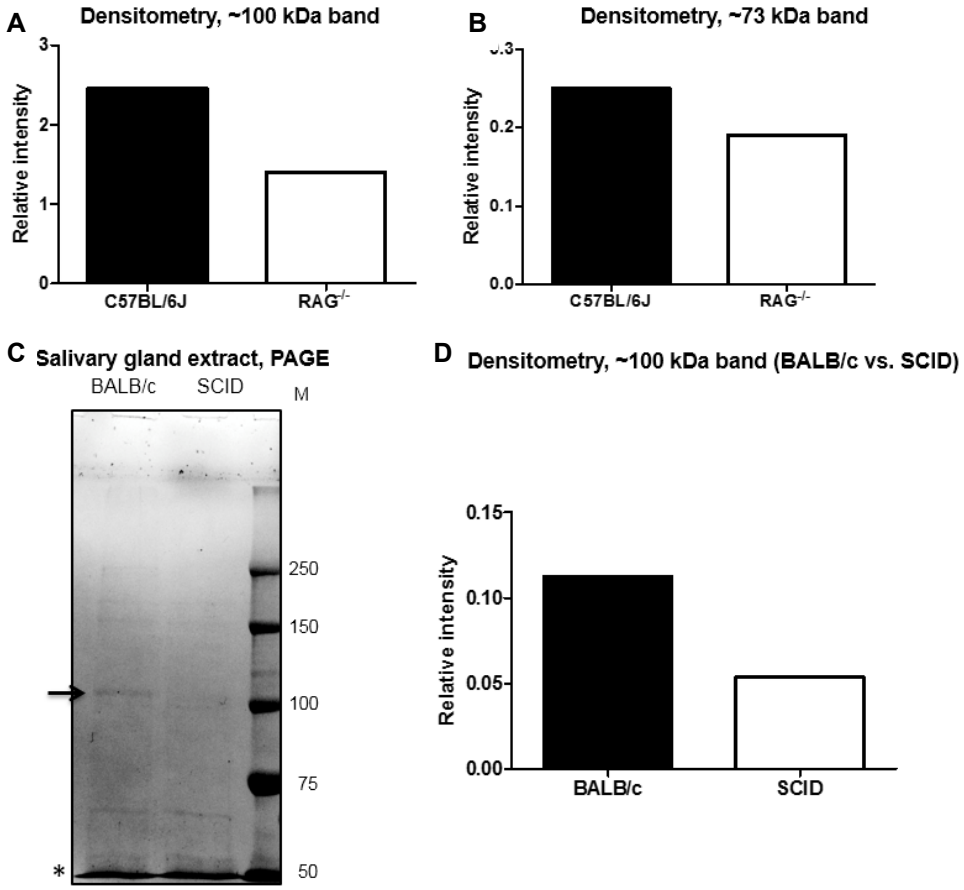

Figure 26. SDS-PAGE Analysis of Total Protein Profiles in Ticks Fed on Immunocompetent or Immunodeficient Animals

(A and B) Densitometry analysis for the SDS-PAGE gel image from Figure 25A showing levels of ~100 kDa (A) and ~ 73 kDa (B) protein band in ticks fed on C57BL/6J or RAG$^{-/-}$ mice.

(C) 1-D SDS-PAGE analysis of total protein profile in salivary glands of ticks fed on BALB/c or SCID is shown. Solid arrow indicates band around ~ 100 kDa that was upregulated in salivary gland lysates prepared from ticks fed on BALB/c mice in comparison to salivary gland lysates prepared from ticks fed on SCID mice.

(D) Densitometry analysis using control bands indicated using the asterisk in (C).

Table 2. LC-MS/MS Data Showing Presence of Arthropod HSP70-Like Proteins in Salivary Gland Lysates Prepared from Ticks Fed on Immunocompetent Mice.

Uniprot accession number	Description	GenBank Accession number	# PSMs	Molecular Function	Biological Process	MW (kDa)
B7PEN4	Heat shock protein, putative OS=Ixodes scapularis GN=IscW_ISCW017754 PE=3 SV=1 - [B7PEN4_IXOSC]	XM_002433611	35	catalytic activity; nucleotide binding	cell organization and biogenesis; metabolic process; response to stimulus	72.5
B7PAR6	Heat shock protein, putative OS=Ixodes scapularis GN=IscW_ISCW017456 PE=3 SV=1 - [B7PAR6_IXOSC]	XM_002407088	41	catalytic activity; nucleotide binding	cell organization and biogenesis; metabolic process; response to stimulus	71.1
B7P4X5	Heat shock protein 70, putative (Fragment) OS=Ixodes scapularis GN=IscW_ISCW024057 PE=3 SV=1 - [B7P4X5_IXOSC]	XM_002406516	12	nucleotide binding	cell organization and biogenesis; response to stimulus	23.1
B7Q7S0	Heat shock protein, putative (Fragment) OS=Ixodes scapularis GN=IscW_ISCW011425 PE=3 SV=1 - [B7Q7S0_IXOSC]	XM_002412155	15	catalytic activity; nucleotide binding	cell organization and biogenesis; response to stimulus	64.3
B7QL71	Heat shock protein, putative (Fragment) OS=Ixodes scapularis GN=IscW_ISCW024910 PE=3 SV=1 - [B7QL71_IXOSC]	XM_002415881	14	nucleotide binding	cell organization and biogenesis; response to stimulus	67.8
B7P8Q5	Hsp70, putative (Fragment) OS=Ixodes scapularis GN=IscW_ISCW017192 PE=3 SV=1 - [B7P8Q5_IXOSC]	XM_002402518	14	catalytic activity; nucleotide binding; protein binding	cell organization and biogenesis; metabolic process	72.2

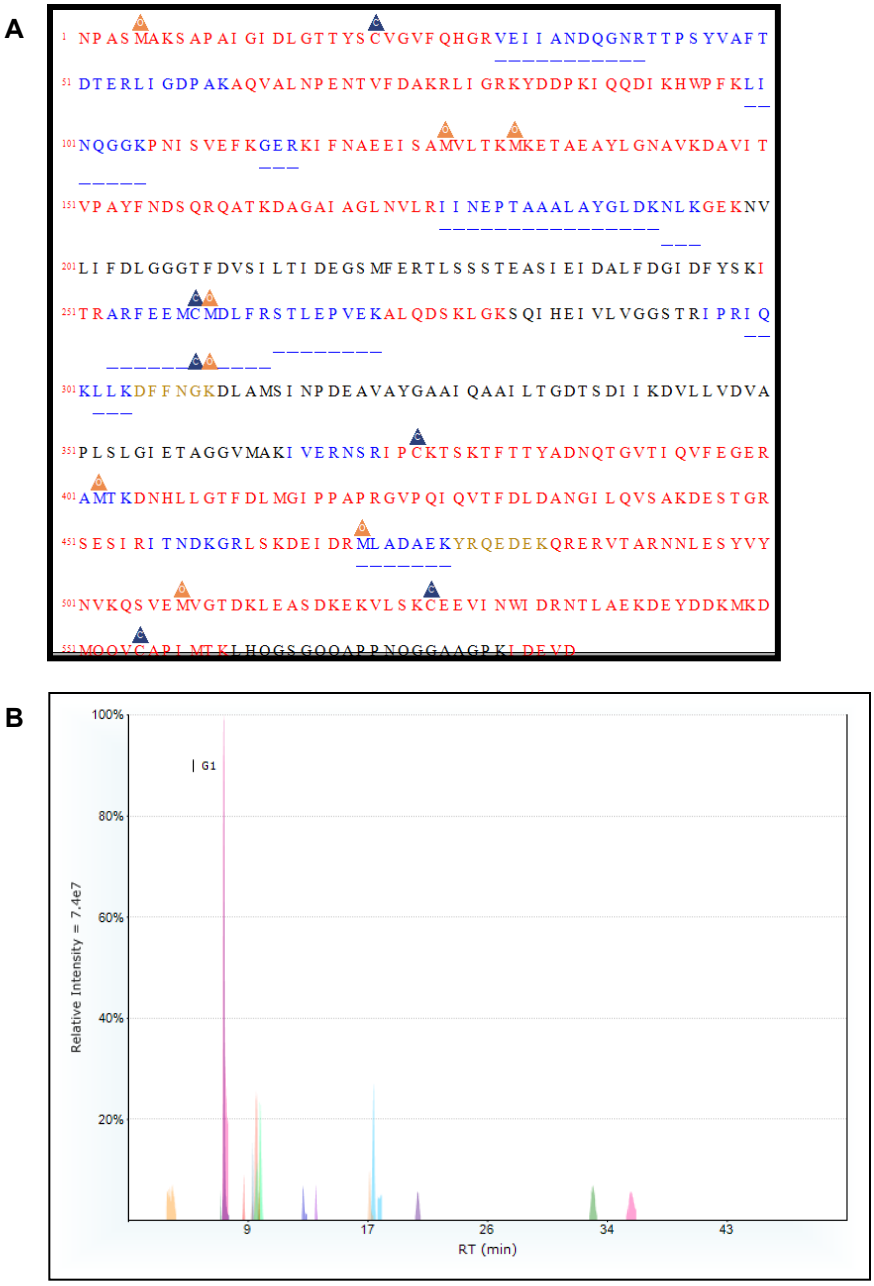

Figure 27. Extracted Ion Chromatogram from LC-MS/MS Analysis

(A) The Uniprot sequence for XM_002412155 identified in the MS analysis are colored in blue or red text. Orange triangles indicate oxidation sites and blue triangles indicate carbamidomethylation sites.

(B) Extracted Ion Chromatograms for all identified peptides for Uniprot sequence (B7Q7S0) with GenBank acc. no. XM_002412155. Dr. Sucharita Dutta performed the LC-MS/MS analysis.

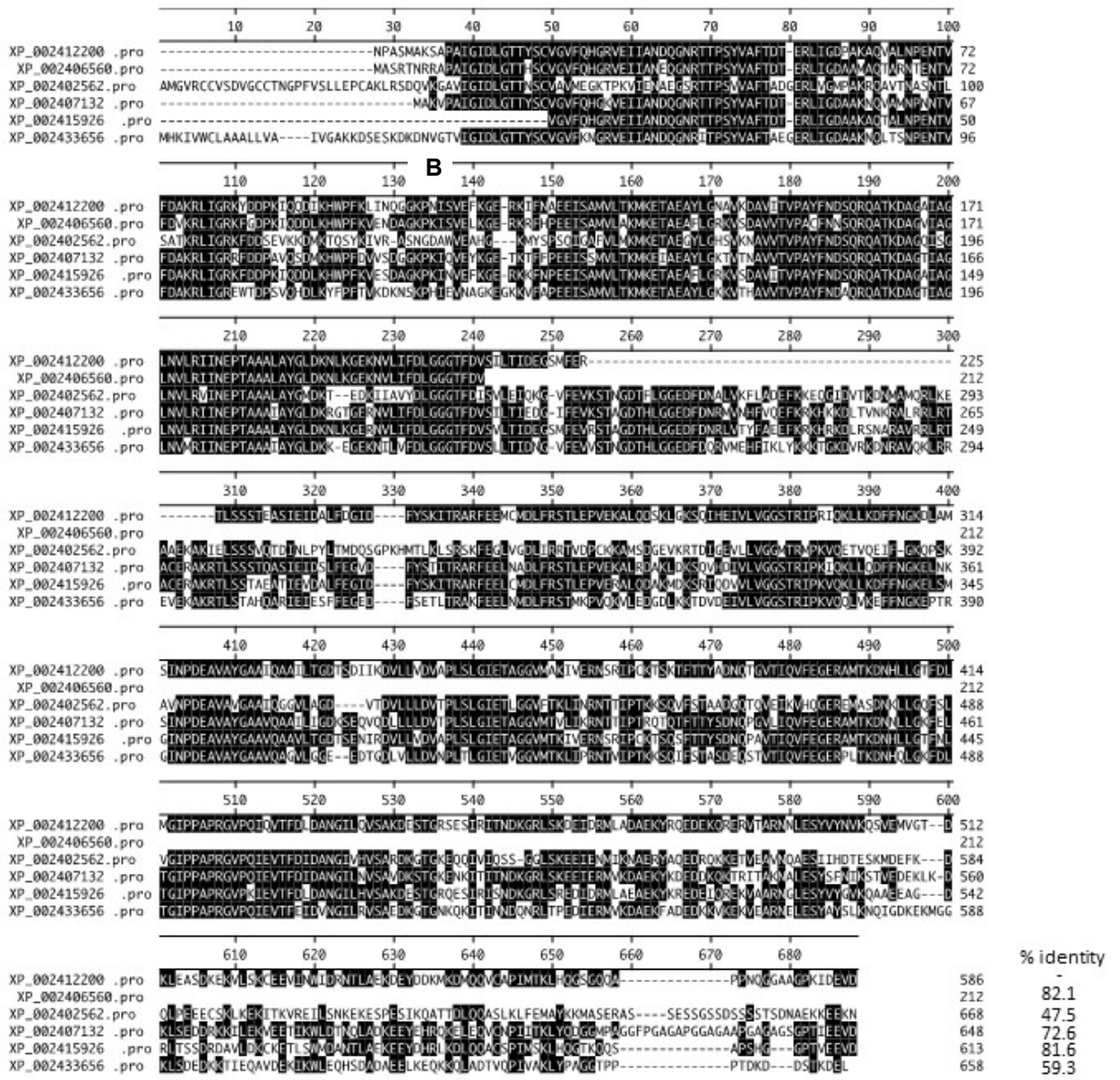

Figure 28. Alignment of *I. scapularis* HSP70-Like Molecules Identified from LC-MS/MS Analysis

Amino acid sequence alignments were performed using Clustal W program in DNASTAR Lasergene. Residues that match are shaded as black color. The GenBank accession numbers for proteins XP_002412200, XP_002406560, XP_002402562, XP_002407132, XP_002415926 and XP_002433656 corresponds to the nucleotide accession numbers XM_002412155, XM_002406516, XM_002402518, XM_002407088, XM_002415881 and XM_002433611, respectively. Percent identities for XP_002412200 (GenBank nucleotide acc. no. XM_002412155) in comparison to other HSP70-like molecules are shown at the bottom of the alignment.

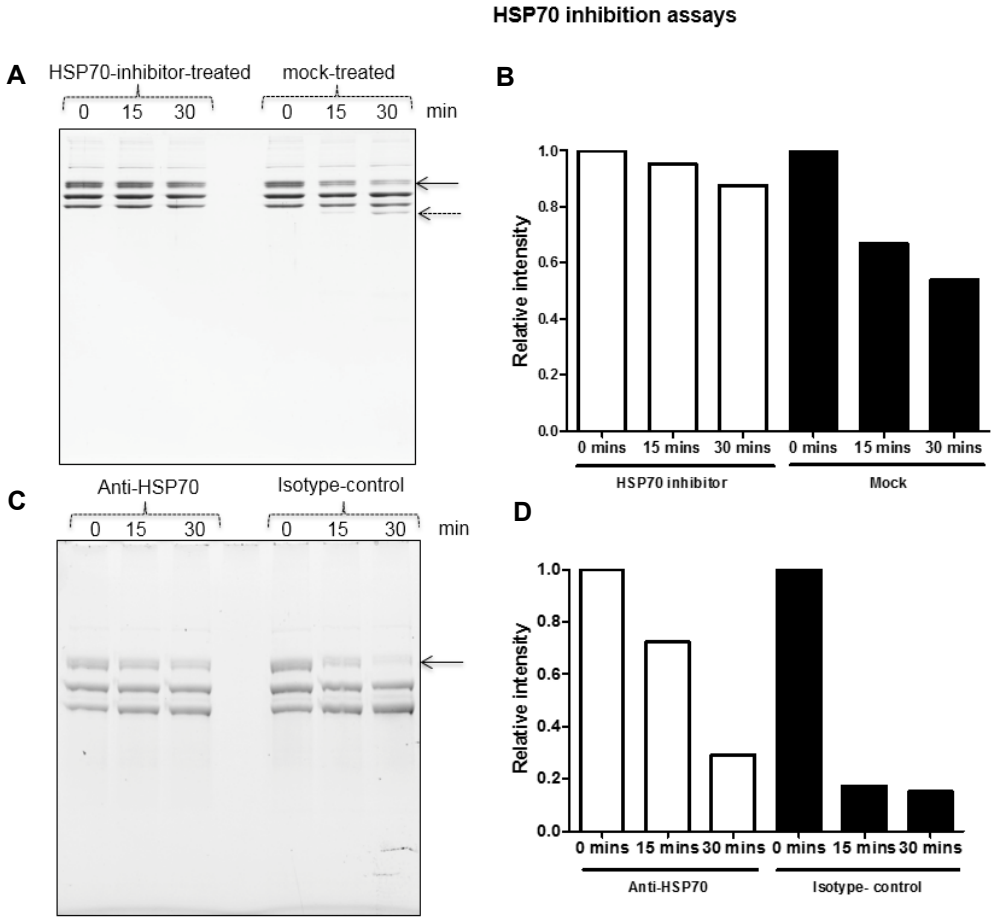

Figure 29. Tick HSP70-Like Protein Participates in Variable Fibrinogenolysis

(A) Fibrinogenolysis assays performed with salivary gland lysates prepared from ticks fed on immunocompetent animals in the presence of a HSP70 inhibitor or equal volume of mock control and incubated over time. Solid arrow indicates increased Aα chain fibrinogen degradation and dotted arrow indicates increased fibrinogen-degraded product at 30 min in mock control in comparison to inhibitor-treated samples.

(B) Densitometry analysis for data shown in (A).

(C) Fibrinogenolysis performed with salivary gland lysates prepared from ticks fed on immunocompetent animals in the presence of anti-HSP70 antibody or an isotype control and incubated over time. Arrow indicates increased fibrinogen degradation in the presence of isotype-matched control antibody.

(D) Densitometry analysis for data shown in (C).

In (B and D), the intensity of Aα was measured relative to the intensity of Aα chain at 0 min time point.

DISCUSSION

Acquiring a blood meal is a multi-step process for ticks. It involves attachment to the host, insertion of their proboscis, secretion of their saliva into the host's dermis and blood stream, engorgement on host blood, and detachment after repletion. To accomplish this while evading detection and immune defense mechanisms, the ticks produce many tick molecules (Brossard and Wikel, 2004; Francischetti et al., 2009; Hovius et al., 2008; Ramos and Selistre-de-Araujo, 2006; Ribeiro and Francischetti, 2003; Wikel, 2013). Fibrinogenolysis at the bite site is once such evasive mechanism elicited by ticks to achieve suppressed host coagulation. We report through this study a novel role for arthropod HSP70-like molecules in tick-induced fibrinogenolysis. The hypothesis is that the increase in post-engorgement weight of ticks fed on immunodeficient mice is due to reduced fibrin/fibrinogen clotting in these mice. The results show a lower expression of an *hsp70-like* molecule in ticks that fed on immunodeficient animals with respect to the immunocompetent cohort (Figure 25A and G). This is consistent with the reduced fibrinogen degradation around the tick bite site on these animals (Figure 18, 19, 20, 21 and 22). The increased transcriptional expression for only one of the HSP70-like molecule out of six molecules analyzed in this study does not rule out involvement of the other HSP70-like molecules at different stages of engorgement in ticks. The reduced presence of murine D-dimer in ticks fed on immunodeficient mice in comparison to ticks fed on immunocompetent mice strongly supports this hypothesis (Figure 18). Decreased fibrin/ fibrinogen clotting could account for higher blood in-take and weight of ticks fed on the immunodeficient animals (Figure

17) and possibly increased transmission of pathogens. The case for higher chance of pathogen transmission is supported by a study that has reported an increased rate of transmission of pathogens from ticks to immunodeficient animals in comparison to the immunocompetent animals (Bockenstedt et al., 2006).

A previous study has shown that antibodies generated against recombinant *Haemaphysalis longicornis* HSP70 recognized bands at approximately 100, 72 and 28 kDa in the egg lysates prepared from these ticks (Tian et al., 2011). This suggests that insects like *Haemaphysalis longicornis* or *I. scapularis* may be expressing a molecule similar to HSP70 but with a different size or that the tick HSP70-like molecules undergo several posttranslational modifications. HSP70s also form antiparallel dimers stabilized by post-translational modifications to position them for transfer to HSP90 (Morgner et al., 2015). Taken together, the observation of an HSP70-like peptide sequence recording the highest peptide match and scores in our LC-MS/MS analysis for a ~100 kDa band is not surprising.

From the works of Tytell and Hightower one can draw precedent that HSP70 could transit through the extracellular spaces (Hightower and Guidon, 1989; Tytell et al., 1986). Human serum contains significant amounts of HSP70s suggesting this molecules existence in extracellular spaces or as secreted proteins (Pockley et al., 1998). This, in combination with evidence that a proteasome component Sec61p and HSP70 are involved in the degradation of fibrinogen in the mammalian cells (Xia and Redman, 2001) confirms our data in Figures 21, 22 and 29. These data provide the evidence that arthropod HSP70-like molecules play a role in fibrinogenolysis during tick blood feeding. The differential *ex vivo* fibrinogenolysis between salivary gland lysates

prepared from ticks fed on SCID and $RAG^{-/-}$ mice could be due to the two different genetic backgrounds (BALB/c and C57BL/6 J, respectively). They could also be due to the leakiness in the generation of some clones of T and B cells in the SCID mice. A role for five the other HSP70-like molecules in fibrinogenolysis cannot be excluded in ticks during feeding on diverse vertebrate hosts (deer, rabbits, birds…etc.). Future comparative studies on all tick HSP70-like molecules would reveal whether they have similar or redundant function during arthropod blood meals. VER155008 is an ATP-competitive inhibitor and arrests the N-terminal domain of HSP70 that subsequently affects substrate binding (Schlecht et al., 2013). Figure 29 shows reduced fibrinogenolysis upon treatment of salivary glands lysates generated from ticks fed on immunocompetent animals with VER155008.

This data suggests that the N-terminal domain of the tick HSP70-like protein is critical for recognition of its substrate proteins that are responsible for fibrinogen degradation. $RAG^{-/-}$ mice do not produce any mature T or B-lymphocytes and this is described as a “non-leaky” immune deficiency animal model while some SCID mice have a “leaky” mutation which leads to the development of a few clones of T and B cells (Bosma et al., 1988). T and B-cells play important roles in the host immune responses against tick bites (Anguita et al., 2002). The lack of T and B cells or other metabolites in the host blood could also account for increased blood in ticks fed on immunodeficient animals independent of the host blood clotting factors. Several studies have now characterized various tick salivary proteins involved in T and B cell inhibition (Anguita et al., 2002; Gillespie et al., 2001; Kotsyfakis et al., 2006). Further investigation is required to determine whether tick HSP70-like proteins affect activation of host T and B cells

facilitating arthropod blood feeding. The data showing a decreased fibrinogenolysis from salivary gland lysates prepared from ticks fed on T and B-cell deficient background host provides important future avenues in understanding the role of these cells in blood clotting during tick feeding. It also provides direction to discover their involvement in coagulation pathways around the feeding cavity formed by the arthropod bites.

We further hypothesize that HSP70-like molecules secreted in tick saliva may aid in proper folding of proteins that are involved in fibrinogenolysis at the arthropod bite site to facilitate blood feeding. However, the contribution of arthropod HSP70 molecules to fibrinogenolysis either directly or indirectly would not rule out other salivary activities by these molecules important during feeding.

In summary, using *I. scapularis* as a model, this study provides evidence that ticks elicit variable fibrinogenolysis upon feeding on hosts with different genetic background and/or immune status. This study is not only important in understanding the molecular basis of the interactions at the tick-host interface but may also potentially lead for the development of anti-tick vaccines to interfere with the life cycle of this and perhaps other medically important vectors.

METHODS AND MATERIALS

Ticks and Mice

Laboratory-reared specimens of *Ixodes scapularis* ticks were used throughout this study. Ticks used in this study were larvae and nymphs obtained from a continuously maintained tick colony at the Department of Epidemiology and Public Health, Yale University (New Haven, CT) or at the Connecticut Agricultural Experiment Station (New Haven, CT). All animal work in this study was carried out in strict accordance with the recommendations in the Guide for the Care and Use of Laboratory Animals of the National Institute of Health. The protocol (#16-017) approved by the Old Dominion University Institutional Animal Care and Use Committee (Animal Welfare Assurance Number: A3172-01) was used in this study. Animal husbandry was provided in accordance with criteria approved by the Association for Assessment and Accreditation of Laboratory Animal Care Program at ODU. Acepromazine (Phoenix, St. Joseph, Missouri) tranquilizer was administered to the animals prior to handling to minimize anxiety and/or discomfort and all efforts were made to minimize suffering. To generate fed larvae or nymphs, unfed ticks were allowed to feed on naïve 6-8 weeks C57BL/6J and B6.129S7-*Rag1*^{tm1Mom}/J (RAG$^{-/-}$) mice (Jackson laboratories) or BALB/c and SCID NCr (Charles River Laboratories) to repletion and were collected immediately after drop-off for tick weight measurements and RNA extractions. At least three mice per experimental group were used. For D-dimer immunoblotting assays, ticks that were collected from individual mouse were used for the analysis. For salivary gland lysates preparation, ticks were pooled from three mice and used for further analysis. Tick

rearing was conducted in a Parameter Generation and Control incubator (Black Mountain, North Carolina) at 23°C with 95% relative humidity and a 14/10 hour light/dark photoperiod regiment. The IBC number for this study are 15-012 and 15-013.

Fibrinogenolysis Assays

The fibrinogen (2.5 mg/mL) purchased from Sigma (USA) was dissolved in solution with pH 7.4 containing 50 mM HEPES and 150 mM NaCl and distributed in two portions, one with 1 mM $CaCl_2$ and the other with 1 mM EDTA. Five micrograms of salivary gland extracts were pre-incubated with 1 µL of 150 mM NaCl. The samples were incubated for 90 min. In some cases, salivary gland lysates and 150 mM NaCl solution was incubated with mock (4 µL of 1x phosphate buffered saline that corresponds to equal volume of HSP70-inhibitor solution) or 100 µM VER155008 (HSP70-inhibitor) or with 50 µg of isotype control or anti-HSP70 antibodies (Cell Signaling technologies, USA). The whole mix of salivary glands with 150 mM NaCl was then added to 15 µL of fibrinogen solutions making up a total volume of 20 µL. From 20 µL reaction mix, 3 µL was immediately taken out and considered as 0 min time point sample. Incubation was then continued and 3 µL sample was collected at different time points (15, 30, 120 and 240 minutes). The collected samples were stored on ice until further use. All samples were heated at 70°C for 3 min before loading on to 4-20% gradient stain-free SDS-PAGE gels (BioRad). 12% SDS-PAGE gels were used for HSP70-inhibitor or antibody-blocking fibrinogenolysis assays. Images for fibrinogen degradation were captured using Chemidoc MP Imager (BioRad).

RNA Isolation and qRT-PCR

Total RNA from fed larvae or salivary glands from nymphs was generated using the Aurum Total RNA mini kit (BioRad, USA) following the manufacturer's instructions. RNA was converted to cDNA using cDNA synthesis kit (BioRad, Hercules, USA). Standard curve was prepared using 10-fold serial dilutions starting from 1 ng to 0.00001 ng of known quantities of *hsp70*-like molecules *or* actin fragments and qRT-PCR reactions were performed as described (Kotsyfakis et al., 2006). The generated cDNA was used as a template for quantifying transcripts of tick *hsp70*-like molecules. As an internal control and to normalize the amount of template, *I. scapularis actin* transcripts were quantified using oligonucleotides 5' GGTATCGTGCTCGACTC3' and 5' CAGGGCGACGTAGCAG 3'. QRT-PCR was performed using iQ-SYBR Green Supermix (Biorad, USA). Following are the oligonucleotide primers used in this study: XM_002433611, 5'-GAGTTTTCAAGAATGGGCGTGT-3' and 5'-GTGAGGCTTGCTGTTCTTGTCC-3'; XM_002407088, 5'-CGGCTGATCGGTCGTCGT-3' and 5' CGCTGCGAGTCGTTGAAGT 3'; XM_002406516, 5'-GCGGAACACGGAGAACACAGT-3' and 5'-GAACCTCTTCCGCTCTCCCT-3'; XM_002412155, 5'-GATGACCCCAAGATTCAGCAG-3' and 5'-GCCTCGGCTGTTTCTTTCATCT-3'; XM_002415881, 5'-GAAAGAAACGGCGGAGGCT-3' and 5'-CGTGGGCTCGTTGATGATG-3'; XM_002402518, 5'-GTGTAGCAGTGATGGAAGGGAAGA-3' and 5'-CAGAGAGGGTGTTGGACGCA-3'.

Tick Weight Measurements

Fed ticks were collected immediately after repletion, cleaned with brushes to remove any mice hair or feces and weighed using a Cahn C-31 microbalance (Thermoelectric Co., West Chester, PA) set to a range from 25 mg to 0.1 µg. Total body weight measurements were obtained by directly placing each tick on a balance pan. Data in Figure 17 shows the total tick body weights for at least 75 larvae/group.

Immunoblotting and Densitometry

Total lysates from 5-7 ticks fed on C57BL/6J or $RAG^{-/-}$ mice and BALB/c or SCID NCr was prepared in modified RIPA buffer (BioExpress) supplemented with EDTA-free protease inhibitor cocktail (Sigma, USA). Protein concentrations were determined by BCA protein assay kit (Pierce, USA). Thirty micrograms of total lysates from each group were loaded onto a 12% non-reducing stain-free SDS-PAGE gel (BioRad) for D-dimer immunoblotting. In addition, D-dimer protein that was purified from human plasma was purchased from Lee Biosolutions (MO, USA) and was used in immunoblotting assays performed on 10% SDS-PAGE gels. The protein gels were further processed for immunoblotting as described (Sultana et al., 2010). D-dimer antibody (Biorbyt, UK) and Rabbit polyclonal anti-IgG HRP-conjugated antibody (Santa Cruz Biotechnology Inc.) was used to detect D-dimer. ECL reactions were performed using Advanced WesternBright ECL HRP substrate kit (Advansta, USA) and chemi-luminescence reaction images were captured using Chemidoc MP Imager (BioRad). Densitometry analysis was performed using image lab software 4 by measuring intensity of D-dimer bands relative to the control band (equal loading control) from the stain-free image. For

fibrinogenolysis assays, densitometry analysis was performed by measuring intensity of the degraded product band relative to the level of fibrinogen Aα at 0 min time point.

Salivary Gland Dissection

Salivary glands and gut tissues were dissected from individual freshly fed nymphal ticks in sterile 1X phosphate buffer saline. The tissues were then pooled in one vial and homogenized using Kontes homogenizer and disposable pestles (VWR, USA). Protein concentrations were determined by BCA protein assay kit (Pierce, USA). Five micrograms of salivary gland extracts were used for fibrinogenolysis assays.

Mass Spectrometry Analysis

The tick samples were run on a 1-D gel for dual purposes of sample concentration and sample clean-up. This gel is stained with Coomassie Blue was de-stained and washed with a series of three washing buffers (50 mM ammonium bicarbonate, 50% acetonitrile and 80% acetonitrile). The bound proteins were reduced with 1 mL of 40 mM dithiothreitol for 25 minutes at 56°C. The gels were rinsed with 1 mL of 50 mM ammonium bicarbonate buffer and the reduced proteins were alkylated with 1 mL of 50 mM Iodoacetamide for 30 minutes at 25°C in the dark with constant mixing. The Iodoacetamide was discarded and the gel bound proteins were digested with 0.5 mL of trypsin (20 ng/µL; Promega, Madison, WI) in 50 mM ammonium bicarbonate buffer at 37°C with constant mixing for 12 h. After digestion, the tryptic fraction was collected, and the gels were washed with 50mM ammonium bicarbonate to collect any remaining tryptic peptides. The eluent containing the tryptic peptides were dried using a Speed-Vac apparatus (Thermo Fisher Scientific, San Jose, CA) and

stored at 4°C prior to mass spectrometric analysis. The LC-MS/MS analysis was performed by Dr Sucharita Dutta for our published study (Vora et al., 2017).

Peptide/Protein Acquisition by ESI-MS/MS Analysis

The dried samples were dissolved with 20 µL of 0.1% formic acid/water. 2 µL of each sample was analyzed by LC/ESI-MS/MS using a Q-Exactive (Thermo Fisher) mass spectrometer with an Easy NanoLC-1000 system using data dependent acquisition with dynamic exclusion (DE = 1) settings. The data dependent acquisition settings used were a top 12 higher energy collision induced dissociation (HCD) for the Q-Exactive MS. The Q-Exactive mass spectrometer was used with capillary temperature, 250°C; spray voltage, 1600V; and S-lens voltage, 55%. The automatic gain control (AGC) target was3e6 for Full MS scans and 2e5 for MS/MS scans. Resolving power for Q-Exactive was set at 70,000 for the full MS scan, and 17,500 for the MS/MS scan at m/z 200. LC/ESI-MS/MS analyses was conducted using a C18 column (75 µm x 150 mm). The mobile phases for the reverse phase chromatography were (A) 0.1% HCOOH/water and (B) 0.1% HCOOH in acetonitrile. A four-step, linear gradient was used for the LC separation (2% to 30% B in the first 47 minutes, followed by 80%B in the next 1 minute and holding at 80% B for 12 minutes). The LC-MS/MS analysis was performed by Dr. Sucharita Dutta for our published study (Vora et al., 2017).

Peptide/Protein Identification from Tick Samples

The Sequest algorithm was used to identify peptides from the resulting MS/MS spectra by searching against the combined tick protein database extracted from Uniprot using the appropriate taxonomy using Proteome Discoverer (version 1.3, ThermoScientific). Searching parameters for parent and fragment ion tolerances were set as 20 ppm and 30 mmu for the Q Exactive MS. Other parameters used were a fixed modification of carbamidomethylation –Cys, variable modifications of oxidation (Met). Trypsin was set as the protease with a maximum of 2 missed cleavages. Raw files and proteome discoverer search results for the target protein were input into the quantitative package; Pinpoint (version 1.1, ThermoScientific). The raw file was imported into the software which analyzed the data and determined the optimal peptide targets for the protein of interest. The software determines the retention time window and accurate m/z ratio for each targeted peptide and produced a mass list used directly in the acquisition method for scheduled MS/MS. Target m/z lists were generated automatically based on tryptic cleavage, specified modifications and retention time on the chromatogram obtained from the gel spots. Quantitation analysis was performed in an automated fashion using the software with a 5 ppm window for extracted ion chromatograms. The optimized acquisition method for the targeted peptides was run in triplicate to validate the quantitative differences observed in the samples from the discovery experiment. Label free differential analysis was performed to compare the four sets of tick samples after sample normalization. The LC-MS/MS analysis was performed by Dr. Sucharita Dutta for our published study (Vora et al., 2017).

Statistics

The statistical significance of differences observed in data sets was analyzed using GraphPad Prism6 software and Microsoft Excel. For data to compare two means, the non-paired Student *t* test was performed. p values of < 0.05 were considered significant in all tests. Wherever necessary, statistical test and p values are reported.

CONCLUSION

These two studies provide an insight into how vector molecules could influence pathogen transmission in different ways. This adds to the range of the vector and pathogen molecular repertoire that can be used upon the host to make infections easier to transmit and establish in arthropod and vertebrate hosts. In the first study involving the transmission of dengue virus through EVs and facilitated by Tsp29Fb, some very important new phenomenon were observed. This study is the first to show that mosquito cells can produce EVs. Recent studies from Dr. Sultana's laboratory shows the production of EVs by tick cells and that these can mediate Langat virus and West Nile Virus infection *in vitro* (Zhou et al., 2018)**.** This study is also the first to show the presence of an entire genome of DENV2 inside EVs. The study was also able to show the presence of RNA from another serotype, DENV3 inside EVs which together with (Zhou et al., 2018) indicates that other flaviviruses could be exhibiting similar strategies. In addition, the study showed the presence of dengue proteins in the EVs, indicating that once the RNA is introduced inside naïve cells, it has some viral proteins available to readily start replicating. Although this study is not the first in showing that EVs derived from virus infected cells can propagate infection, the data showing flaviviral content-carrying EVs being infectious is of special importance. It indicates that receptor-mediated endocytosis may not be the only way for flaviviral entry, since EVs have been shown to directly fuse with recipient cells (Barile and Vassalli, 2017; Colombo et al., 2014; Schorey et al., 2015; Théry et al., 2002). The identification of a mosquito ortholog of the human exosome marker CD63 provides a useful target for the abrogation of

dengue transmission. Inhibition of Tsp29Fb leads to the reduction in dengue load and transmission (through EVs) which fits the first criteria of a good candidate for blocking the transmission of VBDs (Neelakanta and Sultana, 2015).

In the second study, a novel approach in studying VBDs was undertaken. The study was designed to see the effect of the host on the vectors rather than the other way around as many other studies have done (Brossard and Wikel, 2004; Formaglio et al., 2018; Hovius et al., 2008; Ribeiro et al., 2007; Wikel, 2013, 1996). While trying to determine if the immunocompetence of hosts has an effect on the vector, the study discovered that *I. scapularis* ticks have a higher engorgement weight when they feed on immunocompromised hosts. The salivary gland extracts from the same ticks when exposed to fibrinogen showed greater fibrinogenolysis in the immunocompetent host-fed cohort. This indicates that a vector factor was not being induced during feeding and that it was probably involved in the disruption of the host's coagulation machinery, which was not being triggered due to the absence of or weak effect of that pathway in immunocompromised hosts. Though the tested metalloproteases were not involved in this effect, the tick HSP70-like molecule was shown to be involved in the proteolysis of fibrinogen. Thus indicating its role in disruption of the host's coagulation response. The significance of this study is that since the vectors take a larger blood meal or feed for longer, they may have a higher chance of transmitting any pathogens they may be carrying to hosts that are already immunocompromised. To firmly place this molecule as a good candidate for transmission blocking, further studies involving pathogens need to be performed.

In summary, the development of vector-borne disease prevention and cure needs urgent attention due to its high mortality rate. Vector-borne diseases also offer exciting avenues for infectious disease research through the sheer number of interactions and players that are involved at the vector-host-pathogen interface. Strategies for establishing safe, effective and cheap transmission blocking vaccines remain under investigation.

REFERENCES

Ader, D.B., Celluzzi, C., Bisbing, J., Gilmore, L., Gunther, V., Peachman, K.K., Rao, M., Barvir, D., Sun, W., and Palmer, D.R. (2004). Modulation of dengue virus infection of dendritic cells by Aedes aegypti saliva. Viral Immunol. *17*, 252–265.

Alenquer, M., and Amorim, M.J. (2015). Exosome Biogenesis, Regulation, and Function in Viral Infection. Viruses *7*, 5066–5083.

Anderson, J.F., and Armstrong, P.M. (2012). Prevalence and Genetic Characterization of Powassan Virus Strains Infecting Ixodes scapularis in Connecticut. Am. J. Trop. Med. Hyg. *87*, 754–759.

Anderson, J.F., and Magnarelli, L.A. (2008). Biology of Ticks. Infect. Dis. Clin. N. Am. *22*, 195–215.

Anguita, J., Ramamoorthi, N., Hovius, J.W.R., Das, S., Thomas, V., Persinski, R., Conze, D., Askenase, P.W., Rincón, M., Kantor, F.S., et al. (2002). Salp15, an Ixodes scapularis Salivary Protein, Inhibits CD4+ T Cell Activation. Immunity *16*, 849–859.

Apte-Sengupta, S., Sirohi, D., and Kuhn, R.J. (2014). Coupling of replication and assembly in flaviviruses. Curr. Opin. Virol. *9*, 134–142.

Arakelyan, A., Fitzgerald, W., Zicari, S., Vanpouille, C., and Margolis, L. (2017). Extracellular Vesicles Carry HIV Env and Facilitate Hiv Infection of Human Lymphoid Tissue. Sci. Rep. *7*.

Barile, L., and Vassalli, G. (2017). Exosomes: Therapy delivery tools and biomarkers of diseases. Pharmacol. Ther. *174*, 63–78.

Benoit, J.B., Lopez-Martinez, G., Phillips, Z.P., Patrick, K.R., and Denlinger, D.L. (2010). Heat shock proteins contribute to mosquito dehydration tolerance. J. Insect Physiol. *56*, 151–156.

Bhatt, S., Gething, P.W., Brady, O.J., Messina, J.P., Farlow, A.W., Moyes, C.L., Drake, J.M., Brownstein, J.S., Hoen, A.G., Sankoh, O., et al. (2013). The global distribution and burden of dengue. Nature *496*, 504–507.

Bockenstedt, L.K., Liu, N., Schwartz, I., and Fish, D. (2006). MyD88 Deficiency Enhances Acquisition and Transmission of Borrelia burgdorferi by Ixodes scapularis Ticks. Infect. Immun. *74*, 2154–2160.

Bosma, G.C., Fried, M., Custer, R.P., Carroll, A., Gibson, D.M., and Bosma, M.J. (1988). Evidence of functional lymphocytes in some (leaky) scid mice. J. Exp. Med. *167*, 1016–1033.

Brady, O.J., Gething, P.W., Bhatt, S., Messina, J.P., Brownstein, J.S., Hoen, A.G., Moyes, C.L., Farlow, A.W., Scott, T.W., and Hay, S.I. (2012). Refining the Global Spatial Limits of Dengue Virus Transmission by Evidence-Based Consensus. PLoS Negl. Trop. *6*, e1760.

Brossard, M., and Wikel, S.K. (2004). Tick immunobiology. Parasitology *129 Suppl*, S161-176.

Bunggulawa, E.J., Wang, W., Yin, T., Wang, N., Durkan, C., Wang, Y., and Wang, G. (2018). Recent advancements in the use of exosomes as drug delivery systems. J. Nanobiotechnology *16*, 81.

Calvo, E., Sanchez-Vargas, I., Favreau, A.J., Barbian, K.D., Pham, V.M., Olson, K.E., and Ribeiro, J.M. (2010). An insight into the sialotranscriptome of the West Nile mosquito vector, Culex tarsalis. BMC Genomics *11*, 51.

Cesarman-Maus, G., and Hajjar, K.A. (2005). Molecular mechanisms of fibrinolysis. Br. J. Haematol. *129*, 307–321.

Cheng, G., Cox, J., Wang, P., Krishnan, M.N., Dai, J., Qian, F., Anderson, J.F., and Fikrig, E. (2010). A C-type lectin collaborates with a CD45 phosphatase homolog to facilitate West Nile virus infection of mosquitoes. Cell *142*, 714–725.

Chia, B.S., Low, Y.P., Wang, Q., Li, P., and Gao, Z. (2017). Advances in exosome quantification techniques. TrAC Trends Anal. Chem. *86*, 93–106.

Colombo, M., Raposo, G., and Théry, C. (2014). Biogenesis, Secretion, and Intercellular Interactions of Exosomes and Other Extracellular Vesicles. Annu. Rev. Cell Dev. Biol. *30*, 255–289.

Conway, M.J., Colpitts, T.M., and Fikrig, E. (2014). Role of the Vector in Arbovirus Transmission. Annu. Rev. Virol.*1*, 71–88.

Cruz-Oliveira, C., Freire, J.M., Conceição, T.M., Higa, L.M., Castanho, M.A.R.B., and Da Poian, A.T. (2015). Receptors and routes of dengue virus entry into the host cells. FEMS Microbiol. Rev. *39*, 155–170.

Cvjetkovic, A., Lötvall, J., and Lässer, C. (2014). The influence of rotor type and centrifugation time on the yield and purity of extracellular vesicles. J. Extracell. Vesicles *3*, 23111.

Emeis, J.J., Jirouskova, M., Muchitsch, E.-M., Shet, A.S., Smyth, S.S., and Johnson, G.J. (2007). A guide to murine coagulation factor structure, function, assays, and genetic alterations. J. Thromb. Haemost. *5*, 670–679.

Formaglio, P., Hovius, J.W., Aditya, C., Tavares, J., Mason, L.M.K., Ménard, R., Boulanger, N., and Amino, R. (2018). Chapter 12 - Tools to Decipher Vector-Borne

Pathogen and Host Interactions in the Skin. In Skin and Arthropod Vectors, N. Boulanger, ed. (Academic Press), pp. 431–467.

Foster, W.A., and Hancock, R.G. (1994). Nectar-related olfactory and visual attractants for mosquitoes. J. Am. Mosq. Control Assoc. *10*, 288–296.

Fragnoud, R., Flamand, M., Reynier, F., Buchy, P., Duong, V., Pachot, A., Paranhos-Baccala, G., and Bedin, F. (2015). Differential proteomic analysis of virus-enriched fractions obtained from plasma pools of patients with dengue fever or severe dengue. BMC Infect. Dis.*15*, 518.

Francischetti, I.M.B., Mather, T.N., and Ribeiro, J.M.C. (2003). Cloning of a salivary gland metalloprotease and characterization of gelatinase and fibrin(ogen)lytic activities in the saliva of the Lyme disease tick vector Ixodes scapularis. Biochem. Biophys. Res. Commun. *305*, 869–875.

Francischetti, I.M.B., Sa-Nunes, A., Mans, B.J., Santos, I.M., and Ribeiro, J.M.C. (2009). The role of saliva in tick feeding. Front. Biosci. (Landmark Ed) *14*, 2051–2088.

Gillespie, R.D., Dolan, M.C., Piesman, J., and Titus, R.G. (2001). Identification of an IL-2 Binding Protein in the Saliva of the Lyme Disease Vector Tick, Ixodes scapularis. The J. Immunol.*166*, 4319–4326.

Glaser, R.L., and Meola, M.A. (2010). The native Wolbachia endosymbionts of Drosophila melanogaster and Culex quinquefasciatus increase host resistance to West Nile virus infection. PLoS ONE *5*, e11977.

Gonzales, P.A., Pisitkun, T., Hoffert, J.D., Tchapyjnikov, D., Star, R.A., Kleta, R., Wang, N.S., and Knepper, M.A. (2009). Large-Scale Proteomics and Phosphoproteomics of Urinary Exosomes. J. Am. Soc. Nephrol. *20*, 363–379.

Green, S.A., Smith, M., Hasley, R.B., Stephany, D., Harned, A., Nagashima, K., Abdullah, S., Pittaluga, S., Imamichi, T., Qin, J., et al. (2015). Activated platelet-T-cell conjugates in peripheral blood of patients with HIV infection: coupling coagulation/inflammation and T cells. AIDS *29*, 1297–1308.

Gritsun, D.J., Jones, I.M., Gould, E.A., and Gritsun, T.S. (2014). Molecular Archaeology of Flaviviridae Untranslated Regions: Duplicated RNA Structures in the Replication Enhancer of Flaviviruses and Pestiviruses Emerged via Convergent Evolution. PLOS ONE *9*, e92056.

Guzman, M.G., Halstead, S.B., Artsob, H., Buchy, P., Farrar, J., Gubler, D.J., Hunsperger, E., Kroeger, A., Margolis, H.S., Martínez, E., et al. (2010). Dengue: a continuing global threat. Nat. Rev. Microbiol. *8*, S7–S16.

Hackenberg, M., and Kotsyfakis, M. (2018). Exosome-Mediated Pathogen Transmission by Arthropod Vectors. Trends Parasitol. *34*, 549–552.

Hadinegoro, S.R., Arredondo-García, J.L., Capeding, M.R., Deseda, C., Chotpitayasunondh, T., Dietze, R., Hj Muhammad Ismail, H.I., Reynales, H., Limkittikul, K., Rivera-Medina, D.M., et al. (2015). Efficacy and Long-Term Safety of a Dengue Vaccine in Regions of Endemic Disease. N. Engl. J. Med. *373*, 1195–1206.

Halstead, S.B. (2015). Pathogenesis of Dengue: Dawn of a New Era. F1000Research.

Halstead, S.B., and O'Rourke, E.J. (1977). Antibody-enhanced dengue virus infection in primate leukocytes. Nature *265*, 739–741.

Harris, A.F., McKemey, A.R., Nimmo, D., Curtis, Z., Black, I., Morgan, S.A., Oviedo, M.N., Lacroix, R., Naish, N., Morrison, N.I., et al. (2012). Successful suppression of a field mosquito population by sustained release of engineered male mosquitoes. Nat. Biotechnol. *30*, 828–830.

Hightower, L.E., and Guidon, P.T. (1989). Selective release from cultured mammalian cells of heat-shock (stress) proteins that resemble glia-axon transfer proteins. J. Cell. Physiol. *138*, 257–266.

Hovius, J.W.R., Levi, M., and Fikrig, E. (2008). Salivating for Knowledge: Potential Pharmacological Agents in Tick Saliva. PLOS Med. *5*, e43.

Jones, L.D., Hodgson, E., and Nuttall, P.A. (1989). Enhancement of Virus Transmission by Tick Salivary Glands. J. Gen. Virol. *70*, 1895–1898.

Kato, N., Mueller, C.R., Fuchs, J.F., Mcelroy, K., Wessely, V., Higgs, S., and Christensen, B.M. (2008). Evaluation of the Function of a Type I Peritrophic Matrix as a Physical Barrier for Midgut Epithelium Invasion by Mosquito-Borne Pathogens in Aedes aegypti. Vector Borne Zoonotic. Dis. *8*, 701–712.

Katzelnick, L.C., Gresh, L., Halloran, M.E., Mercado, J.C., Kuan, G., Gordon, A., Balmaseda, A., and Harris, E. (2017a). Antibody-dependent enhancement of severe dengue disease in humans. Science eaan6836.

Katzelnick, L.C., Coloma, J., and Harris, E. (2017b). Dengue: knowledge gaps, unmet needs, and research priorities. Lancet Infect. Dis.*17*, e88–e100.

Korbie, D.J., and Mattick, J.S. (2008). Touchdown PCR for increased specificity and sensitivity in PCR amplification. Nat. Protoc. *3*, 1452–1456.

Kotsyfakis, M., Sá-Nunes, A., Francischetti, I.M.B., Mather, T.N., Andersen, J.F., and Ribeiro, J.M.C. (2006). Antiinflammatory and Immunosuppressive Activity of Sialostatin L, a Salivary Cystatin from the Tick Ixodes scapularis. J. Biol. Chem. *281*, 26298–26307.

Krause, P.J., Narasimhan, S., Wormser, G.P., Barbour, A.G., Platonov, A.E., Brancato, J., Lepore, T., Dardick, K., Mamula, M., Rollend, L., et al. (2014). Borrelia miyamotoi

sensu lato Seroreactivity and Seroprevalence in the Northeastern United States. Emerg. Infect. Dis. *20*, 1183–1190.

Kročová, Z., Macela, A., Hernychová, L., Kroča, M., Pechová, J., and Kopecký, J. (2003). Tick salivary gland extract accelerates proliferation of francisella tularensis in the host. J. Parasitol. *89*, 14–20.

Labuda, M., Jones, L.D., Williams, T., and Nuttall, P.A. (1993). Enhancement of tick-borne encephalitis virus transmission by tick salivary gland extracts. Med. Vet. Entomol. *7*, 193–196.

Lancaster, G.I., and Febbraio, M.A. (2005). Exosome-dependent Trafficking of HSP70: a novel secretory pathway for cellular stress proteins. J. Biol. Chem. *280*, 23349–23355.

Le Coupanec, A., Babin, D., Fiette, L., Jouvion, G., Ave, P., Misse, D., Bouloy, M., and Choumet, V. (2013). Aedes mosquito saliva modulates Rift Valley fever virus pathogenicity. PLoS Negl. Trop. Dis. *7*, e2237.

Li, G., Endsley, M.A., Somasunderam, A., Gbota, S.L., Mbaka, M.I., Murray, J.L., and Ferguson, M.R. (2014). The dual role of tetraspanin CD63 in HIV-1 replication. Virol. J. *11*, 23.

Madison, M., and Okeoma, C. (2015). Exosomes: Implications in HIV-1 Pathogenesis. Viruses *7*, 4093–4118.

Morgner, N., Schmidt, C., Beilsten-Edmands, V., Ebong, I., Patel, N.A., Clerico, E.M., Kirschke, E., Daturpalli, S., Jackson, S.E., Agard, D., et al. (2015). Hsp70 Forms Antiparallel Dimers Stabilized by Post-translational Modifications to Position Clients for Transfer to Hsp90. Cell Rep. *11*, 759–769.

Mousson, L., Zouache, K., Arias-Goeta, C., Raquin, V., Mavingui, P., and Failloux, A.-B. (2012). The native Wolbachia symbionts limit transmission of dengue virus in Aedes albopictus. PLoS Negl. Trop. Dis. *6*, e1989.

Neelakanta, G., and Sultana, H. (2015). Transmission-Blocking Vaccines: Focus on Anti-Vector Vaccines against Tick-Borne Diseases. Arch. Immunol. Ther. Exp. *63*, 169–179.

Neelakanta, G., Sultana, H., Fish, D., Anderson, J.F., and Fikrig, E. (2010). Anaplasma phagocytophilum induces Ixodes scapularis ticks to express an antifreeze glycoprotein gene that enhances their survival in the cold. J. Clin. Invest. *120*, 3179–3190.

Ødegaard, F. (2000). How many species of arthropods? Erwin's estimate revised. Biol. J. Linn. Soc. *71*, 583–597.

Pal, U., Li, X., Wang, T., Montgomery, R.R., Ramamoorthi, N., deSilva, A.M., Bao, F., Yang, X., Pypaert, M., Pradhan, D., et al. (2004). TROSPA, an Ixodes scapularis Receptor for Borrelia burgdorferi. Cell *119*, 457–468.

Perera-Lecoin, M., Meertens, L., Carnec, X., and Amara, A. (2013). Flavivirus Entry Receptors: An Update. Viruses *6*, 69–88.

Peters, L.L., Cheever, E.M., Ellis, H.R., Magnani, P.A., Svenson, K.L., Von Smith, R., and Bogue, M.A. (2002). Large-scale, high-throughput screening for coagulation and hematologic phenotypes in mice. Physiol. Genomics *11*, 185–193.

Pockley, A.G., Shepherd, J., and Corton, J.M. (1998). Detection of heat shock protein 70 (Hsp70) and anti-Hsp70 antibodies in the serum of normal individuals. Immunol. Invest. *27*, 367–377.

Pritt, B.S., Sloan, L.M., Johnson, D.K.H., Munderloh, U.G., Paskewitz, S.M., McElroy, K.M., McFadden, J.D., Binnicker, M.J., Neitzel, D.F., Liu, G., et al. (2011). Emergence of a New Pathogenic Ehrlichia Species, Wisconsin and Minnesota, 2009. N. Engl. J. Med. *365*, 422–429.

Ramakrishnaiah, V., Thumann, C., Fofana, I., Habersetzer, F., Pan, Q., Ruiter, P.E. de, Willemsen, R., Demmers, J.A.A., Raj, V.S., Jenster, G., et al. (2013). Exosome-mediated transmission of hepatitis C virus between human hepatoma Huh7.5 cells. Proc. Natl. Acad. Sci. *110*, 13109–13113.

Ramos, O.H.P., and Selistre-de-Araujo, H.S. (2006). Snake venom metalloproteases — structure and function of catalytic and disintegrin domains. Comp. Biochem. Physiol. Part C Toxicol. Pharmacol. *142*, 328–346.

Ribeiro, J.M.C., and Francischetti, I.M.B. (2003). Role of Arthropod Saliva in Blood Feeding: Sialome and Post-Sialome Perspectives. Annu. Rev. Entomol. *48*, 73–88.

Ribeiro, J.M.C., Arcà, B., Lombardo, F., Calvo, E., Phan, V.M., Chandra, P.K., and Wikel, S.K. (2007). An annotated catalogue of salivary gland transcripts in the adult female mosquito, Aedes aegypti. BMC Genomics *8*, 6.

Rodenhuis-Zybert, I.A., Wilschut, J., and Smit, J.M. (2010). Dengue virus life cycle: viral and host factors modulating infectivity. Cell. Mol. Life Sci. *67*, 2773–2786.

Rupert, D.L.M., Claudio, V., Lässer, C., and Bally, M. (2017). Methods for the physical characterization and quantification of extracellular vesicles in biological samples. Biochim. Biophys. Acta BBA - Gen. Subj. *1861*, 3164–3179.

Sanders, H.R., Evans, A.M., Ross, L.S., and Gill, S.S. (2003). Blood meal induces global changes in midgut gene expression in the disease vector, Aedes aegypti. Insect Biochem. Mol. Biol. *33*, 1105–1122.

Schlecht, R., Scholz, S.R., Dahmen, H., Wegener, A., Sirrenberg, C., Musil, D., Bomke, J., Eggenweiler, H.-M., Mayer, M.P., and Bukau, B. (2013). Functional Analysis of Hsp70 Inhibitors. PLOS ONE *8*, e78443.

Schneider, B.S., Soong, L., Zeidner, N.S., and Higgs, S. (2004). Aedes aegypti salivary gland extracts modulate anti-viral and TH1/TH2 cytokine responses to sindbis virus infection. Viral Immunol. *17*, 565–573.

Schoepp, R.J., and Beaty, B.J. (1984). Titration of dengue viruses by immunofluorescence in microtiter plates. J. Clin. Microbiol. *20*, 1017–1019.

Schorey, J.S., Cheng, Y., Singh, P.P., and Smith, V.L. (2015). Exosomes and other extracellular vesicles in host–pathogen interactions. EMBO Rep. *16*, 24–43.

Sherman, M.B., Guenther, R.H., Tama, F., Sit, T.L., Brooks, C.L., Mikhailov, A.M., Orlova, E.V., Baker, T.S., and Lommel, S.A. (2006). Removal of Divalent Cations Induces Structural Transitions in Red Clover Necrotic Mosaic Virus, Revealing a Potential Mechanism for RNA Release. J. Virol. *80*, 10395–10406.

Sherman, M.B., Freiberg, A.N., Holbrook, M.R., and Watowich, S.J. (2009). Single-particle cryo-electron microscopy of Rift Valley fever virus. Virology *387*, 11–15.

Styer, L.M., Lim, P.-Y., Louie, K.L., Albright, R.G., Kramer, L.D., and Bernard, K.A. (2011). Mosquito saliva causes enhancement of West Nile virus infection in mice. J. Virol. *85*, 1517–1527.

Sultana, H., Foellmer, H.G., Neelakanta, G., Oliphant, T., Engle, M., Ledizet, M., Krishnan, M.N., Bonafé, N., Anthony, K.G., Marasco, W.A., et al. (2009). Fusion Loop Peptide of the West Nile Virus Envelope Protein Is Essential for Pathogenesis and Is Recognized by a Therapeutic Cross-Reactive Human Monoclonal Antibody. J. Immunol. *183*, 650–660.

Sultana, H., Neelakanta, G., Kantor, F.S., Malawista, S.E., Fish, D., Montgomery, R.R., and Fikrig, E. (2010). Anaplasma phagocytophilum induces actin phosphorylation to selectively regulate gene transcription in Ixodes scapularis ticks. J. Exp. Med. *207*, 1727–1743.

Sultana, H., Neelakanta, G., Foellmer, H.G., Montgomery, R.R., Anderson, J.F., Koski, R.A., Medzhitov, R.M., and Fikrig, E. (2012). Semaphorin 7A Contributes to West Nile Virus Pathogenesis through TGF-β1/Smad6 Signaling. J. Immunol. *189*, 3150–3158.

Surasombatpattana, P., Ekchariyawat, P., Hamel, R., Patramool, S., Thongrungkiat, S., Denizot, M., Delaunay, P., Thomas, F., Luplertlop, N., Yssel, H., et al. (2014). Aedes aegypti Saliva Contains a Prominent 34-kDa Protein that Strongly Enhances Dengue Virus Replication in Human Keratinocytes. J. Invest. Dermatol. *134*, 281–284.

Takeuchi, T., Suzuki, M., Fujikake, N., Popiel, H.A., Kikuchi, H., Futaki, S., Wada, K., and Nagai, Y. (2015a). Intercellular chaperone transmission via exosomes contributes to maintenance of protein homeostasis at the organismal level. Proc. Natl. Acad. Sci. *112*, E2497–E2506.

Takeuchi, T., Suzuki, M., Fujikake, N., Popiel, H.A., Kikuchi, H., Futaki, S., Wada, K., and Nagai, Y. (2015b). Intercellular chaperone transmission via exosomes contributes to maintenance of protein homeostasis at the organismal level. Proc. Natl. Acad. Sci. *112*, E2497–E2506.

Tauro, B.J., Greening, D.W., Mathias, R.A., Ji, H., Mathivanan, S., Scott, A.M., and Simpson, R.J. (2012). Comparison of ultracentrifugation, density gradient separation, and immunoaffinity capture methods for isolating human colon cancer cell line LIM1863-derived exosomes. Methods *56*, 293–304.

Théry, C., Zitvogel, L., and Amigorena, S. (2002). Exosomes: composition, biogenesis and function. Nat. Rev. Immunol. *2*, 569–579.

Théry, C., Amigorena, S., Raposo, G., and Clayton, A. (2006). Isolation and Characterization of Exosomes from Cell Culture Supernatants and Biological Fluids. Curr. Protoc. Cell Biol. *30*, 3.22.1-3.22.29.

Tian, Z., Liu, G., Zhang, L., Yin, H., Wang, H., Xie, J., Zhang, P., and Luo, J. (2011). Identification of the heat shock protein 70 (HLHsp70) in Haemaphysalis longicornis. Vet. Parasitol. *181*, 282–290.

Tytell, M., Greenberg, S.G., and Lasek, R.J. (1986). Heat shock-like protein is transferred from glia to axon. Brain Res. *363*, 161–164.

Vega-Almeida, T.O., Salas-Benito, M., De Nova-Ocampo, M.A., del Angel, R.M., and Salas-Benito, J.S. (2013). Surface proteins of C6/36 cells involved in dengue virus 4 binding and entry. Arch. Virol. *158*, 1189–1207.

Villar, M., López, V., Ayllón, N., Cabezas-Cruz, A., López, J.A., Vázquez, J., Alberdi, P., and de la Fuente, J. (2016). The intracellular bacterium Anaplasma phagocytophilum selectively manipulates the levels of vertebrate host proteins in the tick vector Ixodes scapularis. Parasit. Vectors *9*, 467.

Villarroya-Beltri, C., Baixauli, F., Gutiérrez-Vázquez, C., Sánchez-Madrid, F., and Mittelbrunn, M. (2014). Sorting it out: Regulation of exosome loading. Semin. Cancer Biol. *28*, 3–13.

Vora, A., Taank, V., Dutta, S.M., Anderson, J.F., Fish, D., Sonenshine, D.E., Catravas, J.D., Sultana, H., and Neelakanta, G. (2017). Ticks elicit variable fibrinogenolytic activities upon feeding on hosts with different immune backgrounds. Sci. Rep. *7*, 44593.

Vora, A., Zhou, W., Londono-Renteria, B., Woodson, M., Sherman, M.B., Colpitts, T.M., Neelakanta, G., and Sultana, H. (2018). Arthropod EVs mediate dengue virus transmission through interaction with a tetraspanin domain containing glycoprotein Tsp29Fb. Proc. Natl. Acad. Sci. 201720125.

Whitehorn, J., and Simmons, C.P. (2011). The pathogenesis of dengue. Vaccine *29*, 7221–7228.

WHO (2004). The world health report 200- changing history. World Health Organization, Geneva.

WHO (2017). Vector- borne diseases fact sheet. World Health Organization, Geneva.

Wikel, S. (2013). Ticks and tick-borne pathogens at the cutaneous interface: host defenses, tick countermeasures, and a suitable environment for pathogen establishment. Front. Microbiol. *4*.

Wikel, S.K. (1996). Host Immunity to Ticks. Annu. Rev. Entomol. *41*, 1–22.

Wiley, R.D., and Gummuluru, S. (2006). Immature dendritic cell-derived exosomes can mediate HIV-1 trans infection. Proc. Natl. Acad. Sci. *103*, 738–743.

Xia, H., and Redman, C.M. (2001). Differential Degradation of the Three Fibrinogen Chains by Proteasomes: Involvement of Sec61p and Cytosolic Hsp70. Arch. Biochem. Biophys. *390*, 137–145.

Yacoub, S., Mongkolsapaya, J., and Screaton, G. (2013). The pathogenesis of dengue. Curr. Opin. Infect. Dis. *26*, 284–289.

Zhou, W., Woodson, M., Neupane, B., Bai, F., Sherman, M.B., Choi, K.H., Neelakanta, G., and Sultana, H. (2018). Exosomes serve as novel modes of tick-borne flavivirus transmission from arthropod to human cells and facilitates dissemination of viral RNA and proteins to the vertebrate neuronal cells. PLOS Pathog. *14*, e1006764.

VITA

ASHISH NARESH VORA

Dept. of Biological Sciences, 110 Mills Godwin Life Sciences Bldg., ODU.

EDUCATION

- MS, Cancer, Cell and Molecular Biology, University of Leicester, UK, 2009.
- BS with Honors, Biomedical Science, University of Central Lancashire, UK, 2008.

PEER-REVIEWED PUBLICATIONS

- Vora, A., Taank, V., Dutta, S.M., Anderson, J.F., Fish, D., Sonenshine, D.E., Catravas, J.D., Sultana, H., and Neelakanta, G. (2017). Ticks elicit variable fibrinogenolytic activities upon feeding on hosts with different immune backgrounds. Sci. Rep. *7*, 44593.
- Vora, A., Zhou, W., Londono-Renteria, B., Woodson, M., Sherman, M.B., Colpitts, T.M., Neelakanta, G., and Sultana, H. (2018). Arthropod EVs mediate dengue virus transmission through interaction with a tetraspanin domain containing glycoprotein Tsp29Fb. Proc. Natl. Acad. Sci. 201720125.

ABSTRACTS, CONFERENCE ORAL PRESENTATIONS & POSTERS

- ” A novel arthropod exosomal marker- tetraspanin domain containing glycoprotein Tsp29Fb mediates dengue transmission” American Society for Virology. Poster number P16-8 (2018)
- “Ticks elicit variable fibrinogenolytic activities upon feeding on hosts with different immune backgrounds”. Virginia Academy of Sciences/ Virginia Entomological Society (2017).
- “Dengue uses mosquito cell-derived exosomes as a vehicle for transmission to humans.” American Society for Virology, Oral presentation (2016).
- “Evaluation of IGF-1 and IGF-1R in triple negative breast cancer.” AMP Abstracts, *JMD* November Vol: 14 No. 6, pp 723, Article number: ST104 (2012).
- “Correlation of Histopathologic and Molecular Characteristics for Prognostication in Neuroblastoma.” AMP Abstracts, *JMD* November Vol: 12 No. 6, pp 903, Article number: ST32 (2010).